THESIS FOR THE DEGREE OF DOCTOR OF PHILOSOPHY

Mobilization and Management of Tellurium in Severe Accident Scenarios

ANNA-ELINA PASI

Department of Chemistry and Chemical Engineering
CHALMERS UNIVERSITY OF TECHNOLOGY
Gothenburg, Sweden 2022

Mobilization and Management of Tellurium in Severe Accident Scenarios

ANNA-ELINA PASI

ISBN: 978-91-7905-736-7

Doktorsavhandlingar vid Chalmers Tekniska Högskola
Ny serie nr 5202
ISSN: 0346-718X

Nuclear Chemistry
Department of Chemistry and Chemical Engineering
Chalmers University of Technology
SE-412 96 Gothenburg
Sweden
Telephone: +46 (0)31-7721000

Cover: Three forms of tellurium: tellurium dioxide (left), dimethyl telluride (middle), elemental tellurium (right)

Printed by Chalmers digitaltryck
Gothenburg, Sweden 2022

Mobilization and Management of Tellurium in Severe Accident Scenarios

ANNA-ELINA PASI

Nuclear Chemistry
Department of Chemistry and Chemical Engineering
Chalmers University of Technology

Abstract

Safety is one of the highest priorities in any industry. In the nuclear industry, safety is in the essence since in case of a nuclear accident, the consequences can be long-lasting, hazardous, and devastating to the public, environment, and the industry. Although only two accidents of highest significance have occurred, their influence is still present today. One of the most severe consequences of a severe nuclear reactor accident is the release of radioactive material to the environment. Different characteristics, such as volatility, toxicity, and half-life, of the released elements determine their effect and significance. Among the released radionuclides is tellurium. The tellurium isotopes released in the major accidents are highly volatile and have half-lives long enough to make tellurium important especially in the early stages of an accident. The released tellurium isotopes can cause increased radiation dose to the public during the first weeks after the accident. Moreover, many of the tellurium isotopes released decay to iodine isotopes which is also a concern due to the increased risk of thyroid cancer iodine can cause.

The aim of this work was to investigate phenomena involving tellurium occurring inside the containment building during a severe nuclear accident. The work is divided into mobilization of tellurium species and their management. The results obtained in this research provide valuable information on the behavior of tellurium in severe accident scenarios. The reactions leading to increased solubility and volatility were shown. High emphasis was put on the formation, stability, and mitigation of organic tellurides. The formation of a variety of organic tellurides from paint solvents under gamma irradiation was observed. This causes concerns about possible re-volatilization leading to post-accident releases. In addition to the increased mobility, this work provides information on the mitigation of tellurium species in accident scenarios. The containment spray system was found to be relatively effective in removing tellurium species from the containment atmosphere. In addition, activated charcoal materials trapped dimethyl telluride well. However, some reversibility was observed which raises interest on the adsorption mechanism. The results presented in this work lay the foundation for further studies on tellurium behavior in the containment. The evidence showing the formation of organic tellurides is especially significant since that could potentially lead to increased releases.

Keywords: tellurium, severe accident, source term, nuclear, gamma irradiation

List of Publications

(I) Kärkelä, T., **Pasi, A. E.,** Espegren, F., Sevón, T., Tapper, U., & Ekberg, C. (2021). Tellurium retention by containment spray system. *Annals of Nuclear Energy*, *164*, 108622.

(II) **Pasi, A. E.,** Glänneskog, H., Foreman, M. R. S. J., & Ekberg, C. (2021). Tellurium behavior in the containment sump: dissolution, redox, and radiolysis effects. *Nuclear Technology*, *207*(2), 217-227.

(III) **Pasi, A. E.,** Foreman, M. R. S. J., & Ekberg, C. (2022). Organic Telluride Formation from Paint Solvents Under Gamma Irradiation. *Nuclear Technology*, 1-11.

(IV) **Pasi, A. E.,** Foreman, M. R. S. J., & Ekberg, C. Radiolytic Degradation of Dimethyl Telluride in Aqueous Solutions (Submitted to *Radiation Physics and Chemistry*)

(V) **Pasi, A. E.,** Foreman, M. R. S. J., & Ekberg, C. Study of the Removal Efficiency of Activated Charcoals for Organic Tellurides (Submitted to *Nuclear Technology*)

(VI) **Pasi, A. E.,** Kärkelä, T., Börjesson Sandén, F., Ekberg, C. Gas phase interactions between tellurium and organic material in severe nuclear accident conditions (Manuscript)

Related publications not included in the thesis:

Espegren, F., Kärkelä, T., **Pasi, A.E**., Tapper, U., Kučera, J., Lerum, H.V., Omtvedt, J.P. and Ekberg, C., 2021. Tellurium transport in the RCS under conditions relevant for severe nuclear accidents. *Progress in Nuclear Energy*, 139, p.103815.

Kučera, J., **Pasi, A.E**., Espergen, F., Kärkelä, T., Lerum, H.V., Omtvedt, J.P. and Ekberg, C., 2020. Tellurium determination by three modes of instrumental neutron activation analysis in aerosol filters and trap solutions for the simulation of a severe nuclear accident. *Microchemical Journal*, 158, p.105139.

Pasi A.E. (2022) The evolution of severe accident research at Chalmers University of technology- State of the art. *Proceedings of the 10th European Review Meeting on Severe Accidents Research (ERMSAR2022)* Karlsruhe, May 16-19th 2022

Contribution report

(I) Part of the experimental work, part of data analysis, not part in modelling, co-author

(II) All experimental work, data analysis and writing

(III) All experimental work, data analysis and writing

(IV) All experimental work, data analysis and writing

(V) All experimental work, data analysis and writing

(VI) Corresponding author, part of the experimental work, part of the data analysis

Table of Contents

1. INTRODUCTION 1

2. BACKGROUND 5

2.1. TYPES OF SEVERE ACCIDENTS 6

2.2. CONSEQUENCES OF SEVERE ACCIDENTS 7
2.2.1. HEALTH EFFECTS 7
2.2.2. SOCIO-POLITICAL EFFECTS 7
2.2.3. TECHNICAL IMPROVEMENTS 8
2.2.4. RELEASE OF FISSION PRODUCTS IN SEVERE ACCIDENTS 8
2.2.5. TELLURIUM IN SEVERE ACCIDENTS 10

2.3. SEVERE ACCIDENT RESEARCH 12
2.3.1. MOBILIZATION OF FISSION PRODUCTS 12
2.3.2. MANAGEMENT OF RELEASES 12
2.3.3. MODELLING 13

2.4. TELLURIUM IN SEVERE ACCIDENT RESEARCH 14

3. THEORY 15

3.1. SOLUTION CHEMISTRY IN SEVERE ACCIDENT SCENARIOS 15
3.1.1. CONTAINMENT SPRAY SYSTEM (CSS) 15
3.1.2. THE SUMP 15

3.2. CHEMISTRY OF FISSION PRODUCTS 16

3.3. TELLURIUM CHEMISTRY 17
3.3.1. ORGANOTELLURIUM CHEMISTRY 18

3.4. RADIOLYSIS 20
3.4.1. WATER RADIOLYSIS 20
3.4.2. RADIOLYSIS OF ORGANIC MOLECULES 21

4. EXPERIMENTAL 23

4.1. MATERIALS 23

4.2. MOBILIZATION METHODS 24
4.2.1. DISSOLUTION OF TELLURIUM UNDER GAMMA IRRADIATION 24
4.2.2. ORGANIC TELLURIDE FORMATION 24
4.2.3. DEGRADATION OF DIMETHYL TELLURIDE 25
4.2.4. GAS PHASE INTERACTIONS 25

4.3. MANAGEMENT METHODS 27
4.3.1. SPRAY REMOVAL EFFICIENCY 27
4.3.2. ADSORPTION ON CHARCOALS 29

4.4. ANALYTICAL METHODS 31
4.4.1. INDUCTIVELY COUPLED PLASMA MASS SPECTROMETRY, ICP-MS 31
4.4.2. GAS CHROMATOGRAPHY MASS SPECTROMETRY, GC-MS 31
4.4.3. ION CHROMATOGRAPHY 31
4.4.4. X-RAY DIFFRACTION, XRD 31
4.4.5. SCANNING AND TRANSMISSION ELECTRON MICROSCOPY, SEM/TEM 31
4.4.6. SPECIFIC SURFACE AREA ANALYSIS 32

5. RESULTS AND DISCUSSION 33

5.1. MOBILIZATION 33
5.1.1. SOLUBILITY OF TELLURIUM 33
5.1.2. ORGANIC TELLURIDE FORMATION 38
5.1.3. DEGRADATION OF DIMETHYL TELLURIDE 45
5.1.4. GAS PHASE INTERACTIONS 52

5.2. MANAGEMENT 54
5.2.1. SPRAY REMOVAL EFFICIENCY 54
5.2.2. ADSORPTION ON CHARCOALS 57

6. CONCLUSION 63

FUTURE WORK 67

ACKNOWLEDGEMENTS 69

REFERENCES 70

Abbreviations

ABS	Alkaline Borate Solution
AC	Activated Charcoal
BWR	Boiling Water Reactor
CSS	Containment Spray System
DMT	Dimethyl telluride
ECCS	Emergency Core Cooling System
ECURIE	European Community Urgent Radiological Information Exchange
EDX	Energy Dispersive X-ray Spectroscopy
FDNPP	Fukushima Dai-ichi Nuclear Power Plant
GC-MS	Gas Chromatography Mass spectrometry
IAEA	International Atomic Energy Agency
IC	Ion Chromatography
ICP-MS	Inductively Coupled Plasma Mass Spectrometry
INES	International Nuclear Event Scale
LET	Linear Energy Transfer
LOCA	Loss of Coolant Accident
LWR	Light Water Reactor
MEK	Methyl Ethyl Ketone
MIBK	Methyl Isobutyl Ketone
NPP	Nuclear Power Plant
PWR	Pressurized Water Reactor
RBMK	Reaktor Bolshoy Moshchnosti Kanalnyy
RCS	Reactor Coolant System
RIA	Reactivity Initiated Accident
SBO	Station Blackout
SEM	Scanning Electron Microscopy
TMI	Three Mile Island
TSP	Trisodium Phosphate
XRD	X-ray Diffraction
ZNPP	Zaporizhzhya Nuclear Power Plan

“Nothing in life is to be feared, it is only to be understood.
Now is the time to understand more, so that we may fear less.”
— Marie Curie

1. Introduction

For as long as nuclear power has been in commercial operation, safety has been of the highest priority. Despite the growing interest from the 1950s and 60s up until today, nuclear technology has been associated with a stigma of unreliability and uncertainty. In the early era of the commercial use of nuclear power, the concerns revolved around the military use of nuclear materials, which had been demonstrated just years prior. These concerns were replaced by nuclear reactor accidents which raised concerns in terms of the safety of nuclear power. The accidents that have occurred, one might say in regular intervals, have not only resulted in social bias and stigma but also in safety developments and need for severe accident research.

Although there have only been two major accidents in over 19 000 reactor years of experience[1], the legacy of these major events still lives on, and has recently been brought to the forefront due to the ongoing war in Ukraine. Once the Russian troops invaded the Chernobyl exclusion zone in February 2022, concerns were expressed about whether a second accident could take place at the same site. Another, more concerning event has been the invasion and shelling of the Zaporizhzhya nuclear power plant (ZNPP). This site has, since its invasion, repeatedly lost connection to the power line, and the ongoing attacks around the ZNPP are putting nuclear safety and security at risk[2]. The ZNPP has six VVER type pressurized light water reactors (PWRs), and therefore a Chernobyl type accident is inconceivable. However, severe accidents in PWR type of reactors can also lead to catastrophic consequences and should this happen, the consequences would be far-reaching.

While nuclear accidents can potentially have severe consequences, and in worst cases, long lasting and ultimately lethal outcomes, no industry is immune to accidents. Whether it is a catastrophic dam break in China[3], wind turbine failure in Japan[4], or coal mine explosion in Turkey[5], no accident is improbable. However, it can be argued that the highest negative impact for an industry that can result from an accident is for nuclear power. The reason for the severity of nuclear accidents compared to other industries is the release of radioactive elements. The released activities of the radionuclides from the major accidents are in the order of several Peta becquerels (10^{15} Bq)[6,7]. These releases can pose a great threat to the public and environment, especially those living near the accident site. While the threats certainly include serious illnesses resulting from increased radiation doses, direct health effects are not the only concern. Research has shown that people affected by such accidents and the subsequent evacuations, have a very high risk of experiencing psychological consequences[8–10]. In addition, strengthening of the anti-nuclear movement has been apparent after the accidents[11]. All this magnifies to a larger scale and ultimately impacts the whole nuclear industry.

Of the large activity released in a severe accident scenario, the highest fraction is contributed to the elements with the highest volatility. These elements include noble gases, iodine, cesium, and tellurium. While all activity released during a nuclear accident is unwanted, the released elements have characteristics that affect their significance. The most significant element in terms of direct health consequences is iodine. The high affinity of iodine to the

thyroid gland increases the risk of thyroid cancer in accident scenarios[12]. For long-term contamination, cesium is the major contributor. Due to the long half-life of specifically ^{137}Cs, the effects of the major accidents are still measurable in the environment decades later.

The third most significant element in the list of volatile elements is tellurium. Its high volatility resulting in releases comparable to those of iodine, makes tellurium one of the significant radionuclides in accident scenarios. Although the half-lives of the released tellurium isotopes are relatively short, it has been estimated that tellurium was a major contributor to the dose of public after the Fukushima accident[13]. Moreover, after both of the major accidents, tellurium had significantly delayed releases to the environment which cannot be fully explained[14]. To add to the significance, many of the tellurium isotopes released during an accident decay to iodine isotopes.

Scientifically, tellurium is interesting due to its complex chemistry, metalloid behavior, redox reactions, and interaction with a variety of other chemical species. The dissolution of tellurium deposits, formation of organic tellurides and the migration of these species inside the containment are of great interest in severe accident scenarios. This thesis focuses on the behavior of tellurium in severe nuclear accident conditions. The schematic presentation of each part of the containment and phenomena examined in this work is presented in Figure 1.1. The thesis is focused on the reactions and interactions leading to higher mobility of tellurium inside the containment building, and the removal efficiency of different mitigating systems towards these mobile tellurium species. Interaction with water radiolysis products leading to tellurium redox reactions (PAPER II), the formation and stability of organic tellurides (PAPER III, IV) and gas phase interactions with organic material leading to increased transport of tellurium (PAPER VI) in the containment were investigated. To study the management of these mobile species, the removal efficiency of the containment spray system (PAPER I) and adsorption of organic tellurides on activated charcoal materials (PAPER V) were examined. Here, small scale experiments have been conducted in order to gain insight into the behavior of tellurium in simulated severe nuclear reactor accident conditions.

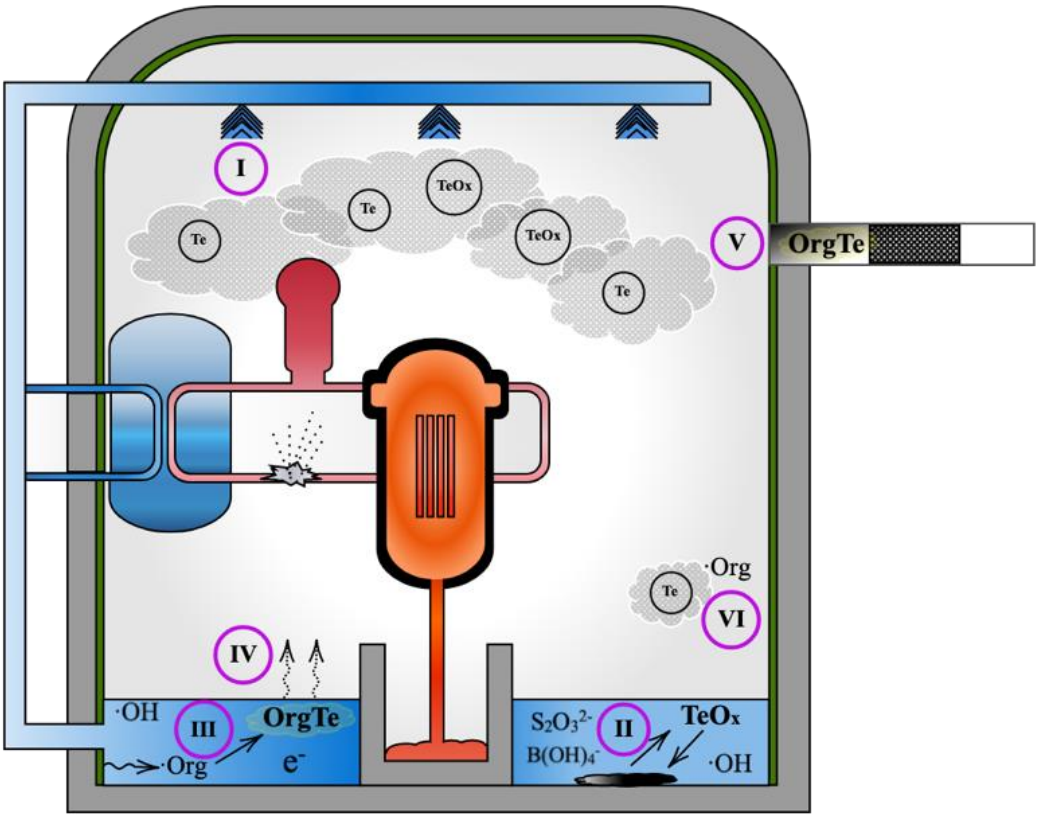

Figure 1.1. The schematic presentation of the phenomena investigated in this work. The Roman numerals and their placing refer to the articles on which this thesis is based on, and the phenomena investigated in each part: I. Efficiency of the containment spray system, II. Dissolution of tellurium in the sump, III. Formation of organic tellurides, IV. Radiolytic degradation of dimethyl telluride, V. Trapping of organic tellurides on activated charcoals, VI. Gas phase interactions between tellurium and organic material

2. Background

Nuclear power has been an important source of electricity for decades. Today, over 10 % of the electricity in the world is produced by nuclear fission[15]. Unfortunately, events that have led to the release of radioactive material into the environment have tainted the nuclear industry and halted the development of nuclear reactors. Although it is the major accidents that receive the most attention, there are a multitude of events in nuclear facilities that do not result in loss of life or long-term consequences. All of these are reported to the International Atomic Energy Agency and categorized by the International Nuclear Event Scale (INES) presented in Figure 1[16]. The 7-step scale is used to categorize nuclear events by their severity and probability, shown in color and grayscale in Figure 2.1., respectively. In addition to major accidents, the radiological events might include events such as the discovery of a radiation source in scrap metal (INES 0), damaged radiation source out of regulatory control (INES 3) or an automatic trip of two reactors following the loss of off-site electric supplies (INES 2)[17]. All of the events mentioned fall under the "incident" category where the consequences to the public and the environment are not considered severe. Higher up on the scale are accidents that are more severe events with varying significance. Major accident, generally referred to as severe accident, is the highest level, INES 7, and only two events have received this status: Chernobyl and Fukushima. Both of these accidents progressed to a point where the core melt could not be terminated for a long time, and releases to the environment could not be prevented.

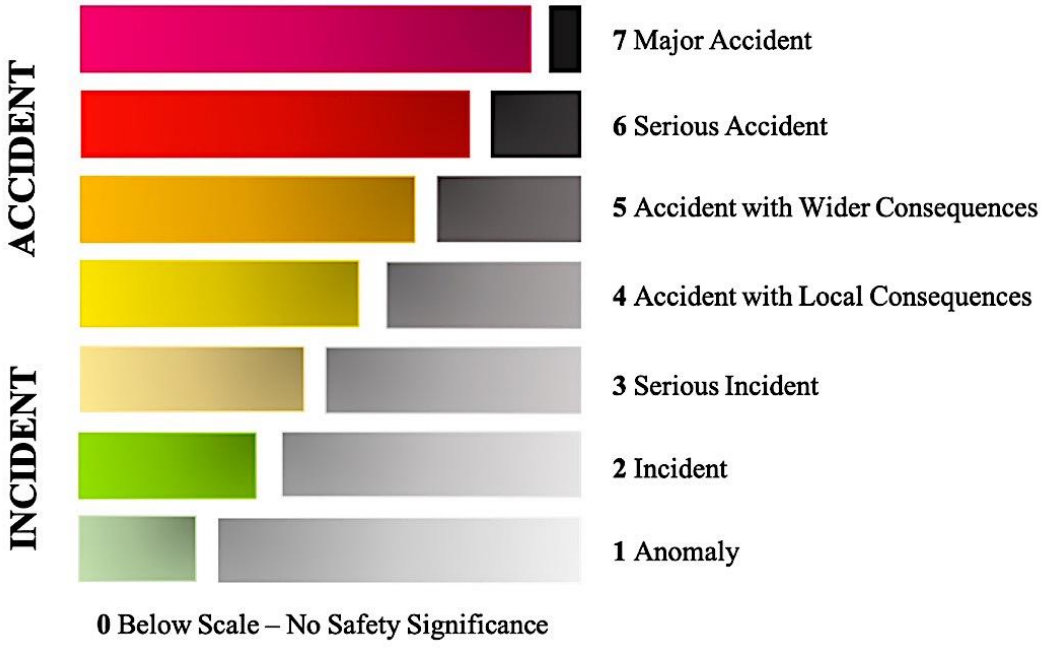

Figure 2.1. A schematic presentation of the INES scale

2.1. Types of severe accidents

Two of the main causes of severe accident are insufficient cooling of the core leading to a loss-of-cooling accident (LOCA) and a sudden rapid increase in the reactivity resulting in a reactivity-initiated accident (RIA). The two major accidents that have occurred provide examples of both accident types, Chernobyl being an RIA and Fukushima a LOCA.

An unwanted and sudden increase of the fission rate and reactor power in the reactor core will, in the worst case scenario, cause an RIA[18]. In Chernobyl, the events leading to the accident involved a questionable test use of the reactor and an inherent feedback mechanism facilitating the accident progression in an RIA scenario. A Chernobyl type RIA is very unlikely in the majority of the reactors currently in operation. This is due to the differences in the reactor designs. The Chernobyl reactor number four was a graphite-moderated and water-cooled channel type reactor (RBMK, Reaktor Bolshoy Moshchnosty Kanalny) whereas the majority of the current fleet consists of water-moderated and water-cooled reactors, mostly light water reactors (LWRs). There are eight RBMK type reactors still operating, all in Russia, compared to the over 400 water-cooled designs in the world[19]. In addition, after the Chernobyl accident, the design faults of the RBMKs were recognized and improved. Some of the shortcomings of the RBMKs that were improved were the reduction of the void coefficient reactivity and the prevention of the emergency system bypass when the reactor is in operation[20]. However, RIAs are not impossible events in LWRs. An event leading to an RIA in a LWR is related to the control rods, which are the elements responsible for regulating the fission reaction[21]. A faulty injection or ejection of control rods could initiate an increase in the reactivity. Nevertheless, emergency systems are in place and the opposite feedback mechanism compared to Chernobyl makes an RIA a very unlikely event in LWRs.

A LOCA is initiated by an event leading to the loss of cooling. Fukushima, which had six boiling water reactors (BWR) at the time of the accident, suffered from LOCA in three of the six reactors. The power plant experienced a loss of off- and on-site power due to the tsunami initiated by an earthquake, leading to a total station blackout (SBO). Although in case of a LOCA, there are emergency systems in place to provide cooling to the core, these systems require a power supply to operate. In Fukushima, the power after the SBO could have been provided by emergency diesel generators, which were unfortunately lost just minutes after the flooding of the site[22].

SBO is not the only initiating event that can potentially cause a LOCA. Another reason can be a break in the circuit that provides the cooling. A break, denoted by its size, a small, medium, or large break (SB, MB, LB-LOCA) results in coolant, usually water, leaking out of the circuit[23]. This leak can ultimately lead to an uncovering of the core. The events from the break until the release of fission products can all take place in a matter of minutes or up to a few hours depending on the size of the break and the progression of the accident[24]. However, accident management systems are in place to mitigate or delay the releases and aim to provide sufficient time for emergency actions outside the power plant to be put into action.

2.2. Consequences of severe accidents

Not all radiological events lead to major consequences. However, when considering high severity events, the consequences are undisputed. Whether it is direct effects of the high radiation doses, evacuation or phasing out of nuclear power, the consequences can be both local and far-reaching. Radioactive releases from severe nuclear accidents have certainly resulted in acute radiation poisoning cases, increased cancer rates and psychological harm. In addition, the use of the highly contaminated areas by radioactive deposition may be restricted for decades after an event.

2.2.1. Health effects

Of all the consequences, the direct health effects are the most concerning for the general public. High doses of ionizing radiation causes harm in the body and can ultimately be lethal when the tissue damage is too severe[25]. Another concern is when the received dose is not high enough to cause acute radiation damage but might appear years later in a form of cancer[26]. There is evidence of increased thyroid cancer rates in children and adolescents after the Chernobyl accident[12,27–29]. This is due to the high thyroid doses resulting from the accumulation of radioiodine. It should be noted that the cases were among the people who lived close to the accident site. Other types of cancers have conflicting evidence and cannot be statistically confirmed. However, when discussing the health consequences and cancer rates, the numbers given in the statistics are based on probabilities, and the exact number of radiation related illnesses will always be given as an estimation, with the estimations on radiation induced cancer cases from low doses being especially uncertain.

2.2.2. Socio-political effects

Considering the larger scale, the accidents have had a major effect on the nuclear industry. The industry has suffered from stagnation and the development has declined after every event. The Three Mile Island (TMI) accident in Harrisburg Pennsylvania in 1979 was a turning point for the development of nuclear power. It was the first accident in a commercial nuclear reactor. Although the TMI was categorized as level 5 on the INES scale, it had serious outcomes. Before the accident, the number of reactors under construction was increasing rapidly. However, after TMI, many orders for reactors in the US were cancelled[30]. Seven years after TMI, the worst severe nuclear accident, Chernobyl, occurred in the USSR, in today's Ukraine. As a results, the safety concerns that arouse after the TMI were multiplied[31]. This resulted in a halt in the construction of new nuclear reactors in the USA for decades and strengthened the opposition to nuclear power also in Europe[11,32,33].

The most recent major accident, Fukushima, in 2011, also had its consequences. The events in Japan again led to the public doubt regarding the safety of nuclear power and forced the decisionmakers to resign construction plans[34,35]. The most extreme decisions were made in Germany where several nuclear reactors were shut down after the accident, and this ultimately led to the phasing out of nuclear power in Germany[36,37].

Some of the consequences discussed here can be seen in Figure 2.2, which shows the electricity produced by nuclear power in the world over the years. The development in the USA can clearly be seen up to early 1990, after which the fraction of the total produced electricity stays relatively constant. Moreover, there is a clear decrease in the production in 2012 which can be contributed largely to the decision made in Germany. Now in 2022, the production is at the same level it was prior to Fukushima, and this can be, for the most part, attributed to the fast development of the nuclear industry in Asia.

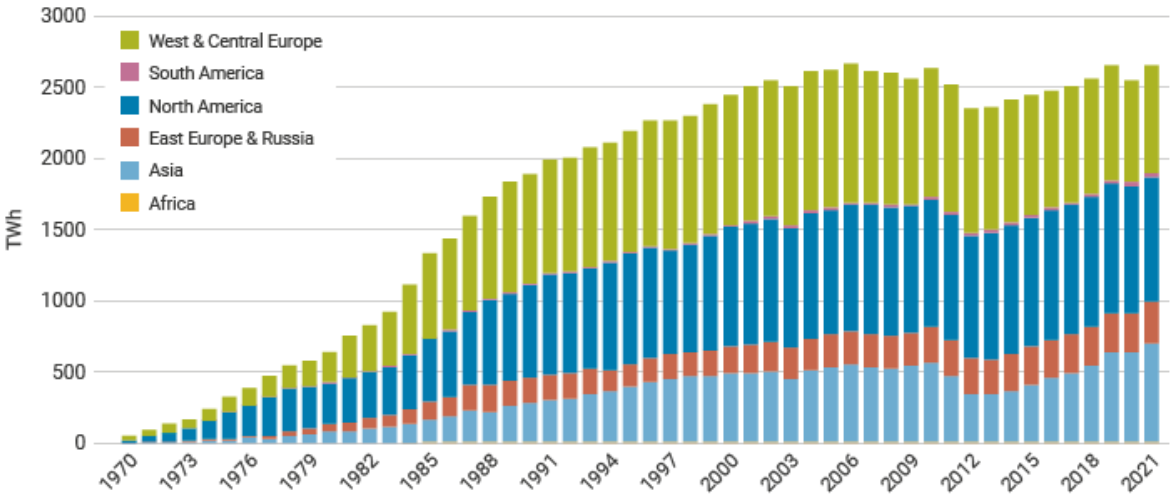

Figure 2.2. Electricity produced by nuclear power in the world[38]

2.2.3. Technical improvements

Not all consequences were detrimental to the nuclear industry. The accidents have resulted in major improvements in reactor design and led to a deeper understanding of the possible phenomena taking place in accident scenarios. New types of safety systems are in constant development and applied to the reactors. Of the improved safety features, the passive safety systems, systems requiring little or no power for operational action, are being tested[39,40] and validated[41,42] with modelling codes to improve the safety of nuclear reactors now and in the future. In addition, the world-wide monitoring systems like the European Community Urgent Radiological Information Exchange (ECURIE) ensure that in case of an accident, the response and data transfer will be rapid[43]. Furthermore, the weaknesses in communication with the public after the accidents have been recognized and improved for future reference[32,44].

2.2.4. Release of fission products in severe accidents

Without the release of radioactive material, all of the consequences of nuclear accidents would arguably be less severe. The radioactive releases are a result of the energy production which comes from the fission of uranium. Therefore, most of the releases in the event of an accident are fission products (FPs) of uranium. The first radionuclides to escape the core are the ones with the highest volatility. These include the noble gases (e.g. ^{133}Xe, ^{85}Kr) and

volatile fission product (e.g. ^{129,131,133}I, ^{134,137}Cs, ^{129m,132}Te). In case the accident proceeds to a point where the temperature increases even higher, or there are direct releases from the core as a result of an explosion, elements with very low volatility can be released into the environment. The released activities of significant radionuclides from the two major accidents are presented in Table 2.1.

Table 2.1. The releases of significant fission products from the Chernobyl and Fukushima accidents

Radionuclide	Half-life[45]	Chernobyl, PBq	Fukushima, PBq
Volatile elements			
^{133}Xe	5.25 d	6500[46]	14 000[47]
^{131}I	8.03 d	1760[6]	150[48]
^{132}Te	33.6 d	1150[6]	180[49]
^{129m}Te	3.20 d	240[46]	15[49]
^{137}Cs	30.1 y	85[6]	12[48]
Intermediate volatility elements			
^{89}Sr	50.5 d	115[6]	0.2[49]
Refractory elements			
^{239}Pu	24 110 y	0.013[6]	-

Although any type of radioactive release is a concern in a nuclear accident scenario, some fission products are considered more significant than others and have received the most attention in severe accident research. The fission product that has received the most attention is iodine. This is due to its high volatility, complex chemistry and the affinity to the thyroid gland, which increases the risk of thyroid cancer[50]. Iodine has been at the center of severe accident management, research, and safety assessment for decades, but there remains more work to be done in order to fully understand iodine behavior. Another fission product in focus has been cesium. The chemistry of cesium is less complex compared to iodine; however, the concerns arise from the long half-life of the main cesium isotope ^{137}Cs. Due to the 30-year half-life, traces of ^{137}Cs from the Chernobyl accident are still present in the environment decades after the event[51–53]. A high amount of ^{137}Cs deposition is one of the main reasons the exclusion zones in both Chernobyl and Fukushima are still restricted or classified as difficult-to-return areas[54,55].

The third element found in the list of the volatile and significant radionuclides is tellurium. Although tellurium has not received as much attention as iodine of cesium, it should still be considered significant. The following section provides information on what is known about tellurium release and behavior in severe accidents and how it related to the other two significant fission products.

2.2.5. Tellurium in severe accidents

The tellurium isotopes released in severe accidents are presented in Table 2.2 with their half-lives and decay products. One of the key details is the decay products of the presented tellurium isotopes. Many of the significant isotopes, including ^{132}Te, decay to iodine isotopes. This increases the significance of tellurium in accident scenarios due to the eventual presence of iodine in places tellurium isotopes have migrated during the accident.

Table 2.2. Relevant tellurium isotopes and their decay products with half-lives

Te isotope	Half-life (Te isotopes)[45]	Decay product	Halflife (I isotopes)[45]
^{127m}Te	109 d	^{127}I	stable
^{129m}Te	33.6 d	^{129}I	1.57 x 10^7 a
^{131m}Te	30 h	^{131}I	8.02 d
^{132}Te	3.2 d	^{132}I	2.295 h
^{133m}Te	55.4 min	^{133}I	20.8 h
^{134}Te	41.8 min	^{134}I	52.5 min

A large fraction of the tellurium inventory in the core is estimated to have been released in both major accidents. During Chernobyl, the estimations of released tellurium vary between 32 to 60 % of the total core inventory of around 2.7×10^{18} Bq was released[56]. In Fukushima, the combined release fraction of tellurium is estimated to be only a few percent as the overall releases were about one tenth of those during Chernobyl[49].

Little is known about the actual behavior of tellurium inside the reactor building during a major accident. This is due to the total destruction of the core and high activity inside the structures, which makes any sample collection nearly impossible. However, the lower severity of the TMI accident has enabled sample collection from the reactor building. Samples were collected from the sump water collected at the bottom of the containment through a drilled hole. Tellurium was found in these sump water samples. In addition, tellurium was found to be a main source of activity on a painted steel plug collected at a position close to the sump surface. The main fraction at the time of the sample collection came from ^{129m}Te with traces of ^{125m}Te and ^{127m}Te[57].

Knowledge of tellurium behavior inside the reactor building is scarce, but can be estimated is the release time, distribution, and deposition of tellurium in the environment. By analyzing the monitoring systems and isotopic ratios of the released radionuclides it was found that tellurium had similar behavior to that of cesium during the Chernobyl accident which suggest that both were likely transported in the same particles at least for a period of time[58]. Interestingly, the rate of release for tellurium was higher in the late stage of the accident which suggests there were changes in the chemical behavior during the accident progression. This might be due to the oxidation of tellurium-bearing material or the formation of volatile species[14].

After Fukushima, both tellurium deposition and distribution were also monitored alongside other fission products. Most of the tellurium was deposited to the north-west of the power

plant which coincides with the deposition of other fission products, such as cesium and iodine (Figure 2.3)[59]. However, there were significant differences in the isotopic ratios, especially $^{123}Te/^{137}Cs$, measured after the accident. The ratio increased and reached the maximum value after around 275 hours after the accident[14]. This again raises interest as to what caused the delayed tellurium releases. In addition, tellurium was found in both particulate and activated charcoal filters in the sampling devices which indicates the possible release of different species of tellurium.

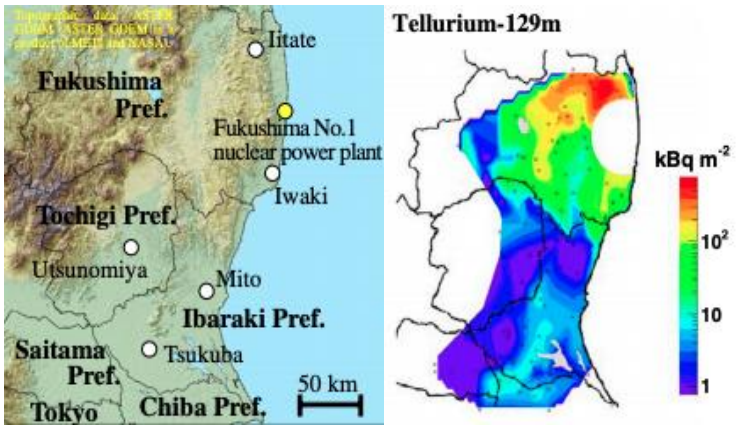

Figure 2.3. The deposition of ^{129m}Te in Japan after the Fukushima accident[59]

After the major accidents, tellurium was not only measured close to the accident site, but it also spread around the world with other fission products. The plumes from Chernobyl were detected widely across central and northern Europe. Moreover, the releases from Fukushima travelled across the Pacific Ocean and were detected in North America[60,61]. In the days following the accident, the plumes travelled towards Europe and were detected in Iceland, Scandinavia[62], and central and eastern Europe. Tellurium was among those radionuclides detected, and the measured activities were of the same magnitude as those of cesium and iodine[63]. Overall, the levels detected outside Japan were significantly lower compared to the ones monitored close to the accident site[64,65].

2.3. Severe Accident Research

The migration and deposition of fission products outside the reactor can be monitored and assessed. However, the events occurring inside the reactor building during an accident are very difficult to track. What cannot be observed or measured during or after an accident can be potentially simulated in a laboratory or with a computer. These are the tools used in severe nuclear reactor accident research. The research is highly based on the major accidents that have occurred. Due to the abundance of light water reactors in operation compared to the Chernobyl type graphite moderated design, the focus of severe accident research leans heavily towards Fukushima type LOCA. In recent years, other types of reactors such as small modular[66] and sodium cooled fast reactors[67,68] have also been considered. In case an accident occurs and progresses to core damage, regardless of the reactor type, the aim is to minimize or terminate the fuel melt, ensure the integrity of the containment building, minimize the amount of radioactive releases, and achieve a long-term stable state in the core. Severe accident research can be divided into two parts: experimental work and modelling. Both aim to gain better estimation of the source term of radionuclides in accident scenarios, where the source term refers to the timing and amount of releases in accident scenarios[23]. In the best cases, experiments are combined with modelling results, both of which validate each other.

2.3.1. Mobilization of fission products

The development of experimental severe accident research worldwide, is largely contributed to the advanced experimental programs such as PHEBUS[69,70], VERCORS[71], THAI[72] and BIP[73]. These programs have focused on the progression of a core melt accident, the release behavior of fission products in a variety of conditions, and the complexity of fission product behavior, mostly iodine. The access to large and complex experimental facilities, such as those used in PHEBUS and VERCORS, have been crucial in investigating severe accident phenomenology in moderately realistic conditions. To complement these large experimental programs, the THAI and BIP have focused on individual phenomena like hydrogen risk and iodine behavior. In addition, the Nuclear Energy Agency (NEA) of the OECD has produced a wide range of valuable results for both individual elements and their behavior as well as the phenomena that occur during an accident[72,74,75]. These programs and collaborations have laid the foundation and continue to be the benchmark of severe accident and especially source term research.

2.3.2. Management of releases

The migration of radionuclides, their chemical characteristics and physical properties highly affect their management. It is crucial to understand the differences in the efficiencies of the spray, scrubber, or filters towards the removal of gaseous and particulate species. Research efforts have accordingly studied these different management actions. The large experimental programs have mostly focused on the behavior of fission products, but some of the management actions have been incorporated into these programs. For example, the THAI and facility was equipped with a spray system to study hydrogen and iodine mitigation. However, most of the experimental research related to accident management concerns individual small-

scale studies. In recent years, pool scrubbing efficiency[76,77] and the development and testing of different filter materials have been in focus[78,79].

2.3.3. Modelling

To scale up the experimental data to realistic scenario, related either to core melt, the behavior of FPs or their management, information is applied to computed codes. Of these codes, MELCOR[80] developed by the Sandia National Laboratory (SNL); ASTEC[81] developed by Institut de Radioprotection et de Sûreté Nucléaire (IRSN) and the German Gesellschaft für Anlagen und Reaktorsicherheit (GSR); and the Modular Accident Analysis Program (MAAP) developed by Fausske and Associates and is being maintained by Electric Power Research Institute are the most used codes in severe accident research. These codes are used to simulate the phenomena that take place during an accident, like the progression of core melt[82–84], thermal hydraulics in the circuit, vessel and containment[85,86] and the release of fission products[87–89]. The complexity of the codes enables the simulation of large-scale events and pinpoints the different release phases with various accident scenarios. However, the codes could not have been developed without experimental research. In order to develop the modeling codes further, more experimental data are needed, and for that, small-scale experiments investigating a specific phenomenon are crucial.

2.4. Tellurium in Severe Accident Research

Although tellurium has not received the same attention that the other volatile fission products in severe accident research have, it has not been completely neglected in the past. Tellurium has been part of the large experimental programs that have provided valuable information, especially on the release behavior from the core. The VERCOS program recognized the volatile nature of tellurium and demonstrated the delayed release of tellurium due to cladding interactions[71]. In terms of containment behavior, tellurium was found to deposit in the sump in the PHEBUS experiments[70]. Apart from the large-scale experimental programs, research has focused on more specific and detailed phenomena, particularly the speciation of tellurium in the fuel[90,91], zirconium-tellurium species[92,93], and the atmosphere affecting tellurium transport[94,95], all of which have been investigated in the past. One of the major factors separating tellurium from the other fission products is its high affinity towards the zircaloy cladding already shown in VERCORS but also in other small-scale experiments. Previous research shows that tellurium can form zirconium-tellurium species in the fuel-cladding gap, which are released after sufficient oxidation of the cladding[92]. In addition, experiments show that the transport of tellurium is highly governed by the atmosphere[94,96,97]. The tellurium speciation changes from elemental to various forms of oxides depending on the partial pressure of oxygen in the atmosphere. In inert or reducing conditions, tellurium has been found to exist in a form of elemental tellurium. In a possible air ingress scenario, which creates more oxidizing conditions, tellurium is converted to an oxide, mono- or dioxide, depending on the amount of oxygen. Moreover, steam creating more humid conditions have been shown to increase the transport of tellurium through the reactor coolant system, likely through the formation of tellurium oxyhydroxide[98,99].

When it comes to the containment behavior of tellurium, the data is scarce. The solubility of tellurium has been expected to be low due to the sump results collected after TMI. The formation of volatile species such as organic tellurides have furthermore been mentioned in severe accident literature[14,100,101], however, no concrete evidence of the formation has been presented. In addition, the efficiency of management actions towards tellurium species is also unclear.

3. Theory

3.1. Solution chemistry in severe accident scenarios

During a severe nuclear accident, several management actions are applied to mitigate the radioactive releases. The safety systems are targeted to either retain fission products in a form where they will be unable to escape the reactor building or changed into a form that is less mobile. Key to achieve this is to use different solutions in the reactor building and by changing the chemistry, mitigate the releases.

3.1.1. Containment Spray System (CSS)

An important safety measures in accident scenarios is the containment spray system (CSS), where the spray nozzles are placed on top of the containment building. The CSS is a means of removing fission products from the containment atmosphere thus transferring them into the aqueous solution which accumulates in the sump. In addition, the CSS is designed to decrease the temperature and pressure in the containment and is consequently an important factor in protecting the containment integrity. As a mitigation action, the CSS is very efficient in removing aerosols or particulate species, but it has also been shown to retain some gaseous products[102,103]. The composition of the spray solution varies highly depending on the power plant design, but generally, it consists of a base and boric acid. The spray can have an additive such as sodium thiosulfate or hydrazine[104], both of which facilitate the mitigation of gaseous species, especially methyl iodide[103,105]. However, both of the additives are either corrosive[106] or toxic[107], and therefore largely abandoned or replaced. The spray solution pH is generally kept alkaline with the base to shift the disproportionation of volatile molecular iodine to the non-volatile iodate/iodide side[108]. Furthermore, boric acid is used to maintain the subcriticality of the reactor core as well as buffer the pH with the base[108].

3.1.2. The sump

The liquid that leaks from the reactor coolant system (RCS) or is introduced through the management systems collects at the bottom of the containment. This liquid is referred to as the sump. The main components of the sump are the base and boric acid originating from the coolant and spray. However, in reality, the sump is a very complex mixture of components, some of which are listed in Table 3.1. In addition to the base and acid, the sump contains different metals like zinc, aluminum and iron, fiber glass and concrete. Lastly, another important category of chemicals is organic material. Different organic material can be found inside the reactor building in insulation material and painted surfaces. The organic species are important since it has been shown that FPs can react with a variety of organic species in accident conditions and form volatile organic compounds[109–113]. Overall, due to the complexity of the sump, it is extremely difficult to predict the behavior of fission products and possible reactions without experimental research.

Table 3.1. Main components in the containment sump during a severe accident[114,115]

Source	**Component**
Cooling water (CSS, Safety Injection System (SIS), Emergency Core Cooling System (ECCS))	B, Li, Na, Cl
pH adjustment	sodium triphosphate (TSP), sodium hydroxide (NaOH), sodium tetraborate (NaTB)
Spray additives	Sodium thiosulfate ($Na_2S_2O_3$), hydrazine (N_2H_4)
Insulation material (e.g. fiberglass, calcium silicate)	Si, Al, Ca, Mg, B,
Concrete	Si, Ca, Al
Metals, steel, coatings	Al, Zn, Fe, Ni, S, Cu, organic material

3.2. Chemistry of fission products

The chemical and physical form of an element highly governs its characteristics and behavior such as volatility, solubility, or reactivity. This is something that needs to be considered when assessing the phenomena occurring during a nuclear accident. Due to the variety of radionuclides present in the core, the number of different species present in accident scenarios is very high. However, here only the highly volatile species are discussed emphasizing the chemistry of tellurium.

The chemistry of an element with multiple oxidation states is very complex. The possibility of an element releasing or gaining an electron, and by that changing its behavior, needs to be considered when assessing the behavior of elements in accident scenarios. One example of an element with multiple oxidation states is iodine. The oxidation states make iodine behavior difficult to control and assess. In its elemental form I_2, iodine is volatile; however, when reduced to the (-I) state, iodine becomes non-volatile. In addition, elemental iodine can also oxidize to form various non-volatile iodine oxides[116]. Controlling the iodine speciation is the basis of many of the management actions. For example, the pH of the sump is kept alkaline to keep the non-volatile state, -I, the predominant iodine species[117,118].

3.3. Tellurium chemistry

Tellurium is an element found on the bottom right part of the periodic table with an atomic number of 52. Its electron configuration is $[Kr]4d^{10}5s^{2}5p^{4}$. This configuration gives tellurium six valence electrons and its highest oxidation state +VI. As a part of the Group 16 elements, also referred to as the oxygen group or chalcogens, tellurium can exist in five different oxidation states ranging from -II to +VI. In addition to tellurium, the chalcogen group also includes oxygen, sulfur, selenium, polonium, and livermorium. The heavier chalcogens, selenium, tellurium and polonium can adopt both metallic and non-metallic properties and are therefore characterized as metalloids. The metalloid nature gives these elements a metallic appearance but a brittle nature and low electrical conductivity[119]. Due to its metalloid properties, tellurium is used to improve machinability in steel alloys and as a semiconductor in CdTe solar panels[120]. In the environment, tellurium is found in very low concentrations, only a few µg per kg on the Earth's crust and is therefore one of the rarer elements. In the bedrock, tellurium is often associated with gold tellurides such as calaverite and krennerite, both polymorphs of $AuTe_2$ [121].

The complex chemistry, and especially the range of oxidation states, enables tellurium to go through several reduction-oxidation, redox, reactions. The occurrence of these reactions depends on the prevailing conditions, mostly the electrical potential, E_h and the pH, and any species affecting them. The effect of these two on tellurium speciation is presented in the Pourbaix diagram in Figure 3.1. For severe accident research purposes, the most relevant conditions are pH around neutral to alkaline, and E_h at almost its entire range. Although some acidic solutions can be present in the containment sump, the more representative conditions are of those controlled by the alkaline management actions. In the diagram, the bolded species present the solids and the rest the soluble species.

In the case of tellurium, pH has a significant effect on tellurium solubility. Elemental tellurium is non-soluble in neutral aqueous solutions but in extremely alkaline solutions (pH>10) or in the presence of an oxidizing agent tellurium becomes more soluble. If elemental tellurium is added to an aerated solution, it is covered by tellurium dioxide[122] as could likely happen in sump conditions. Tellurium dioxide is an amphoteric compound and can protonate or deprotonate depending on the conditions. The dominant Te(IV) species in neutral aqueous solutions is tellurous(IV) acid H_2TeO_3, which can form both cationic and anionic products. The solubility of tellurium dioxide is relatively low, with a minimum at around 2.1×10^{-10} mol/dm^3 at pH 5.5[123]. However, the solubility increases at both extremes of the pH scale when tellurium dioxide dissolves as an ionic species. In its hydrated form, $TeO_2 \bullet H_2O$, the solubility increases significantly and reaches a maximum at 1.6×10^{-2} mol/dm^3 in an alkaline solution.[123] The solubility of tellurium has been considered low in containment sump conditions which originates from the samples collected after the TMI accident. However, the possibility of higher solubility as a result of chemical reactions has been identified especially as a result of oxidation by water radiolysis products[100]. This was investigated in Paper II.

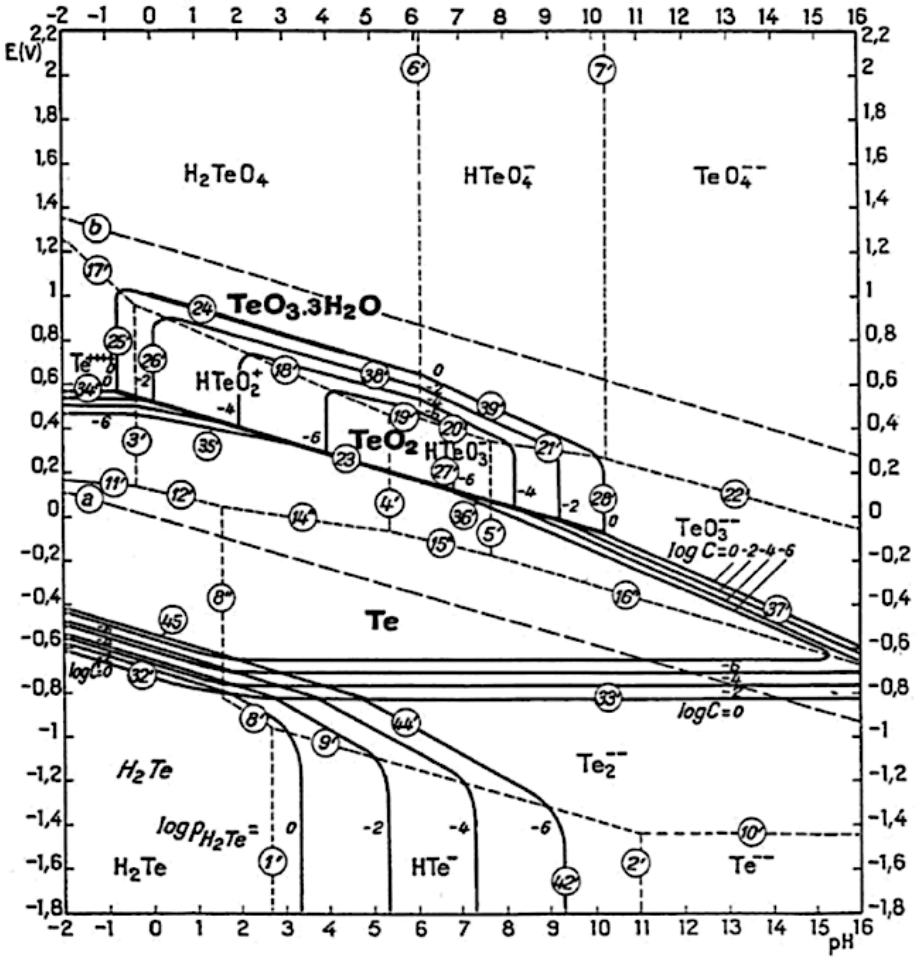

Figure 3.1. Pourbaix diagram of tellurium showing Eh-pH dependency and speciation[123]

3.3.1. Organotellurium chemistry

The presence of organic material in the containment in both aqueous[124,125] and gaseous phases[111] has been a source of concern due to the possible formation of volatile organic species. Organic species of iodine have especially been thoroughly investigated. However, organic tellurides have not been part of severe accident research. Organotellurium chemistry dates back to 1840 when the first organic telluride, diethyl telluride was successfully synthesized[126]. Since then, organic tellurides have been used in some applications, however, they are not as widely used as some of the other organic chalcogens. A feature, that is very characteristic of the organic chalcogens, including organic tellurides, is their odor. In the literature, the odor of dimethyl telluride is described as smelling like garlic and in fact if a person ingests tellurium, they will have a garlic breath due to the methylation of tellurium in the body forming dimethyl telluride (DMT)[127].

Organic tellurides can be synthesized in multiple ways. One of the methods is the production of dimethyl telluride form methyl lithium and methyl iodide[128]. This method was also used to produce DMT used in Papers III, IV and V. The reactions involved in the synthesis are presented below (Reactions 3.1-3.4).

$$CH_3Li + Te \rightarrow CH_3TeLi \quad (3.1)$$

$$CH_3TeLi + CH_3I \xrightarrow[-LiI]{} (CH_3)_2Te \quad (3.2)$$

$$(CH_3)Te + CH_3I \rightarrow [(CH_3)_3Te\,]I \quad (3.3)$$

$$[(CH_3)_3Te\,]I + P(C_6H_5)_3 \xrightarrow{\Delta} (CH_3)_2Te + [CH_3P(C_6H_5)_3]I \quad (3.4)$$

Apart from the synthetic use and formation of organic tellurides, there are other reactions which produce these species. Dimethyl telluride has been found to form from solid tellurium, either from tellurium powder or from so-called tellurium mirrors. Tellurium mirrors have been used to quantify the amount of methyl radicals in the past by depositing a thin layer of tellurium, a mirror, and flushing methyl radicals over the solid tellurium mirror[129]. The result is the formation of dimethyl telluride. This type of interaction is important for severe accident purposes, as in the case where tellurium is either present in the containment atmosphere or deposited on a surface. This interaction was the basis for Paper VI. The formation can be expected to form via Reaction 3.5.

$$Te(s) + 2R\cdot \rightarrow TeR_2 \quad (3.5)$$

$(R = C_xH_y)$

3.4. Radiolysis

One of the important phenomena in the containment and especially in the sump is ionizing radiation. The energy released by the radionuclides as they decay, has the potential to knock electrons out of atoms as the radiation penetrates through material. The missing electron forms a radical, which is a highly reactive species. Depending on the type of radiation, particulate or electromagnetic, and the energy, the damage to the material can vary significantly. The effect of ionizing radiation is often discussed in the terms of linear energy transfer (LET) values. The LET values describe the amount of energy transferred to the material as a function of distance and can be expressed as keV/μm. Alpha radiation has a high LET value. The alpha particles can travel only short distances in material and attenuate their energy quickly. This leads to a high degree of local ionization. Therefore, one of the applications of alpha radiation is radiotherapy where the short distance and high ionization are utilized to cause damage to cancer cells without destroying the surrounding healthy tissue. The electromagnetic gamma radiation has a low LET-value and does not cause as much ionization when passing through matter. However, the formation of radicals due to gamma irradiation has a significant effect on the chemistry of elements and has been shown to change the behavior of, e.g., iodine and ruthenium in severe accident conditions. Gamma irradiation was used in Papers II, III and IV to study its effect on tellurium and organic telluride chemistry.

3.4.1. Water radiolysis

The radiolysis of water produces a variety of oxidizing and reducing species. In neutral conditions, the amount of formation for both redox species is around the same, as presented in Reaction 3.6. The values in the brackets present the G-values of each species as μmol J^{-1} [130]. The LET value of radiation also highly affects the formation of the radiolysis species. High LET radiation has a short distance and deposits the energy very locally. This leads to more recombinations and consequently to the formation of molecular species like H_2O_2. With low LET radiation, the distribution of energy spreads wider, and the result is the formation of radicals such as $^{\bullet}OH$ or $H^{\bullet}$. All the radiolysis experiments were done by using Gammacell 220 ^{60}Co source which emits low LET gamma irradiation (PAPER II, III, IV).

$$H_2O \rightarrow [0.28] \cdot OH + [0.07]H_2O_2 + [0.05]H_2 + [0.27]H_3O^+ + [0.27]e^-_{aq} + [0.06]H^{\cdot} \quad (3.6)$$

By changing the pH or redox potential, the ratio of the different water radiolysis species also changes. In addition, adding components that act as radical scavengers affects the amount of oxidizing and reducing species. Some of the additives reacting with the water radiolysis products are presented in Table 3.2. The conditions used to control the amount of radiolysis species in this work were to change the amount of oxygen by aerating or deaerating the samples (PAPER IV) and using sodium thiosulfate as a radical scavenger (PAPER II, IV).

Table 3.2. Additives reacting with the water radiolysis species

Additive	Reaction	Dominating species
Acid	$e_{aq}^- + H^+ \rightarrow H^\cdot$	$H^\cdot, {}^\cdot OH$
Hydroxyl radical scavenger (thiosulfate, tert-butanol)	$RH + {}^\cdot OH \rightarrow R^\cdot + H_2O$	$e_{aq}^-, H^\cdot,$
Oxygen	$O_2 + e_{aq}^- \rightarrow O_2^{\cdot -}$ $O_2 + H^\cdot \rightarrow OH_2^\cdot$	${}^\cdot OH, OH_2^\cdot, O_2^{\cdot -}$
Nitrous oxide	$N_2O + e_{aq}^- + H_2O \rightarrow OH^\cdot + OH^- + N_2$	$H^\cdot, {}^\cdot OH$

3.4.2. Radiolysis of organic molecules

The water radiolysis products can readily react with any solvent in the aqueous phase. The hydroxyl radical, solvated electron and hydrogen can all change the molecular structure of the dissolved organic species. Moreover, the change in the structure can have a significant effect on the reactivity of the organic molecule. This phenomenon was the focus of PAPER III and IV.

The hydroxyl radical can lead to several different reactions with an organic molecule. The OH radical can attach to the molecule and create an organic radical as shown in Reaction 3.7. Another possibility is an abstraction of hydrogen from the organic molecule leading to the formation of a radical and a water molecule (Reaction 3.8.). The third possible outcome is an electron transfer from the OH radical directly to the organic molecule (Reaction 3.9.). Again, an organic radical is the remaining product. With the solvated electron, the main reaction is likely the addition of the electron leading to bond breakage, as shown in Reaction 3.10.

$$RH + {}^\cdot OH \rightarrow (HO)RH^\cdot \quad (3.7)$$

$$RH + {}^\cdot OH \rightarrow R^\cdot + H_2O \quad (3.8)$$

$$RH + {}^\cdot OH \rightarrow RH^{+\cdot} + OH^- \quad (3.9)$$

$$R_ACR_B + e_{aq}^- \rightarrow (R_ACR_B)^{\cdot -} \rightarrow R_AC^- + \cdot R_B \quad (3.10)$$

Radicals are in general very reactive and only observed in very short time scale. In longer experiments, the final species observed is usually a molecular one formed via reactions with the water radiolysis products. The reactions following the ones shown above include phenomena such as dimerization, degradation, and cleavage. The bond breakage and cleavage sites are important when considering the possible formation of organic tellurides since the radicals resulting from the decompositions of the organic molecules are available to react with the fission products including tellurium. The cleavage sites of texanol ester alcohol, one of the paint solvents used in PAPER III, are presented in Figure 3.2. The main species formed are methyl, •CH3, and isopropyl, •C3H7, radicals.

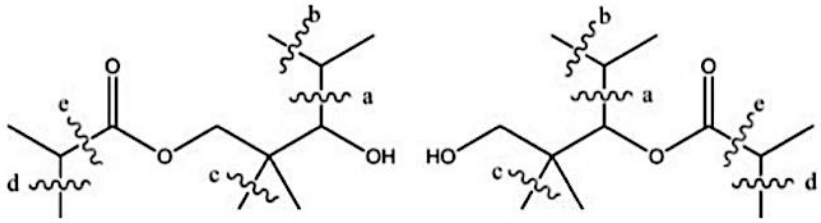

Figure 3.2. Possible cleavage sites of texanol ester alcohol[109]

The degradation of organic molecules occurs often via the oxidative path initiated by Reaction 3.7.-3.9. Methyl ethyl ketone (MEK), a paint solvent relevant in severe accident research has been shown to degrade via hydrogen abstraction leading to the formation of MEK radical. Following the initial step, the MEK radical reacts with dissolved oxygen, and through several steps, finally MEK is decomposed to various organic acids. The degradation and production of organic acids and CO_2 decrease the pH of the solution, which can have further effects. In addition, since MEK reacts with dissolved oxygen, the overall conditions in the aqueous solution become less oxidizing and possibly even reducing with higher MEK concentrations and longer irradiation times[131]. In deaerated aqueous solution, MEK has been found to dimerize to larger molecules before degrading. These reactions were considered when analyzing the results of PAPER IV.

4. Experimental

The experiments conducted in this work are presented in the following sections. The methods and results sections are both divided into two parts, mobilization and management, according to the phenomena studied. The methods give an overview of the procedures and facilities used in each experiment. Following the methods, the analytical techniques are presented.

4.1. Materials

The chemicals, their information and the use in each experiment are presented in Table 4.1. The use, concentration and form are further specified in each method section.

Table 4.1. The chemicals used in the experiments with the relevant information.

Name	**Chemical formula**	**Purity**	**Producer**	**Use**
Tellurium	Te	≥ 99.997%	Sigma Aldrich	Tellurium precursor
Tellurium dioxide	TeO_2	≥ 99%	Sigma Aldrich	Tellurium precursor
Telluric acid	H_6TeO_6	98%	Sigma Aldrich	Ion Chromatography
Sodium tellurite	Na_2TeO_3	99%	Sigma Aldrich	Ion Chromatography
Sodium hydroxide	NaOH	≥ 99%	EMPLURA®	Sump, Spray, traps
Boric acid	H_3BO_3	≥ 99.8%	Merck	Sump, Spray
Sodium thiosulfate	$Na_2S_2O_3$	≥ 99%	Sigma Aldrich	Sump, Spray
Cesium iodide	CsI	99.9%	Sigma Aldrich	Spray Experiments
Texanol Ester Alcohol	$C_{12}H_{24}O_3$	≥ 99%	Sigma Aldrich	Paint solution
Methyl Isobutyl Ketone	$(CH_3)_2CHCH_2C(O)CH_3$	≥ 99.5%	Janssen Chimica	Paint solution
Toluene	C_7H_8	≥ 99.7%	Fluka Analytical	Paint solution
Nitric acid	HNO_3	70%	Suprapur®, Supelco	ICP-MS
Tellurium Standard	Te 10mg/L		High Purity Standards	ICP-MS
Holmium Standard	Ho 10mg/L		High Purity Standards	ICP-MS
Methyl Lithium	CH_3Li	1.6 M in diethyl ether	Sigma Aldrich	Synthesis
Tetrahydrofuran	$(CH_2)_4O$	≥ 97%	Sigma Aldrich	Synthesis
Methyl iodide	CH3I	≥ 99%	Sigma Aldrich	Synthesis
Triphenyl phosphine	$P(C_6H_5)_3$		Sigma Aldrich	Synthesis
Hydrogen peroxide	H_2O_2	30%	Sigma Aldrich	Oxidation of organic tellurides, recovery of DMT from charcoal

4.2. Mobilization methods

4.2.1. Dissolution of tellurium under gamma irradiation

The behavior of tellurium dioxide under gamma irradiation in sump conditions was investigated. The samples were prepared by weighing 30 ± 0.5 mg of tellurium dioxide to glass vials before adding 5 ml of sump simulate. The sump solution was prepared with 0.15 M sodium hydroxide and 0.23 M boric acid. In some samples 0.064 M sodium thiosulfate was added as an additive since it is used in some nuclear power plants to facilitate organic iodide decomposition. The samples were irradiated in the Gammacell 220 ^{60}Co source for a time ranging from 1 to 10 days. The dose rate at the time of the experiments was around 5 kGy/h and the maximum dose delivered to the samples therefore around 1.2 MGy. The dose rate in the containment is expected to be in a range of 1 to 10 kGy/h[125] so the dose rate used in the irradiation experiments represents the accident conditions well. The temperature in the Gammacell was around 313 K, while the temperature of the sump depends on which stage of the accident is referred to; however, it can be over 100 °C[132]. Non-irradiated reference samples were also prepared and kept in the same conditions as the irradiated samples to eliminate the effect of the slightly elevated temperature and ageing. After the irradiation, small samples were taken and filtered with a 0.45μm syringe filter (VWR®) and prepared for ICP-MS analysis for total tellurium concentration. The remaining solid material was dried, ground and analyzed with XRD for tellurium speciation. The speciation of the dissolved tellurium species was analyzed with IC. Irradiated and reference samples were prepared in triplicates for statistical significance.

4.2.2. Organic telluride formation

To investigate organic telluride formation, tellurium dioxide was dissolved and mixed with different paint solvents and irradiated. The samples were prepared by mixing 5 ml of tellurium dioxide (3 mM) dissolved in an alkaline borate solution (ABS) and 5 ml saturated paint solvent solution in ABS in a 20 ml headspace vial in 1:1 ratio. The concentration of tellurium dioxide in the solution was around 1.5 mM in the start of the irradiation. The samples were irradiated in Gammacell 220 giving a dose rate of 4 kGy/h at the time of the experiments. The irradiation time ranged from 1 to 3 days where the maximum dose delivered to the samples was around 280 kGy. After the samples were taken out from the Gammacell, they were analyzed with GC-MS for the presence of organic tellurides after which the samples were centrifuged for 5 min at 3500 rpm and filtered with a syringe filter (polypropylene, VWR®). Solid material formed during the irradiation was analyzed with SEM-EDX and ICP-MS was used for total tellurium concentration analysis. Reference samples were also prepared in the same way but not irradiated. All samples, irradiated and reference, were prepared in triplicates to obtain statistical significance.

4.2.3. Degradation of dimethyl telluride

The radiolytic degradation of dimethyl telluride (DMT) was investigated under gamma irradiation. The stock solutions were prepared by adding approximately 400μL of liquid DMT to 400 ml of solution and mixed. To minimize the possible degradation, the mixing time was kept short before preparing the samples for irradiation. The samples were prepared by adding 10 ml of solution in a 20 ml headspace vial. The samples were then irradiated in the Gammacell 220 giving a dose rate of approximately 3.5 kGy/h at the time of the experiments. The temperature inside the Gammacell was slightly over room temperature at around 300 K. The samples were irradiated for a time ranging from 10 minutes to 6 hours except for the deaerated aqueous samples where the irradiation was continued for 8 hours. After irradiation, the samples were taken out and analyzed with GC-MS for volatile tellurium species and with ICP-MS for total tellurium concentration. ICP-MS samples were prepared by oxidizing the remaining DMT with hydrogen peroxide to avoid any loss during sample preparation. All samples were prepared in triplicates for statistical significance.

4.2.4. Gas Phase interactions

The gas phase interaction experiments were performed at VTT Research Center of Finland. The samples were analyzed partly at VTT and partly at Chalmers.

Possible interactions between tellurium and organic material in the gas phase were investigated. The aim was to study whether high volatility organic material effects the tellurium transport or forms organic tellurides when present in the gas phase under containment conditions.

The experiments were carried out using two tubular flow furnaces (Entech, ETF20/18-II-L and Entech/Vecstar, VCTF 3). An alumina tube made high purity alumina was placed inside the first furnace, and tellurium (1 g) was added to a ceramic crucible placed in the first furnace.

In the next step, heating was set to 540 °C as the volatilization of tellurium was consistent at that temperature (melting point 449 °C). A flow rate of 5 l/min (air or nitrogen or a mixture of argon with 5 % hydrogen – also called as carrier gases) through the system was initiated when the temperature set-point of the furnace had been achieved. The flow rate is a sum of the feed flow rates of the liquid organic precursor (acetone or propanol, fed as droplets by the atomizer using the carrier gas) or gaseous organic precursor methane (5 % CH_4 in argon) as well as the feed flow rate of additional carrier gas to achieve the total flow rate of 5 l/min. The gas flows were only mixed inside the gas phase of the tubular furnace, in which the reactions between the precursors (including the vaporized tellurium species) were expected to occur.

A stainless-steel tube was placed inside the second furnace which simulated the containment part. The temperature of the second furnace was set to 300°C which is close to the maximum estimated temperatures possible in the containment building[133]. The aerosol reaction products

originating from the interaction between tellurium, the atmosphere and organic precursors were filtered out at a location of 106 cm from the outlet of the furnace (at ca. 30°C). Beyond the filter, a trap with NaOH (0.1M) was positioned to capture gaseous species. The schematic presentation of the experimental facility is presented in Figure 4.1 and the experimental matrix in Table 4.2.

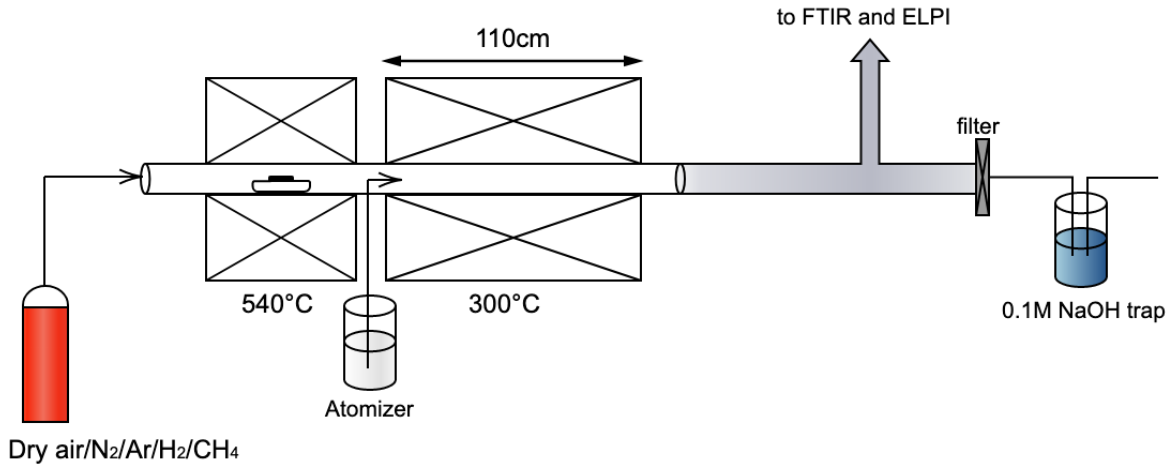

Figure 4.1. Schematics of the experimental facility at VTT used for tellurium studies with organic material

Table 4.2. The conditions used in each gas phase interaction experiment

Experiment #	**Precursor**	**Vaporization temperature, °C**	**Atmosphere**	**Organic precursor**
1	Te	540	Air	Acetone
	Te	540	Air	Propanol
2	Te	540	N_2	Acetone
	Te	540	N_2	Propanol
3	Te	540	H_2/Ar	Acetone
	Te	540	H_2/Ar	Propanol
4	Te	540	H_2/Ar	Methane
4.1.	Te	540	N_2	Methane

The liquid traps and precursors were collected for analysis. The trap samples were analyzed with ICP-MS for tellurium concentration and the precursors with XRD. In addition, the mass size distribution of the aerosols and the possible formation of gaseous species were monitored with an electrical low-pressure impactor (ELPI) and Fourier Transform Infrared Spectroscopy (FTIR), respectively. Lastly, the material on the filters was analyzed with SEM-EDX.

4.3. Management methods

4.3.1. Spray removal efficiency

The spray experiments were performed at VTT Research Center of Finland. The samples were analyzed partly at VTT, Chalmers and the Nuclear Research Insitute ÚJV Řež, in Czech Republic.

The schematics of the "VTT spray chamber" experimental setup is shown in Figure 4.2. The setup consisted of a cylindrical spray chamber made of stainless steel with a spray nozzle (model Lechler 136.330.xx.16) on top. The inner walls of the chamber were coated with Teflon tape to minimize the deposition of tellurium species on the surfaces. The spray droplets (ca. 10 µm in diameter) were generated by the solution in the spray supply bottle and the droplet feed rate was controlled with a pressurized air or nitrogen (approximately 3 bar absolute). Therefore, the spray nozzle output was a mixture of droplets (feed rate 9.0 ml/min) and gas (25.4 l/min). The width of the spray cone was 60 mm at a distance of 150 mm from the spray nozzle, and 120 mm at a distance of 300 mm (spray angle was 20 degrees). The temperature of the spray solution and spray chamber was approximately at room temperature. The generated spray droplets were accumulated at the bottom of the chamber, which simulated the sump. The experimental matrix with all the changing parameters is presented in Table 4.3.

Table 4.3. The experimental matrix of the spray experiments

Experiment [#]	Precursor	Temperature [K]	Atmosphere	Humidity[a]	CsI[b]
1	TeO_2	1150	Air	No	No
2	TeO_2	1150	Air	Yes	No
3	TeO_2	1150	Air	Yes	Yes
4	Te	810	Air	No	No
5	Te	810	Air	Yes	No
6	Te	810	Air	Yes	Yes
7	Te	810	Nitrogen	No	No
8	Te	810	Nitrogen	Yes	No
9	Te	810	Nitrogen	Yes	Yes

[a] Humidity content of the gas flow entering the spray chamber was 21000 ppmV
[b] CsI content of the atomizer supply bottle was 0.15 M

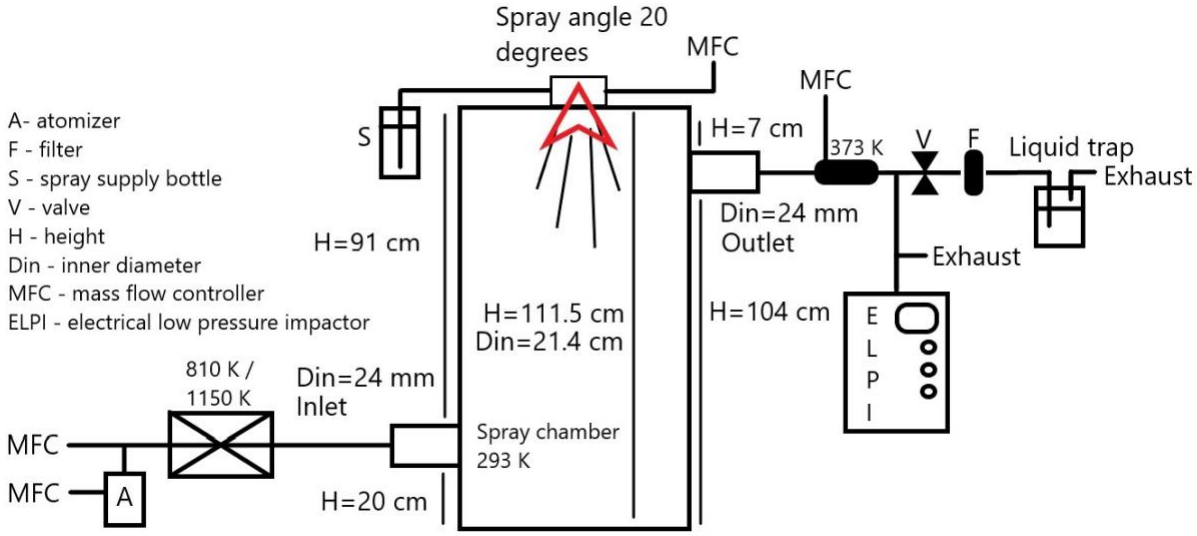

Figure 4.2. Schematic presentation of the experimental setup used for spray experiments

Two different tellurium precursors were used: elemental tellurium and tellurium dioxide, both in powder form. The experiments were conducted by weighing the respective tellurium precursor (1g of elemental tellurium or 1.26g of tellurium dioxide) in a crucible which was placed in the furnace. The furnace was heated to a chosen temperature which was chosen slightly above the boiling point of the respective tellurium precursors, 810 K for tellurium and to 1150 K for tellurium dioxide. A flow rate of 5 L/min (air or nitrogen) through the furnace was used to transport the vaporized tellurium compounds through a stainless-steel line (AISI 316L) to the entrance of the spray chamber. The flow of aerosols entered from the lower half of the chamber opposing the flow of the spray droplets.

The steam content of the flow was adjusted by directing half of the flow via an atomizer generating droplets of water. In the experiments where cesium iodide was used as an additive, cesium iodide was dissolved in the supply bottle (4 g of CsI in 100 g of water). When the generated droplets dried inside the furnace, solid cesium iodide particles were formed.

For the spray, three different solutions were used: **I.** 18 MΩ deionized MilliQ water **II.** an alkaline borate solution (0.23M H_3BO_3, 0.15 M NaOH), and **III.** an alkaline borate solution with sodium thiosulphate (0.23M H_3BO_3, 0.15 M NaOH and 0.064 M $Na_2S_2O_3$). The chemicals were chosen to represent the general composition of the spray solutions used in severe accident scenarios[134,135].

The aerosols not removed by the spray droplets exited the containment from the top of the chamber. The flow of aerosols was captured by a filter and directed to a sodium hydroxide trap place beyond the filter to capture any species possibly passing through the filter.

4.3.2. Adsorption on charcoals

Activated charcoal experiments were conducted to assess the removal efficiency of different charcoal materials for organic tellurides. The experiments can be divided into two parts: the recovery of dimethyl telluride from the charcoal and flow through experiments for the trapping efficiency.

Of the charcoal materials chosen for this study, three were taken from respirator cartridges and one from a filter module used in a Swedish nuclear power plant. The ACs are referred to as Charcoal A received from disassembling a 3 M 60928 respirator cartridge, Charcoal B from Dräger (X-plore 6000) and "Charcoal C" was from a Scott Pro 2000 (CF32 ABEK2) cartridge. Charcoal D was the one used in the filter module.

The recovery of DMT from the charcoals was determined by weighing 50 mg of each charcoal into a glass vial and adding 10 μL of liquid DMT in each vial. The samples were equilibrated for approximately 1 hour after which the charcoal was moved to another glass vial. This was done to determine how much DMT had adsorbed onto the surfaces of the first vial. To recover tellurium from the charcoals and vials, 2 ml of 0.1M sodium hydroxide with 0.6 % hydrogen peroxide was added. The samples were mixed and allowed to stand for around 1 hour before small samples were prepared for ICP-MS measurement for total tellurium concentration.

The schematic presentation of the experimental setup used for the flow-through experiments is presented in Figure 4.3. The setup consisted of nitrogen gas source connected to a flowmeter (AALBORG®). The flow was directed to the borosilicate glass setup with a connector that had a side arm for a hose. The glass column (length 50 cm, inner diameter 1 cm) containing the charcoal pads was partly placed inside the glass connector. The liquid DMT was injected to the entrance of the charcoal column with a syringe needle through a septum. The nitrogen flow had been adjusted and kept on during the injection. Another glass connector was placed at the end of the column which had a hose attached. The flow through the columns was directed to a liquid trap.

The flow rate of 1 L/min and time of 30 minutes was used in the experiments comparing the different ACs. "Charcoal A" was chosen for further investigations in experiments changing the flow duration from 5 to 330 minutes. In addition, the effect of the flow rate was investigated by using 0.5, 1 and 1.7 L/minute.

The column with charcoal was prepared by weighing 250 mg ± 1 mg of charcoal material and packing it into the column by pressing slightly with a glass rod. The pads were separated with a small layer of glass fiber. A total of eight pads were used in each experiment.

After the experiment, the charcoal pads were separated into 20 ml glass vials and 10 ml of 0.1M sodium hydroxide with 0.6% hydrogen peroxide was added. The solid to liquid ratio was the same as in the recovery experiments and the recovery times and sample preparation methods were the same. The recovered tellurium was analyzed with ICP-MS.

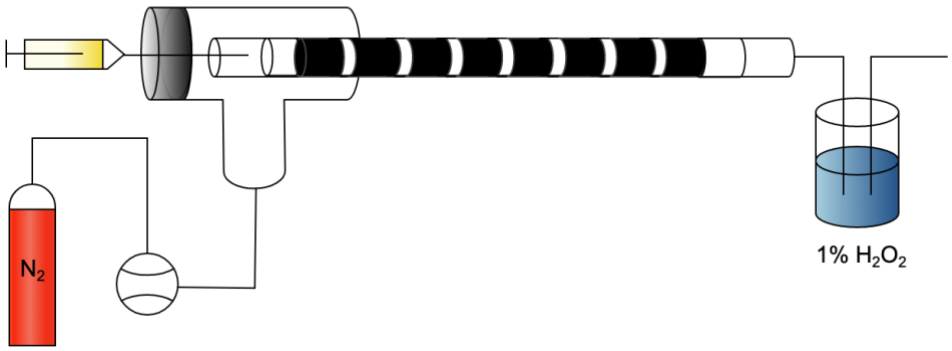

Figure 4.3. Schematic presentation of the setup used for charcoal experiments. The black sections represent the charcoal pads separated by the layers of glass fiber (white sections). The proportions do not correlate with the real experimental setup

4.4. Analytical methods

4.4.1. Inductively Coupled Plasma Mass Spectrometry, ICP-MS

Tellurium concentration in all the liquid samples was measured with Inductively Coupled Plasma Mass Spectrometry (Thermo Scientific iCAP Q). The samples were diluted with 0.5 M nitric acid containing holmium (1 ppb) as an internal standard. Holmium was chosen as an internal standard because of its chemical stability and rareness. Tellurium standards were prepared from a tellurium standard solution. The standards were generally prepared with concentration ranging from 0 ppb to 200 ppb.

4.4.2. Gas Chromatography Mass Spectrometry, GC-MS

Volatile organic tellurides were analyzed with Headspace Gas Chromatography Mass Spectrometry (HS-GC-MS, Thermo Scientific) (5%-Phenyl)-methylpolysiloxane column). The temperature was programmed between 40 and 250°C with a ramp of 10°C/min. The inlet temperature was set to 250°C. The mass spectra were generally analyzed between a mass-to-charge range (m/z) of 50 and 400.

4.4.3. Ion Chromatography

Tellurium speciation in the sump experiments (PAPER II) was investigated using ion chromatography (IC; Dionex DX-100, IonPac AS4A-SC 4 × 250 mm). The eluant used was a carbonate buffer (1.7 mM $NaHCO_3$, 1.8 mM Na_2CO_3). Standard solutions were prepared from Na_2TeO_3 for Te(IV) and from H_6TeO_6 for Te(VI). The samples were compared to the known standards to determine the oxidation state in each sample.

4.4.4. X-Ray Diffraction, XRD

The solid speciation of tellurium precursors from spray experiments as well as the solid material from the sump experiments were investigated with powder X-ray Diffraction (XRD; Siemens D5000 diffractometer with Cu Kα- radiation in the case of the sump experiment and Bruker D8 Advance with samples obtained from the spray experiments). Interpretation of the diffractograms was done with DIFFRAC.EVA 4.1.1. (sump) or 5.2. (spray) software using the International Center for Diffraction Data® database.

4.4.5. Scanning and Transmission Electron Microscopy, SEM/TEM

The size, morphology, and elemental composition of the tellurium samples collected in PAPER III and the charcoal materials in PAPER V were analyzed using scanning electron microscopy (SEM, Phenom ProX, Thermo Scientific). The elemental analyses in SEM were performed through Energy Dispersive X-ray analysis (EDX).

4.4.6. Specific Surface Area analysis

The specific surface areas of the charcoal materials were analyzed with the Brunauer, Emmett and Teller (BET) method using an ASAP 2020 by Micromeritics and nitrogen gas at 77 K (−196 °C) as an absorbate. The samples were pretreated by drying for 25 hours at 100°C.

5. Results and Discussion

5.1. Mobilization

The following sections present the results of the experiments leading to the formation of higher mobility species of tellurium. These experiments include the solubility of tellurium under gamma irradiation, the formation of volatile organic tellurides, the radiolytic degradation of dimethyl telluride and the gas phase interactions between tellurium aerosols and organic material in containment conditions.

5.1.1. Solubility of tellurium

Results presented here are based on those published in PAPER II.

The behavior of tellurium was investigated in a simulated sump solution and under gamma irradiation. The sump consisted of an alkaline borate solution (ABS) with or without sodium thiosulfate. The results for the solubility as a function of time are presented in Figure 5.1. As shown, in the absence of thiosulfate the solubility of tellurium increases with an increasing radiation dose. Compared to the reference samples which reached the maximum solubility at around 15 mM, the concentration of tellurium increased linearly up to 25 mM. Equilibrium was not achieved in the irradiated samples likely due to the excess of tellurium dioxide in the solution. With longer experiments, the solubility would have likely reached equilibrium when either all the tellurium dioxide had dissolved, or the solubility limit had been reached.

In the presence of sodium thiosulfate, the concentration of tellurium decreased linearly with the increased radiation dose. The concentration after about a 1.2 MGy dose was around 6 mM compared to the 15 mM in the respective reference samples. In addition to the decrease in the tellurium concentration, the initially white tellurium dioxide precursor had turned black (see Figure 5.2.). An XRD analysis of the dried precursors showed that the black precipitate was elemental tellurium. This highly suggests that tellurium dioxide had been reduced to elemental tellurium which also explains the decrease in the dissolved concentration. Elemental tellurium is very insoluble in any aqueous solution and therefore as the more soluble tellurium dioxide reduces and precipitates into elemental tellurium, the concentration decreases in the solution.

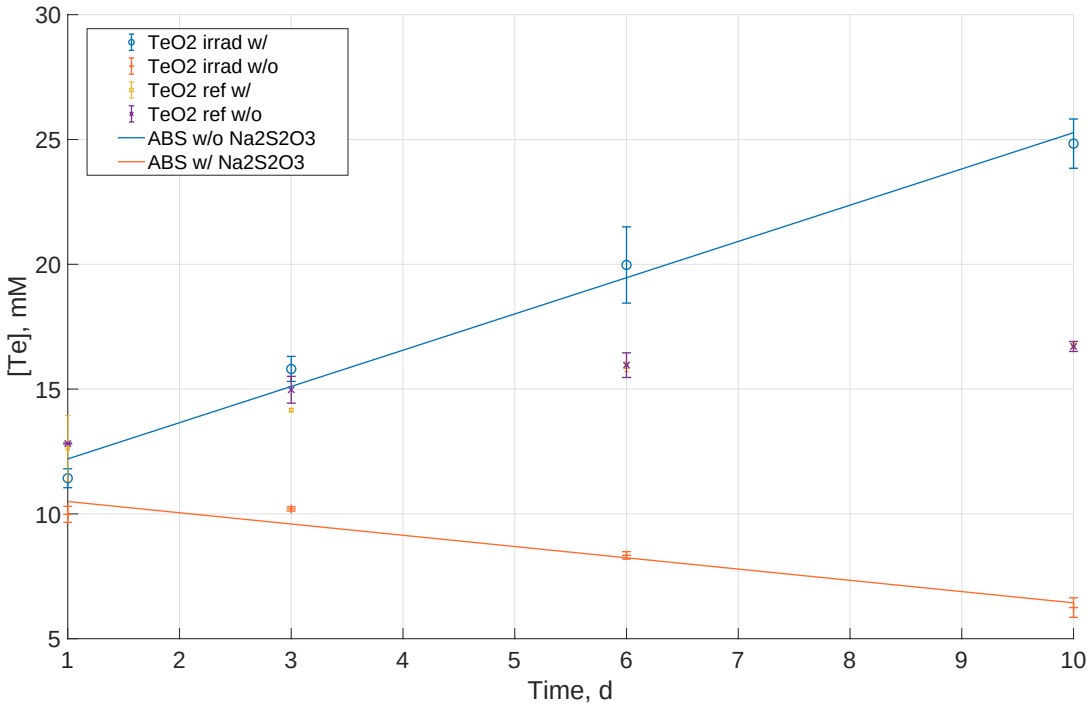

Figure 5.1. The concentration of tellurium as a function of time in the irradiated and non-irradiated reference samples in ABS with (blue) and without (orange) sodium thiosulfate

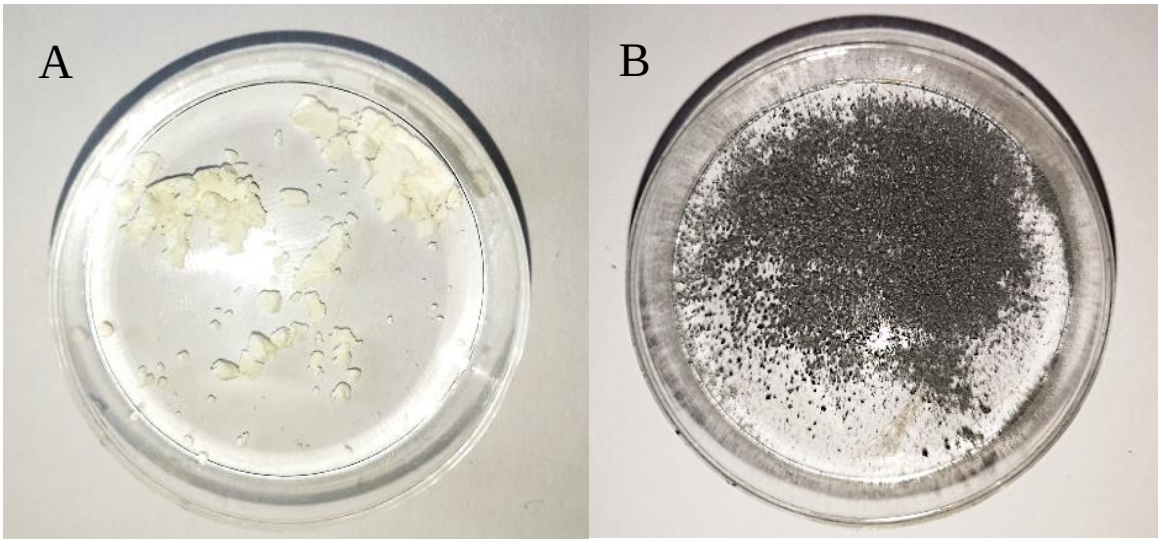

Figure 5.2. Dried tellurium precursor after the irradiation in A. ABS without thiosulfate and B. ABS with thiosulfate

The cause for the increase in the solubility was analyzed using ion chromatography. The aim of the ion chromatography analysis was to determine the oxidation state of tellurium by comparing the samples with known standards and using the literature to estimate the prevailing speciation. The IC results are presented in Figure 5.3. and 5.4. The samples were prepared by filtering the liquid after the experiment. Due to the relatively low concentration of tellurium in all samples, there was no need for dilution. However, this created strong signals for other anionic species present in the solution in higher concentrations (e.g., borate, OH^-, $S_2O_3^{2-}$, SO_4^{2-}).

Tellurium was found to be present in two oxidation states, +IV and +VI, depending on the solution and conditions. In the irradiated samples with ABS without thiosulfate (Figure 5.3.), tellurium was present as Te(VI) which forms an anionic complex tellurate, $HTeO_4^-$ in the alkaline conditions used in these experiments. The retention time for tellurate was around 6 minutes. The oxidation from the initial Te(IV) to Te(VI) explains the increase in solubility observed in ICP-MS measurements, since the Te(VI) species has significantly higher solubility than $Te(IV)O_2$. The oxidation is most likely due to reactions with the strong oxidizing water radiolysis products (e.g., H_2O_2, •OH) formed by the gamma radiation.

In the respective unirradiated reference samples, tellurium was found to exist as $Te(IV)O_3^{2-}$, which is an expected dissolved species for tellurium dioxide in alkaline solution (Figure 5.4.). The retention time for Te(IV) complex was also around 6 minutes. However, the oxidation states could be identified by the shape of the detected peak. For Te(IV), the signal was detected as a negative peak which was used to identify the oxidation state. The negative peak was possibly a result of a high positive hydration tendency of the TeO_3^{2-} species resulting in lower conductivity [136]. On the contrary, the Te(VI) species had a positive peak with relatively good resolution. Although, the retention times were the same, the determination of the exact oxidation state was possible due to the fact that only one species was expected to be present in each sample, and no separation was needed. The standards were prepared in a manner similar to that of the samples, which validated the identification.

In the samples containing sodium thiosulfate, tellurium was found to be present as $Te(IV)O_3^{2-}$ in both irradiated and reference samples. Moreover, this indicated no change in the dissolved species under irradiation, and the decrease in the tellurium concentration can be attributed to the reduction and following precipitation of tellurium dioxide to elemental tellurium.

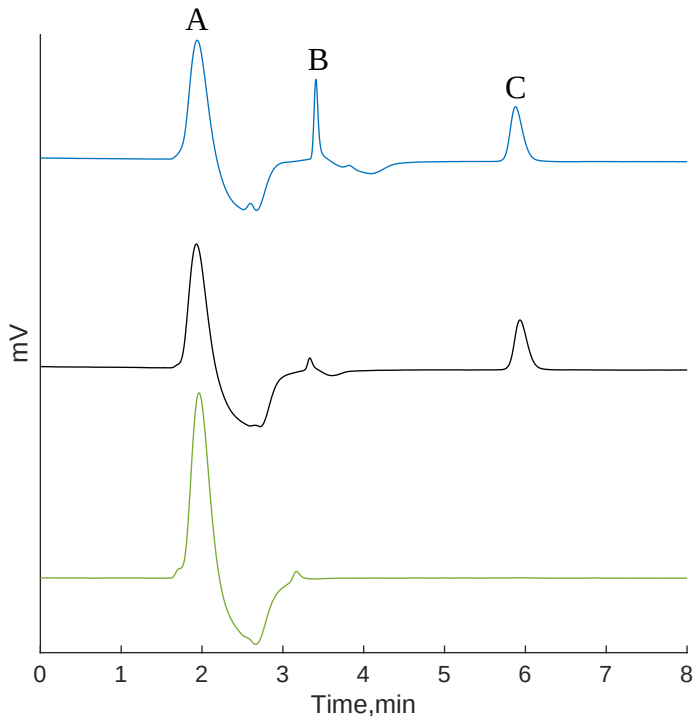

Figure 5.3. The chromatograms for ABS standard with no tellurium (bottom), Te(VI) standard (middle) and TeO_2 in the irradiated ABS (top). The letters correspond to the species A: OH^- B: Borate C: Te(VI)

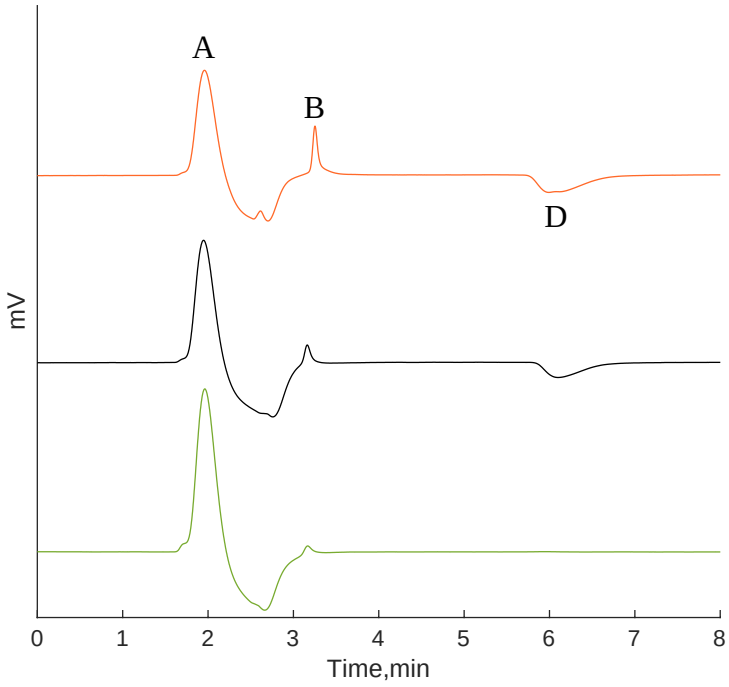

Figure 5.4. The chromatograms for ABS standard with no tellurium (bottom), Te(IV) standard (middle) and TeO_2 in the irradiated ABS with thiosulfate (top). The letters correspond to the species A: OH^- B: Borate C: Te(IV)

By combining the solubility and the solid and liquid speciation results, it seems like tellurium dioxide can react with either the oxidizing or reducing water radiolysis species. In the absence of sodium thiosulfate, a radical scavenger, both oxidizing and reducing species are present in the solution. In addition, since all experiments were performed in the presence of air, the formation of •OH is facilitated, as the oxygen reacts with the reducing species (see Table 3.2.). This leads to Reaction 5.1., which shows the oxidation of Te(IV) to Te(VI) via reaction with e.g. H_2O_2. However, it should be noted that it is not possible to differentiate whether tellurium dioxide reacts with hydrogen peroxide or hydroxyl radicals. It is most likely a combination of several different reactions.

$$TeO_3^{2-}(aq) + H_2O_2 \rightarrow \ HTeO_4^-(aq) + OH^- \quad (5.1)$$

As for the samples with sodium thiosulfate, the reduction of tellurium likely occurs via reactions with reducing water radiolysis products. The reaction between dissolved tellurite and solvated electrons is presented in Reaction 5.2. Again, the system is likely more complex, and it is unlikely that the reduction is just a one step process. The reason for the difference compared to the samples without thiosulfate comes from the strong scavenging tendency of the thiosulfate ions. As shown in Reaction 5.3., thiosulfate reacts rapidly with oxidizing products and forms sulfate ions. Due to this rapid disappearance of the oxidizing species, tellurium only has the reducing species to react with.

$$TeO_3^{2-}(aq) + 4e_{aq}^- + 6H^+{}_{aq} \rightarrow Te(s) + 3\ H_2O \quad (5.2)$$

$$S_2O_3^{2-}(aq) + 5\ H_2O \rightarrow 2SO_4^{2-}(aq) + 8e^- + 10\ H^+ \quad (5.3)$$

5.1.2. Organic telluride formation

Results presented here are based on those published in PAPER III.

The formation of organic tellurides from paint solvents under gamma irradiation was investigated in sump conditions. The simulated sump solution consisted of ABS without sodium thiosulfate where tellurium dioxide was dissolved. Three paint solvents possibly present in the sump were selected: texanol ester alcohol, methyl isobutyl ketone (MIBK) and toluene. The samples were irradiated up to a dose of around 280 kGy and analyzed for total tellurium concentration, solid speciation, and the presence of volatile species.

The results for the tellurium concentration are presented in Figure 5.5. It was observed that the concentration of tellurium decreased with the increasing radiation dose. The most significant effect was observed with texanol where the initial concentration of around 1.5 mM decreased to around 0.4 mM during the irradiations. A similar effect was observed with MIBK where the end concentration was also around 0.4 mM. Toluene seemed to have the least effect and the concentration of tellurium decreased only from 1.5 to around 1.2 mM. The decrease is likely due to a reduction of tellurite leading to precipitation. The reduction is possibly a result of the fast reactions of oxidizing radicals with the organic molecules and the consequent reduction of tellurium dioxide by reducing water radiolysis products.

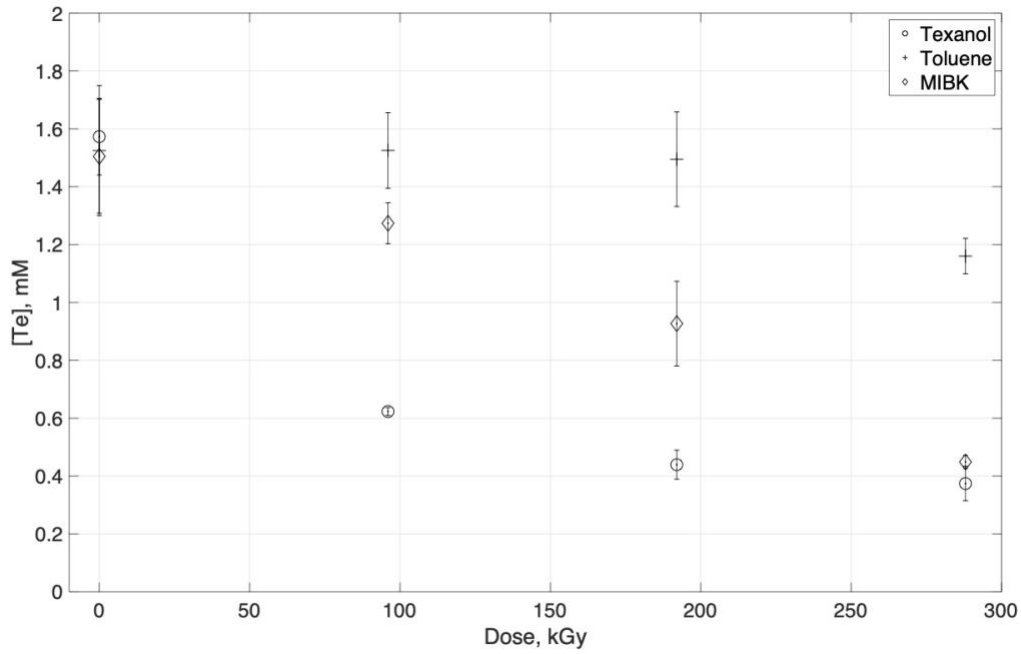

Figure 5.5. The concentration of tellurium as a function of radiation dose with the presence of texanol, toluene and MIBK

In addition to the decrease in concentration, precipitate was also formed in all of the irradiated samples. The SEM-EDX analysis showed that all the precipitates were various forms of tellurium. The results are presented in Figures 5.6, 5.7 and 5.8 for irradiated tellurium samples with texanol, toluene and MIBK, respectively. With texanol and MIBK, the solid material was identified as elemental tellurium whereas the precipitate formed in the toluene samples was more consistent with tellurium dioxide. This coincides with the concentration results determined with ICP-MS where the concentration of tellurium decreased the most in the samples with texanol and MIBK. The differences likely originate from the molecular structures of the chosen paint solvents. Toluene is more persistent towards radiation due to the aromatic structure. The ring structure enables toluene to efficiently delocalize the energy within its structure unlike the aliphatic texanol and MIBK[137]. Therefore, the effects on tellurium behavior are more significant with the aliphatic paint solvents used in this study than with toluene.

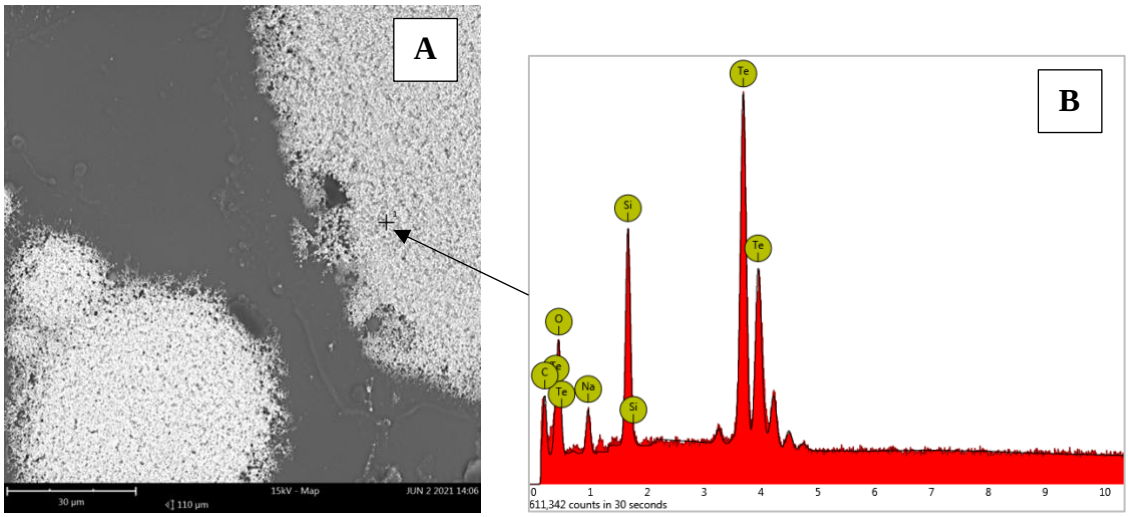

Figure 5.6. SEM (A) and EXD (B) analyses from the irradiated sample with tellurium dioxide and texanol ester showing the presence of elemental tellurium

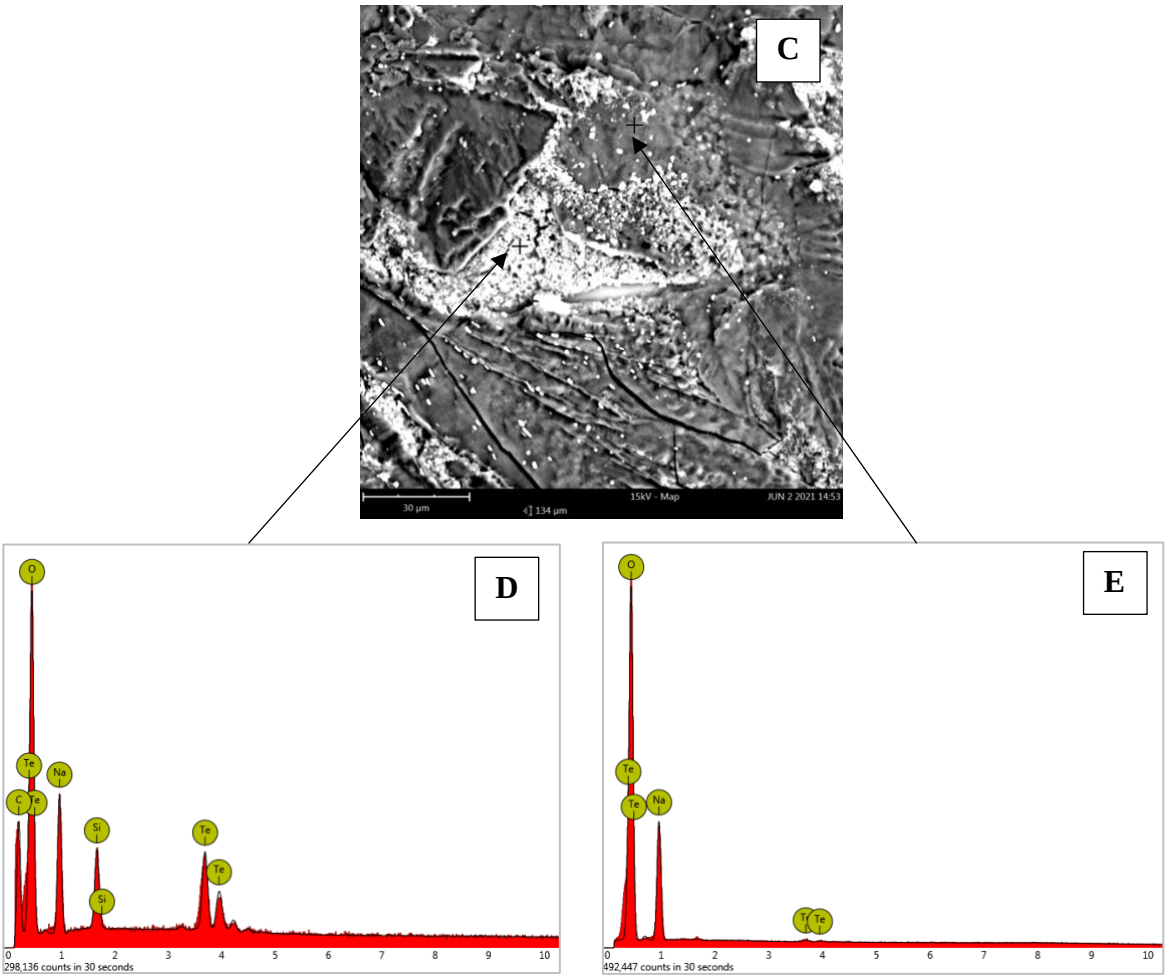

Figure 5.7. SEM (C) and EXD (D, E) analyses from irradiated sample with tellurium dioxide and toluene showing the presence of tellurium dioxide

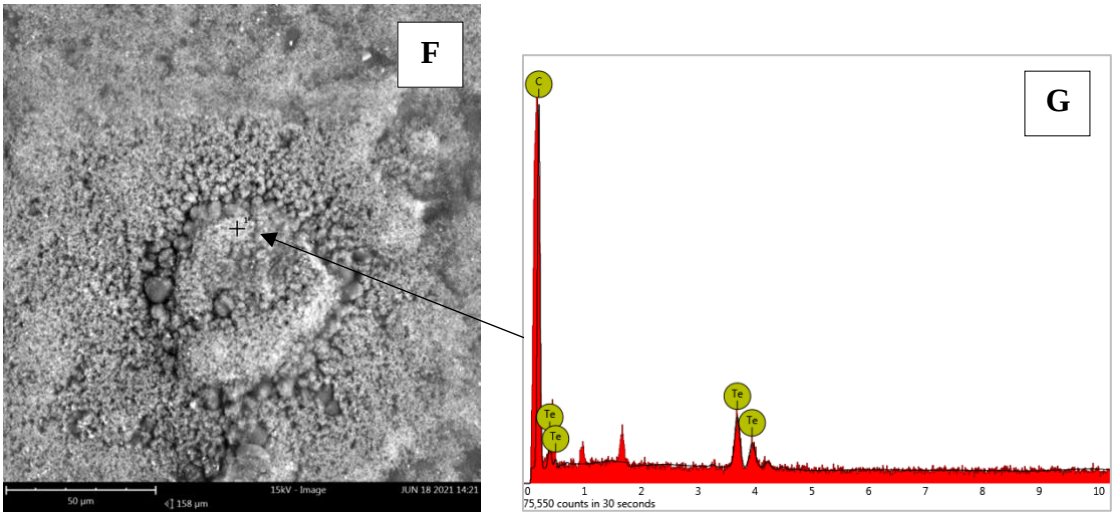

Figure 5.8. SEM(F) and EDX(G) analyses from irradiated sample with tellurium dioxide with MIBK showing the presence of elemental tellurium

The volatile species were analyzed with GC-MS and the results are shown in Figures 5.9, 5.10, and 5.11 for texanol samples and in Figure 5.12. for the sample with MIBK. All of the volatile species containing tellurium had characteristic mass patterns with the lowest mass group at around 128 mass-to-charge (m/z). This group of masses corresponds to the most abundant isotopes of tellurium, 126, 128 and 130 m/z. The other signals were then compared to these masses to find the correct fractions and identify the organic groups.

Three different tellurium bearing volatile species were identified in the samples containing texanol. The most abundant organic tellurium species was detected with a retention time of 4.26 minutes (Figure 5.9). This species was identified as diisopropyl telluride, $((CH_3)_2CH)_2$-Te^+ with a mass ion at 216 m/z. Another group of signals was observed around 172 m/z, which were attributed to isopropyl telluride $C_3H_8Te^+$ fractions. All of the groups had the highest signals with 2 m/z apart, which is due to the most abundant tellurium isotopes being 2 m/z apart from each other. To compare the results to those obtained for iodine, the most abundant organic iodide formed from texanol under gamma irradiation is isopropyl iodide[109]. This supports the fact that isopropyl radicals are a major radiolysis product of texanol and is able to react with the available element.

Another tellurium species was detected at 5.18 minutes (Figure 5.10). This had a mass ion at 214 m/z. The characteristic isotopic pattern for Te^+ fractions was again found at around m/z 130. The strongest signal for the 5.18 min peak is at m/z 170 which likely corresponds to a species with a formula of C_3H_6Te. Although the mass is close to the M^+ of the first peak at 4.26 min, it does not correspond to isopropyl telluride. Instead, this fraction could be an allyl telluride with a C=C double bond. This assumption would also explain the signals at m/z 210, 212 and 214 which would correspond to diallyl telluride.

The third organic telluride species was detected at 7.72 minutes (Figure 5.11). The structure resembles that of diisopropyl telluride with masses at around 172 m/z. However, strong signals were observed at around 256 m/z which indicated ditelluride, Te-Te, species.

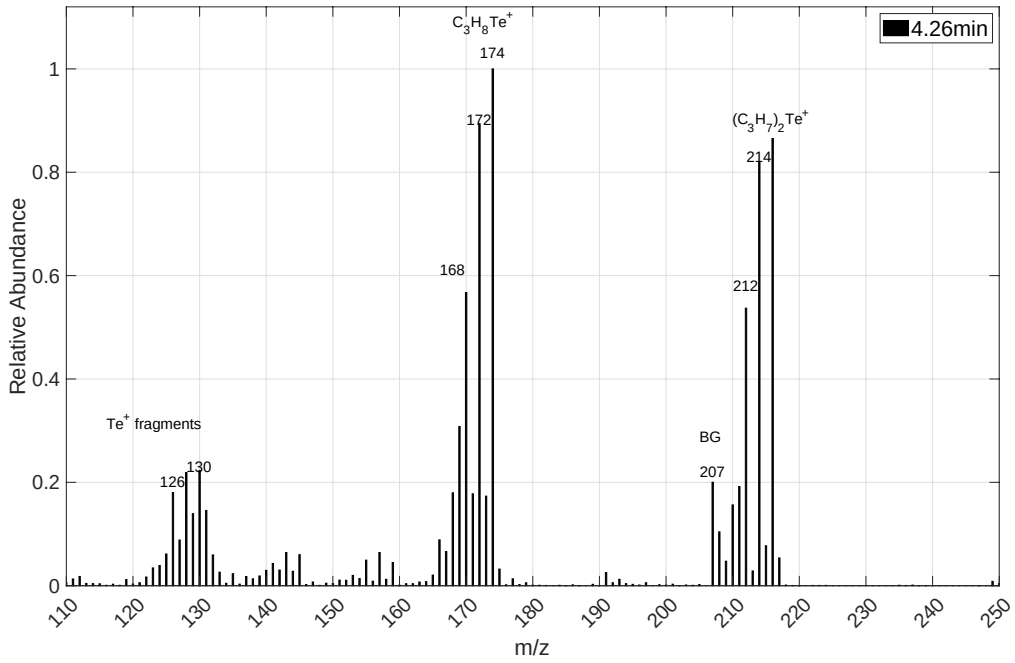

Figure 5.9. Mass spectrum for the irradiated sample containing texanol and TeO_2 for a peak with retention time 4.26 minutes. Mass at 207 m/z, denoted with BG, is a background signal

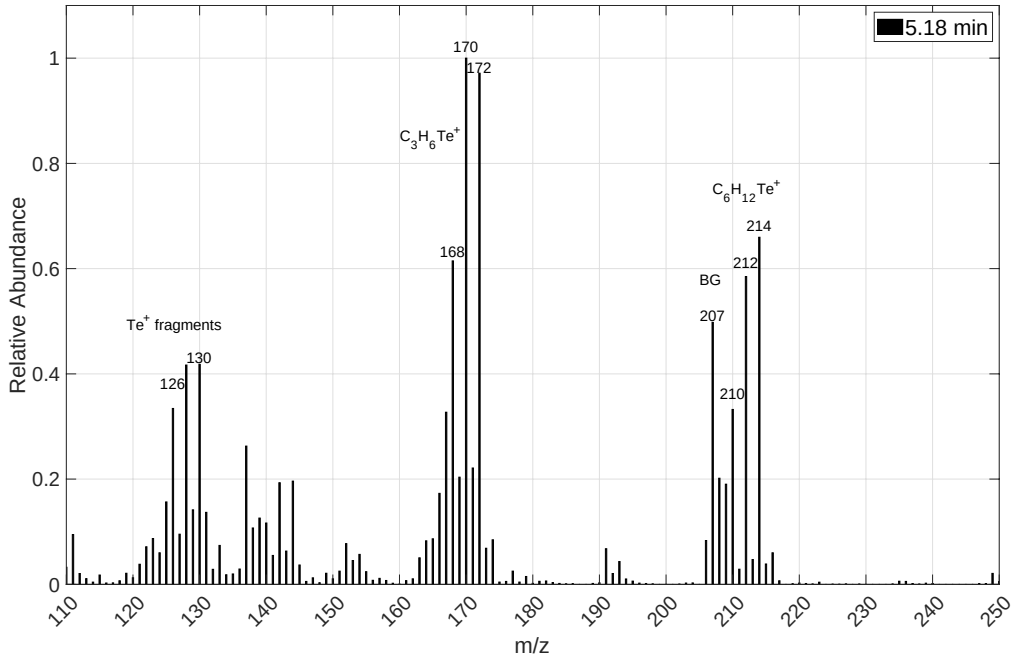

Figure 5.10. Mass spectrum for the irradiated sample containing texanol and TeO_2 for a peak with retention time 5.18 minutes

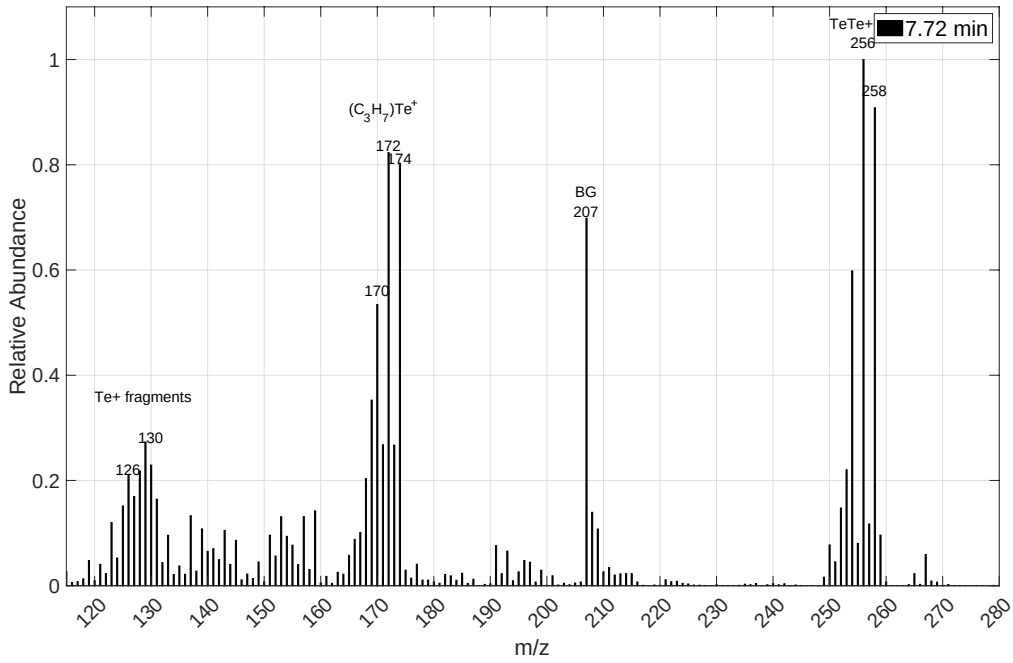

Figure 5.11. Mass spectrum for the irradiated sample containing texanol and TeO_2 for a peak with retention time 7.72 minutes

One organic telluride species was detected in samples with MIBK. The retention time was 3.96 minutes. As in the samples containing texanol, the irradiated MIBK sample had signals for tellurium fragments at m/z 126, 128 and 130 (Figure 5.12.). In addition, there were signals for at around m/z 144 which likely correspond to methyl telluride, CH_3Te fraction. The highest mass was detected at m/z 202 with weaker signals 2 m/z apart at 198 and 200. Compared to the methyl telluride signals, the mass difference between the signals is 57 m/z, a fragment which could correspond to C_4H_9. Therefore, the organic telluride species in question could be methyl-isobutyl-telluride, $C_4H_9TeCH_3$. Considering the possible cleavage sites and leaving groups of MIBK, both methyl and isobutyl groups are plausible which strengthens the analysis of the telluride species.

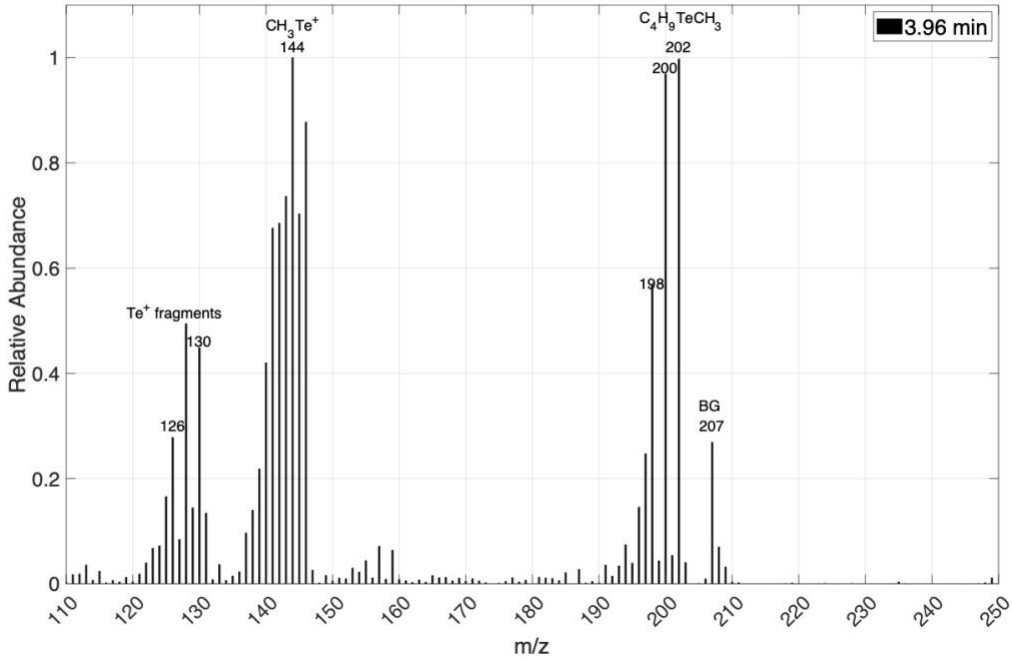

Figure 5.12. The mass spectrum of the tellurium species detected in a sample with TeO_2 and MIBK

5.1.3. Degradation of dimethyl telluride

Results presented here are based on those presented in PAPER IV.

The radiolytic degradation experiments were conducted to gain information on the stability of organic tellurides. In cases where organic tellurides decompose fast under irradiation, the probability for re-volatilization is low. However, if found relatively stable, re-volatilization could occur leading to additional releases. The results presented here are for the radiolytic degradation of dimethyl telluride.

The total concentration of tellurium was analyzed using ICP-MS. This was done to determine whether the loss of volatile tellurium was only due to degradation and not a result of volatilization or any other processes. The results for the concentration of tellurium normalized to the highest value as a result of an irradiation dose in the four aqueous solutions are presented in Figure 5.13. Overall, the concentration stayed constant throughout the experiments regardless of the solution. Some variation was observed in the first samples, which is likely due to the inhomogeneity of the stock solution. As the dimethyl telluride, when added to the aqueous solution, sank to the bottom of the flask, the concentration was likely slightly higher at the bottom, which resulted in slight differences during sample preparation. However, it can be concluded that there was no loss of tellurium during the experiments.

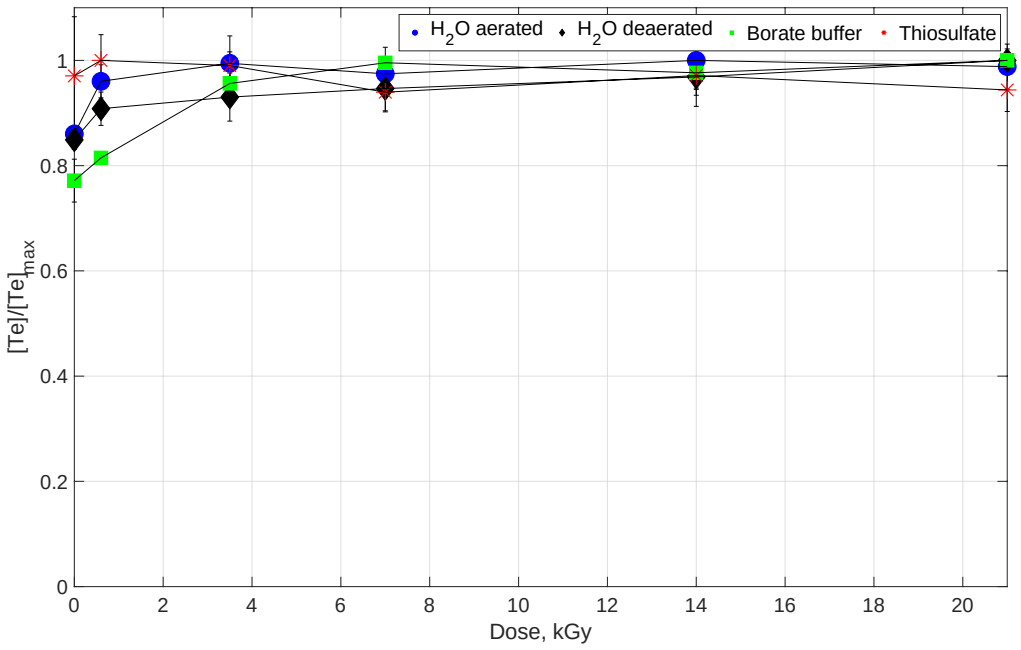

Figure 5.13. The normalized total tellurium concentration as a function of radiation dose

The degradation of dimethyl telluride was analyzed using GC-MS. The chromatograms showing the peaks for DMT are presented in Figure 5.14. The graphs A and B show the results for aerated and deaerated water, respectively. In the aerated solution, the peak intensity decreased with increasing radiation dose whereas in the nitrogen saturated solution,

the peak intensity stayed consistent up to 7 kGy after which the intensity decreased. The graph C shows the results for DMT in ABS. The intensity decreased rapidly from 0 to 0.6 kGy after which the degradation is more consistent and after 21 kGy dose, the intensity is at the background level. Lastly, the results for DMT in the sodium thiosulfate solution are shown in graph C. There, the intensity decreases fast in the first sample but then stays relatively consistent throughout the rest of the experiment.

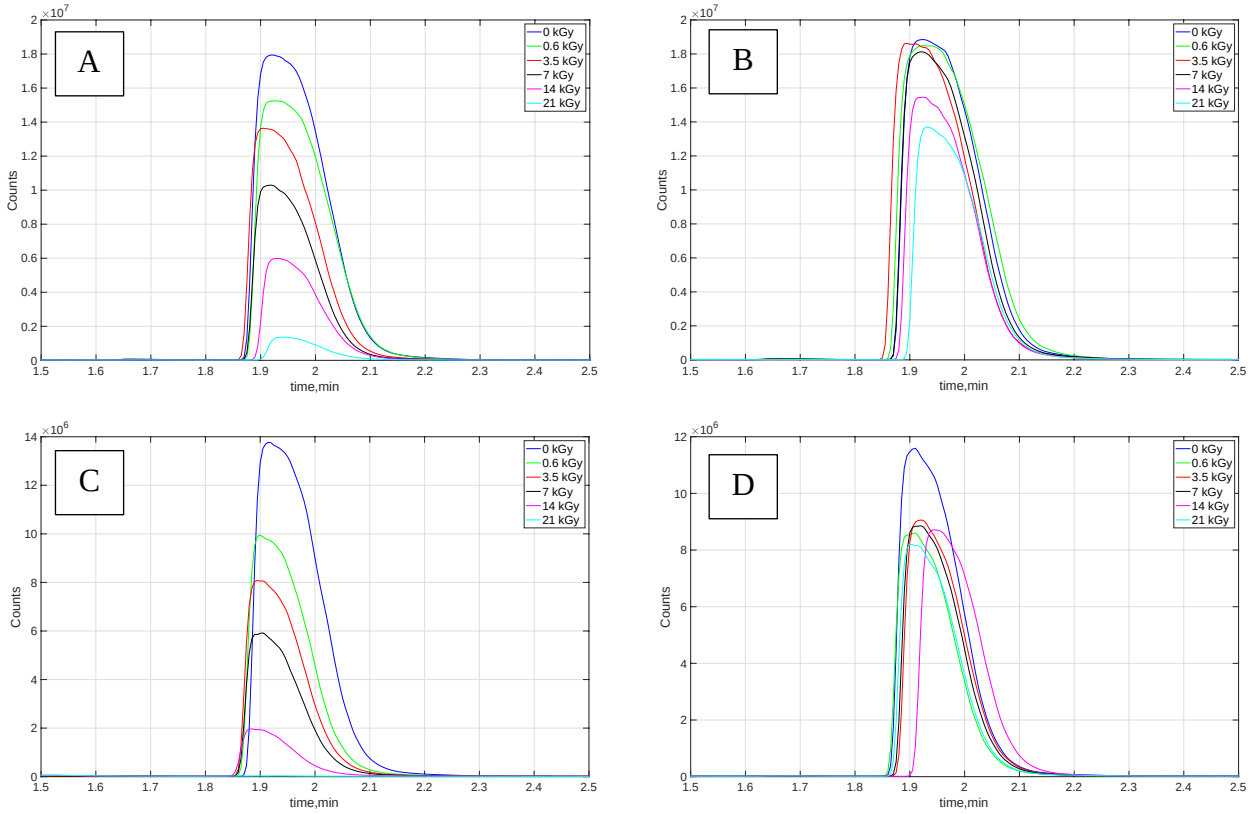

Figure 5.14. Chromatograms for dimethyl telluride degradation in A. aerated water, B. deaerated water, C. ABS and D. sodium thiosulfate solutions

The results obtained from the GC-MS measurements were normalized to the highest value and are presented as the normalized intensity as a function of irradiation dose. Figure 5.15 presents the results for aerated and deaerated water as well as for ABS. The results for sodium thiosulfate are presented separately in Figure 5.16. The intensity of DMT in aerated water decreased down to 6 % of the initial value after 21 kGy. The degradation is relatively linear and follows zero-order kinetics with a more rapid rate in the first 0.6 kGy after which the rate is relatively linear. A similar behavior was observed when using ABS. There, a rapid degradation was observed in the beginning after which the trend followed that of pure aerated water. In the absence of oxygen, DMT only degraded down to 60 % of the initial value. The degradation in the deaerated solution also follows zero-order kinetics but with a slower rate compared to the two aerated solutions. The differences likely originate from the amount of oxygen present in the solutions. Oxygen in the aqueous solutions leads to scavenging of reducing radicals which facilitates the oxidation in the solution but also consumes the oxygen

with long irradiation times (see Table 3.2.). The oxygen is also consumed via reactions with organic material, which further decreases the dissolved oxygen concentration (see Section 3.4.2.). As the decomposition of DMT is assumed to be an oxidative process, the faster rate of degradation at the beginning of the experiment could be explained by the presence of oxygen and its scavenging effect. As the oxygen is consumed, the rate of degradation decreases.

$$CH_3TeCH_3 + \cdot OH \rightarrow (CH_3Te(OH)CH_3)^{\cdot} \quad (5.4)$$

$$CH_3TeCH_3 + \cdot OH \rightarrow (CH_3TeCH_2)^{\cdot} + H_2O \quad (5.5)$$

$$CH_3TeCH_3 + \cdot OH \rightarrow CH_3Te(OH) + CH_3 \quad (5.6)$$

In the presence of borate, there are likely some additional reactions leading to change in the rate of degradation. Like oxygen, boric acid has also been found to react with reducing radicals, the solvated electron and hydrogen, rapidly. Research on radiolysis of boric acid has shown that the production of hydrogen is rapid in the beginning of the irradiation before plateauing [138]. The hydrogen likely comes from Reactions 5.7 and 5.8. These reactions likely explain the faster rate of degradation of DMT in ABS in the beginning of the experiment compared to the pure aerated water where the reducing radicals are scavenged only by the dissolved oxygen.

$$H_3BO_3 + H \cdot \rightarrow H_2BO_3 + H_2 \quad (5.7)$$

$$H_3BO_3 + e_{aq}^- \rightarrow H_2BO_3^- + H \quad (5.8)$$

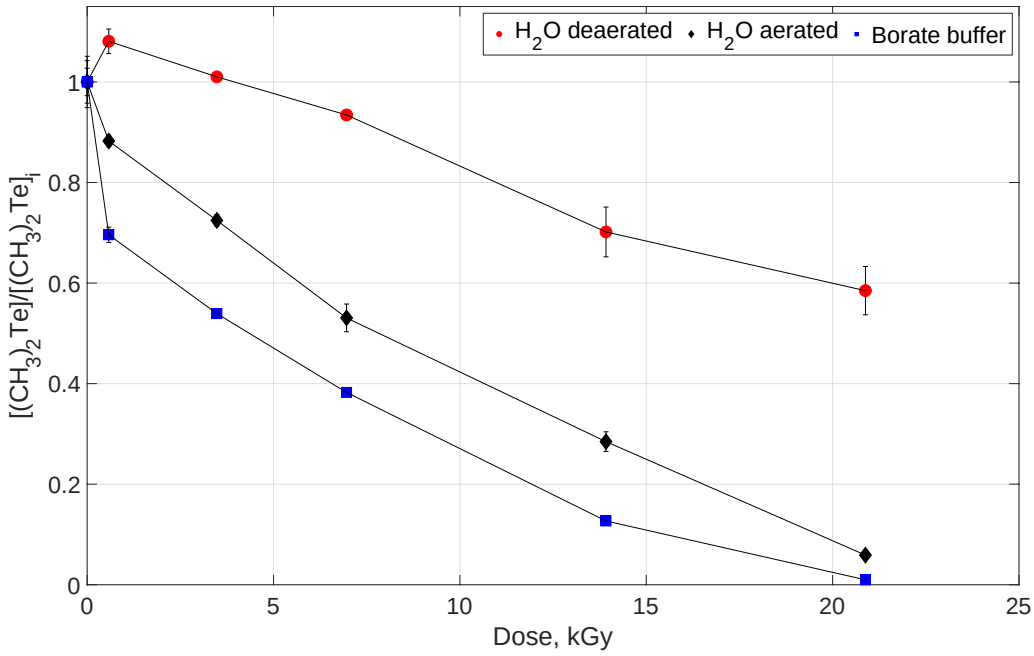

Figure 5.15. The normalized intensity of DMT in aerated (black) and deaerated (red) water and ABS (blue) as a function of the irradiation dose

The most unexpected results were observed in the sodium thiosulfate solution (Figure 5.16.). There, DMT degraded rapidly within the first 10 minutes of irradiation to about 73 %, only slightly decomposing during the rest of the irradiation. After 21 kGy, about 60 % of the initial DMT was left. This behavior was surprising and unexpected, but likely relates to the complex radiolysis behavior of thiosulfate ion. An interesting trend where there is a rapid degradation following a plateau has also been observed for other organic species[139–141]. This can be likely explained by the radiation behavior of thiosulfate. In the presence of oxygen, thiosulfate can form a sulfate radical $SO_4^{\cdot -}$, which is a very strong oxidant. The reactions leading to the formation of $SO_4^{\cdot -}$ are presented below[142,143]. The first step is the formation of thiosulfate or sulfite radical (Reaction 5.9 or 5.10) following further reactions with oxygen forming peroxomonosulfate (Reaction 5.11). The sulfate radical is formed by a recombination of the peroxomonosulfate radicals (Reaction 5.12). The sulfate radical can then react with dimethyl telluride which leads to an oxidative degradation of DMT (Reaction 5.13). It is important to mention that there are likely other reactions involved and here only a simple pathway is presented.

$$S_2O_3^{2-} + O_2 \xrightarrow{\gamma} S_2O_3^{\cdot -} + O_2^{\cdot -} \quad (5.9)$$

$$S_2O_3^{2-} + O_2 \xrightarrow{\gamma} SO_3^{\cdot -} + SO_2^{\cdot -} \quad (5.10)$$

$$SO_3^{\cdot -} + O_2 \xrightarrow{\gamma} SO_5^{\cdot -} \quad (5.11)$$

$$SO_5^{\cdot -} + SO_5^{\cdot -} \xrightarrow{\gamma} 2SO_4^{\cdot -} + O_2 \quad (5.12)$$

$$SO_4^{\cdot -} + \mathrm{DMT} \rightarrow SO_4^{2-} + \mathrm{DMT_{oxidized}} \quad (5.13)$$

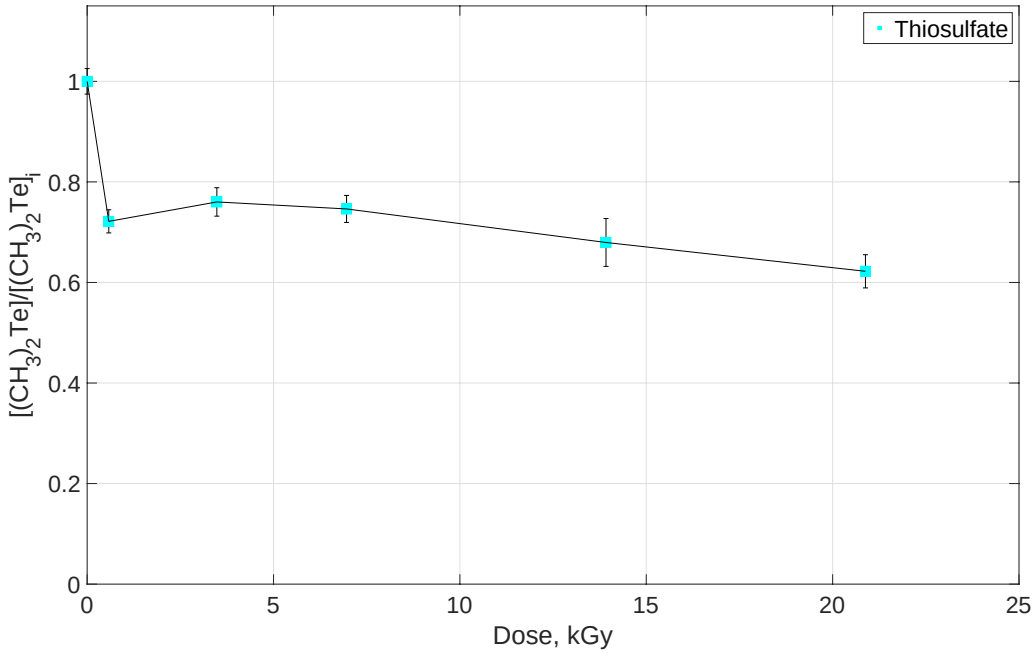

Figure 5.16. The normalized intensity of DMT in aqueous sodium thiosulfate as a function of irradiation dose

In addition to the degradation, the GC-MS analysis also revealed the formation of other volatile tellurides in the deaerated samples. The chromatograms and the corresponding mass spectra are presented in Figure 5.17.A and 5.17.B, respectively. Four new species were identified. It should be noted that the peak for dimethyl telluride (retention time 2.5 minutes) is not presented in Figure 5.17 due to its abundance compared to the other signals. However, the mass spectrum for dimethyl telluride is presented as a reference. The first new peak was observed at around 3 minutes. The corresponding mass spectrum A was used to identify this as methyl-ethyl telluride, $CH_3TeCH_2CH_3$, with a mass ion at 174 m/z. Compared to the reference at 0 kGy, where a small amount was present, the intensity after 28 kGy was over 9 times higher. The next new species was observed at around 3.8 minutes, denoted with B. The mass ion for this species was at 188 m/z and corresponds to methyl propyl telluride, $CH_3TeCH_2CH_2CH_3$. These first two species come from the lengthening of the carbon chain, which likely occurs via a reaction between the DMT radical formed in Reaction 5.5 and a free methyl (Reaction 5.14.).

$$(CH_3TeCH_2)^{\cdot} + \cdot CH_3 \rightarrow CH_3TeCH_2CH_3 \quad (5.14)$$

A further lengthening of the carbon chain to form the methyl propyl telluride likely occurs via a similar reaction but instead of dimethyl telluride, this forms later after around 21 kGy dose, indicating that it forms from the methyl ethyl telluride (Reactions 5.15 and 5.16).

$$CH_3TeCH_2CH_3 + \cdot OH \rightarrow (CH_3TeCH_2CH_2)^{\cdot} + H_2O \quad (5.15)$$

$$(CH_3TeCH_2CH_2)^{\cdot} + \cdot CH_3 \rightarrow CH_3TeCH_2CH_2CH_3 \quad (5.16)$$

Additional two volatile species with higher masses were observed at 8.5 and 11.5 minutes (C and D). The peak at 8.5 minutes had a mass ion at 286 m/z with additional groups at around 130, 140, 256 and 271 m/z and was identified as dimethyl ditelluride, $CH_3TeTeCH_3$. The last species had even higher mass at 304 m/z. In addition, it had a complete mass spectrum for dimethyl telluride between 126 and 160 m/z. This species is a dimethyl ditelluride dimer, $(CH_3)_2TeTe(CH_3)_2$.

The suggested pathways for these dimers include a reaction with either the solvated electron forming a methyl telluride species (Reaction 5.17), following the dimerization (Reaction 5.18), or a substitution of the OH group in $(CH_3Te(OH)CH_3)^{\cdot}$ formed in Reaction 5.19 with another DMT molecule. These reactions are analogous to other organic chalcogens[144] and can therefore also be expected for organic tellurides. However, due to the fast reactivity of all radical species, the detection is not possible, and the pathways cannot be confirmed.

$$CH_3TeCH_3 + e^-_{aq} \rightarrow (CH_3TeCH_3)^{\cdot -} \rightarrow CH_3Te^- + \cdot CH_3 \quad (5.17)$$

$$CH_3Te^- + TeCH_3 \rightarrow + CH_3TeTeCH_3 \quad (5.18)$$

$$(CH_3Te(OH)CH_3)^{\cdot} + CH_3TeCH_3 \xrightarrow{-OH} (CH_3)_2TeTe(CH_3)_2 \quad (5.19)$$

This type of dimerization in the absence of oxygen has been observed with other organic compounds. Methyl ethyl ketone, for example, has been found to go through similar processes where it is decomposed by oxidizing radicals in aerated aqueous solution but forms various dimers in the absence of oxygen [145]. In addition, both dimethyl selenide and dimethyl sulfide have been found to form similar dimers when exposed to gamma irradiation [146,147]. These findings support the results presented here and further strengthen the assumption that the DMT degradation occurs via oxidative decomposition.

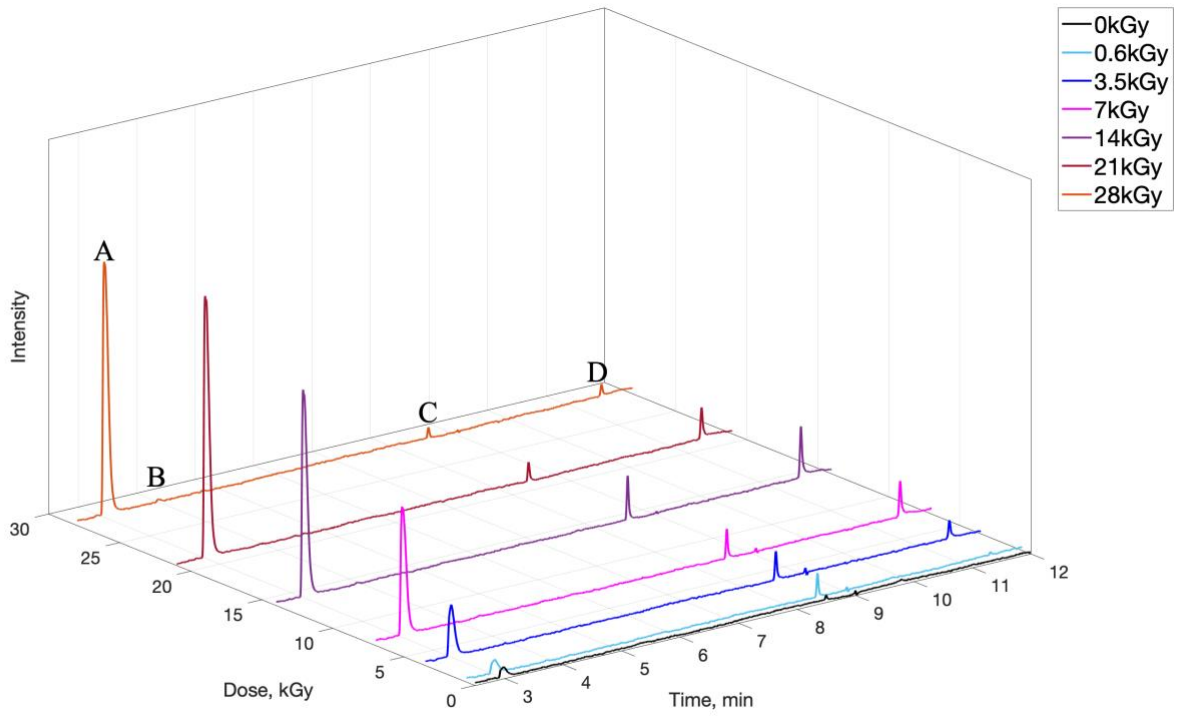

Figure 5.17.A. The chromatograms of the irradiated DMT solution in deaerated conditions with increasing irradiation dose. The letters refer to the corresponding mass spectra presented below

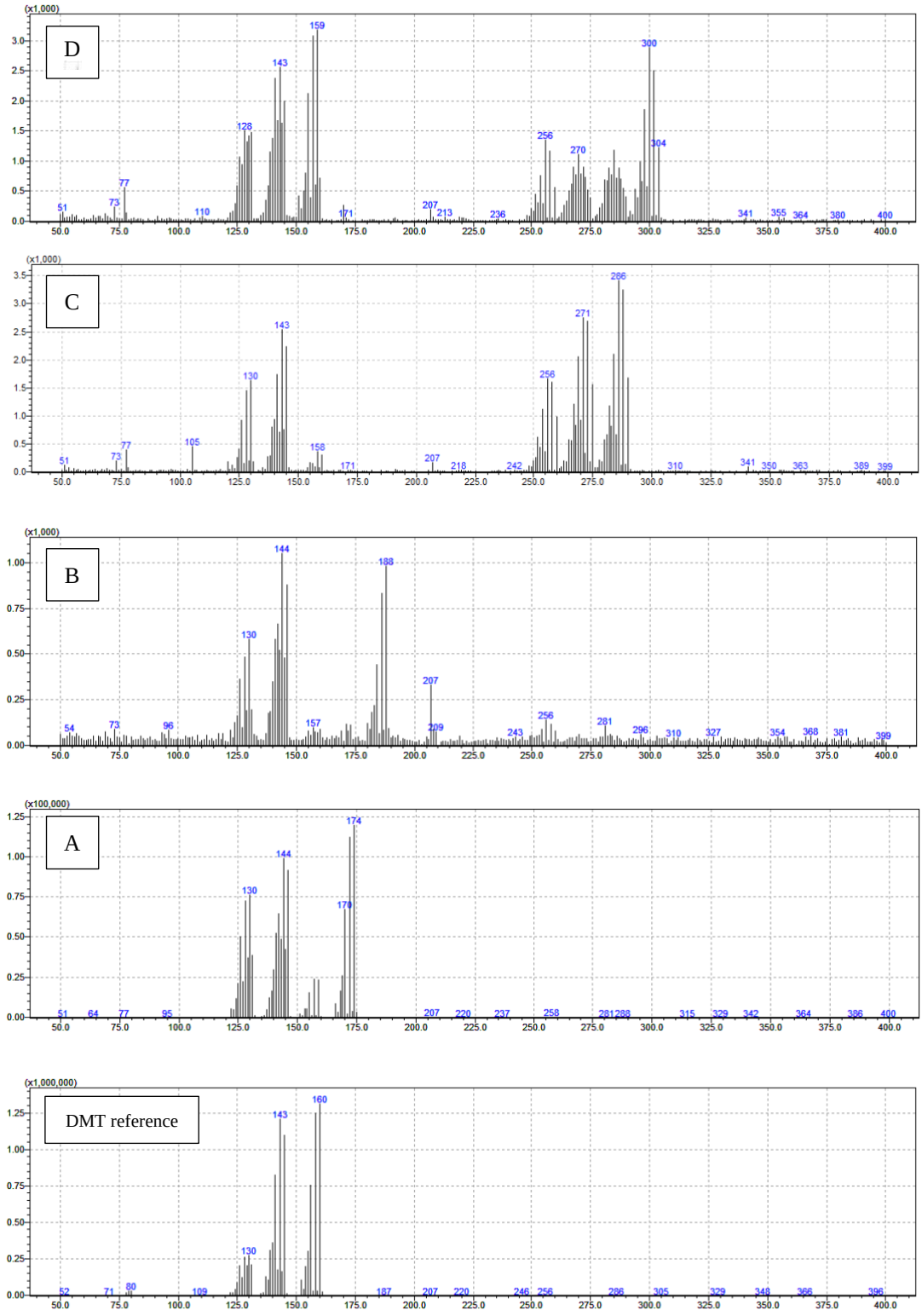

Figure 5.17.B. The mass spectra for the peaks shown above A. *Methyl-ethyl telluride* B. *Methyl-propyl telluride* C. *Dimethyl ditelluride* D. *Dimethyl ditelluride dimer*

5.1.4. Gas phase interactions

Results presented here are based on those presented in PAPER VI.

Possible interactions between tellurium and organic material were investigated. The results for the fraction measured in the trap solutions in each experiment using the two liquid organic additives are presented in Figure 5.18. The first three bars are the tellurium concentration values measured in the reference conditions without any organic precursor. In Experiments 1, where tellurium was exposed in air atmosphere, no significant change was observed in the reference experiment or those with organic material present. However, in Experiments 2 and 3, where the atmospheres were nitrogen and argon/hydrogen, respectively, clear differences were observed. In both conditions, the concentrations in the reference experiments were around the same value as that in Experiment 1. However, when adding organic material to the feed, significantly more tellurium was measured in the trap solutions. In the nitrogen atmosphere, the addition of acetone to the feed increased the transport of tellurium around four times. With propanol in nitrogen atmosphere, the increase was around 2.5 times higher compared to the reference value. In argon/hydrogen (Exp 3), the reference value was slightly higher compared to the first two experiments. The addition of organic material increased the transport approximately 4 times higher than that in the reference conditions. This applied to both acetone and propanol.

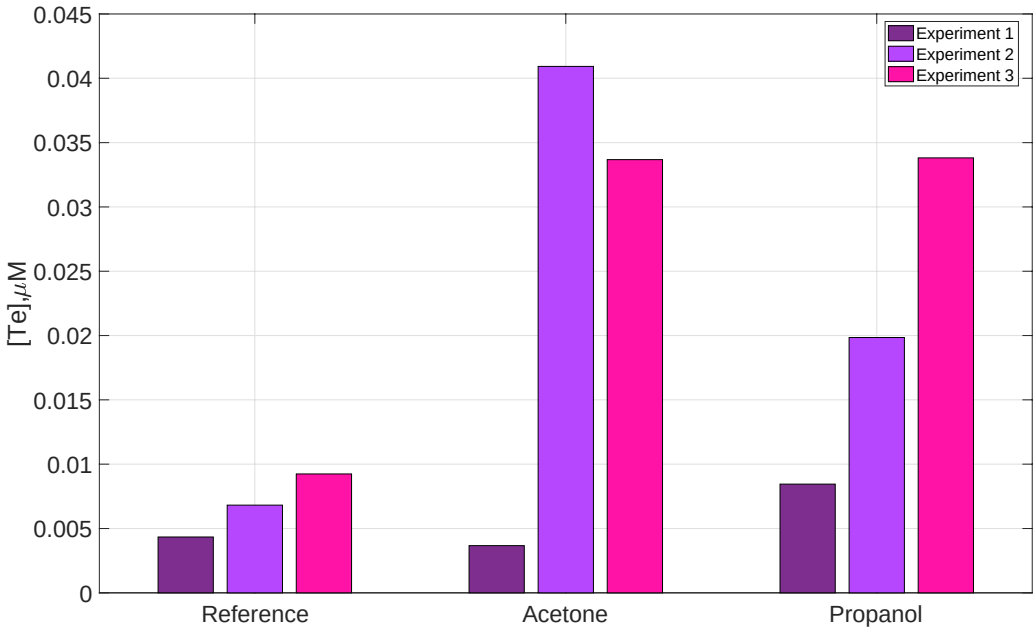

Figure 5.18. The tellurium concentrations in Experiments 1 (air), 2 (nitrogen) and 3 (Argon/hydrogen) measured in the trap solutions in reference conditions (no organic precursor) and with acetone and propanol in added to the feed

The results for the tellurium concentrations in the trap solutions using methane gas in the feed with either argon/hydrogen (Experiment 4) or nitrogen (Experiment 4.1.) are presented in Figure 5.19. An increase was observed in both experimental conditions. In argon/hydrogen,

the value with methane was around 3.5 times higher, and with nitrogen 4 times higher, than the corresponding reference values. Overall, the concentrations measured in the trap solutions were very low, however, the increase in the presence of an organic precursor is inevitable.

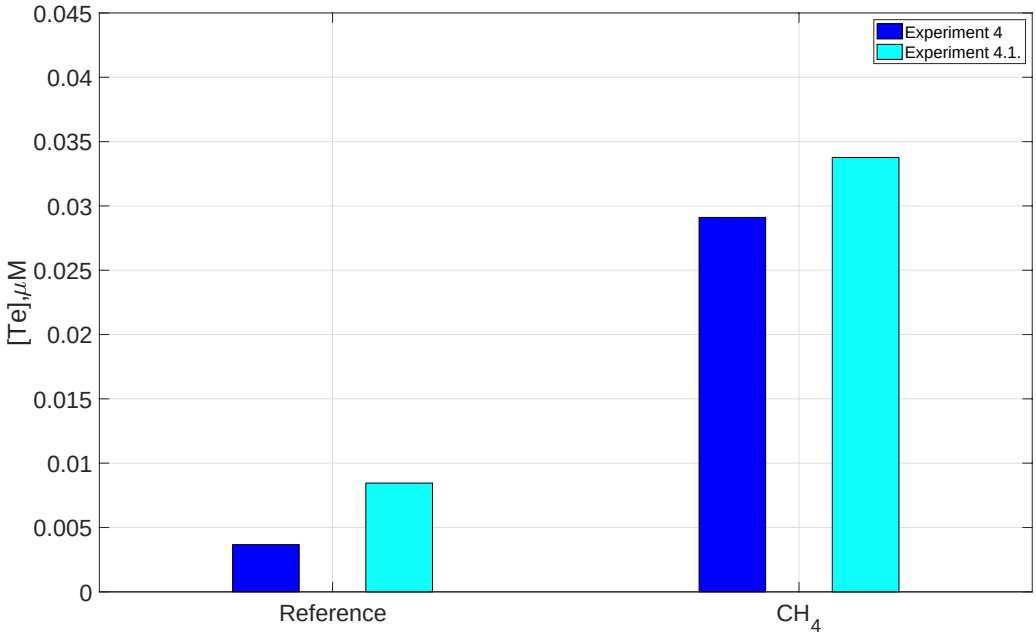

Figure 5.19. The tellurium concentrations in Experiments 4 (methane+argon/hydrogen) and 4.1. (methane+nitrogen) measured in the trap solutions in reference conditions (no organic precursor) and with acetone and propanol in added to the feed

Unfortunately, no speciation analysis was performed in order to determine the exact species in the trap solutions. The online measurements with the FTIR were also inconclusive and the speciation in the gas phase was uncertain. However, the increase in the fraction of tellurium transported to the traps indicated some interactions between tellurium and organic material. Whether this is the formation of organic tellurides in the gas phase, or some other interaction remains unclear. In case organic tellurides had formed in the experiments where an increase was observed, the amounts are likely too low to be detected with the FTIR among other species with higher concentration e.g., acetone, propanol, and water. In an oxidizing atmosphere, no change was observed, which is likely related to the oxidation of tellurium. In air, the elemental tellurium precursor oxidized to tellurium dioxide, which consequently decreases the transport of tellurium aerosols. In addition, previous research has shown that tellurium, in its elemental form, can trap organic radicals and form organic tellurides[129,148]. This has not been observed when using tellurium dioxide. Therefore, the oxidation of tellurium likely inhibits the interaction between organic material and tellurium. In addition, organic tellurides have been found to form in the presence of methane. However, these previous experiments were performed in the liquid phase, using sodium telluride as the starting material, and gamma irradiation to facilitate the reaction[149]. These previous experiments have been performed in higher temperatures or in the presence of gamma irradiation and are therefore not fully comparable with the results presented here.

5.2. Management

5.2.1. Spray removal efficiency

Results presented here are based on those published in PAPER I.

The removal efficiency of a simulated containment spray system was investigated in various conditions. The results here present data on the aerosol mass size distribution and the removal efficiencies of water, ABS and ABS with sodium thiosulfate.

Figure 5.20. presents the average mass size distributions of the fed tellurium aerosols leaving the spray chamber in reference conditions without any spray on. Generally, the aerodynamic mass median diameter (AMMD) of the particles fed into the system was less than 1 µm. Generally, the removal efficiency of the CSS is the most efficient at removing particles larger than 1 µm or smaller than 0.1 µm but the removal efficiency remains low for the accumulation mode particles (between 0.1 and 1 µm)[150]. The particle size distribution of tellurium aerosols (<1 µm) was not within the optimal range and likely affected the removal efficiencies of the sprays.

In Experiment 5, where elemental tellurium was exposed to humid air, the overall amount of the particles was very low. There was no reason found other than an experimental error that could have resulted in the low release. Therefore, the remaining results for Experiment 5 are uncertain as well.

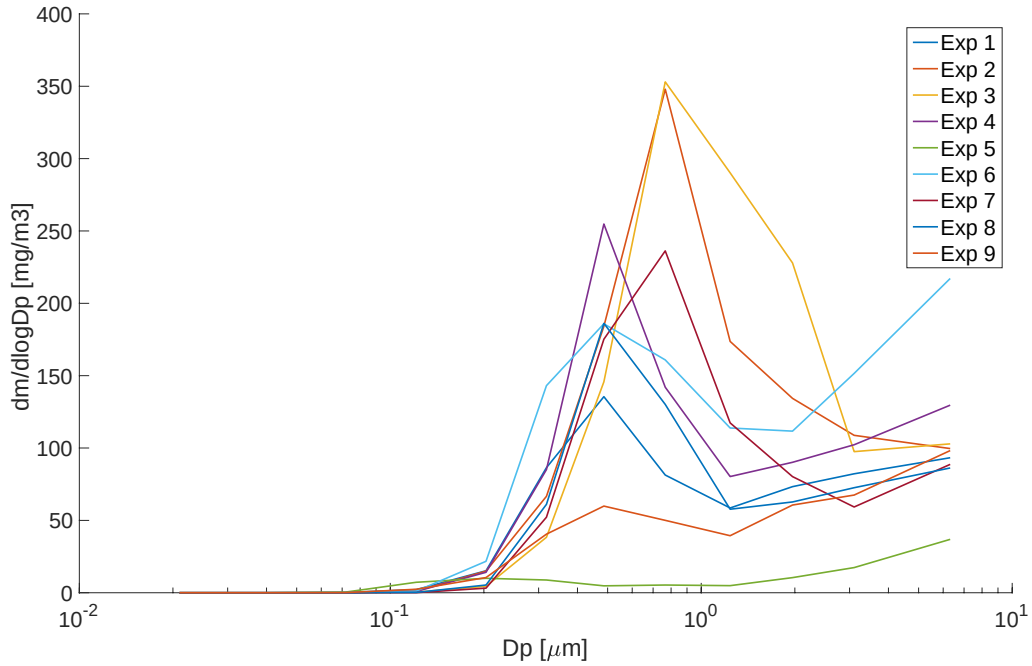

Figure 5.20. Particle size distribution of tellurium aerosols fed into the spray system in reference conditions measuring the aerosols passing through the system without a spay on

The removal efficiencies for the 9 experiments conducted are presented in Figure 5.21. Spray numbers 1, 2, and 3 correspond to water, ABS and ABS with sodium thiosulfate, respectively. Overall, the removal efficiencies were quite high. For water, the efficiency was well over 80% for all experiments except for Experiment 5. For all conditions, the removal increased even higher when using a chemical spray. Then, the percentages were up to 99 %. No significant effect was observed with using thiosulfate additive compared to the plain ABS. This is somewhat expected since sodium thiosulfate is added to the spray solution to decompose and facilitate the removal of methyl iodide[151,152]. Since no organic tellurides or other gaseous species were present in the system, thiosulfate is not expected to increase the removal in any significant way.

More variation was observed in Experiments 7, 8 and 9 where elemental tellurium was exposed to inert conditions. The removal efficiencies with water spray for Experiments 7 and 8 were around 64 and 57 %, respectively. With chemical sprays, the removal percentages increased slightly, however, the removal for both experiments was still less than 75 %. When cesium iodide was added to the feed (Experiment 9), the removal increased again to over 90 % with even higher when using chemical sprays. This is likely due to a larger degree of particle agglomeration and a consequently higher chance of collisions with the spray droplets.

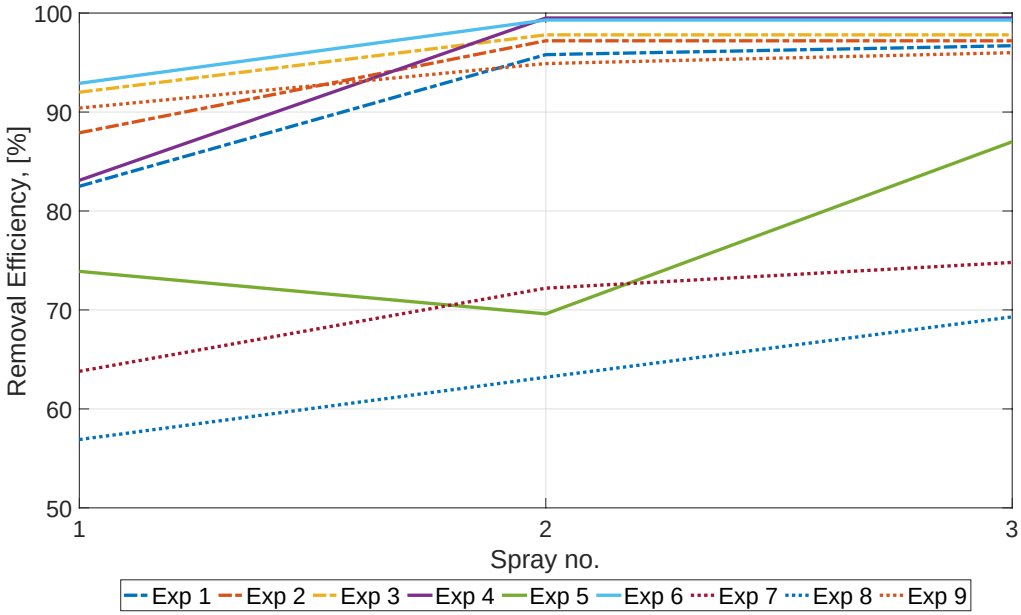

Figure 5.21. Removal efficiencies with the three different sprays used: 1. Water, 2. ABS, and 3. ABS with sodium thiosulfate

The results in inert atmosphere compared to the higher removal efficiencies obtained in oxidizing conditions likely originate from differences in particle size. Although an increase was observed with chemical sprays compared to pure water, chemical reactions are still considered neglectable between the tellurium species and the spray droplets. The chemicals, especially the additives, are often added to enhance the removal of gaseous species, which were not detected in these experiments. The removal likely occurs via physical processes such as impaction and collision. For smaller particles, diffusion on the droplet surface is also plausible, but not the main mechanism in these experiments. Other than the size of the aerosols, the cause of the lower removal efficiency in inert conditions remains unclear.

5.2.2. Adsorption on charcoals

Results presented here are based on those presented in PAPER V.

The formation of organic tellurides raises questions as to whether the management actions present in the containment and used in protective gear are efficient in trapping these volatile species. The following results present results concerning four different activated charcoal (AC) materials. Three of the chosen ACs were obtained from disassembling respirator cartridges, and the last one came from a filter module used at a nuclear power plant.

First, batch experiments were conducted to determine the recovery of DMT from the different ACs. The results for the recoveries are presented in Table 5.1. The values were calculated by comparing the amounts recovered from the ACs to the value analyzed from the empty reference vial. Charcoals B, C and D had a recovery percentage of around 55 % whereas for Charcoal A the recovery was 100 %. The amount left in the vials was also analyzed and determined to be low for all of the samples. Therefore, it can be assumed that all of the DMT added to the vial had adsorbed onto the AC. The differences in the recovered amounts are probably due to differences in the structure and activation mechanism. Moreover, although the recoveries were relatively low for Charcoals B, C and D and could have been higher with repeating the extraction or by using longer times, the main goal was to attain a reproducible not maximal recovery.

Table 5.1. Recovery percentages for the different charcoal materials

Charcoal	**Recovery from Charcoal, %**	**Recovery from vial, %**
A	107 ± 15	1.6 ± 0.7
B	56 ± 11	1.7 ± 0.3
C	54 ± 9	1.4 ± 0.9
D	53 ± 8	2.0 ± 0.9

To compare the efficiencies of the different ACs, they were exposed to same conditions: flow rate of 1 $Lmin^{-1}$ and a duration of 30 minutes. The results of the fractions recovered from each charcoal pad as a function of pad number are presented in Figure 5.22. For all four charcoals, the highest fraction of DMT adsorbed on the first pad was between 56 and 68 %, as expected. Around 30 % was adsorbed on the second pad followed by a few percentages on the third. This applies for all four materials. No tellurium was detected in the samples from pad number four onwards or in the traps.

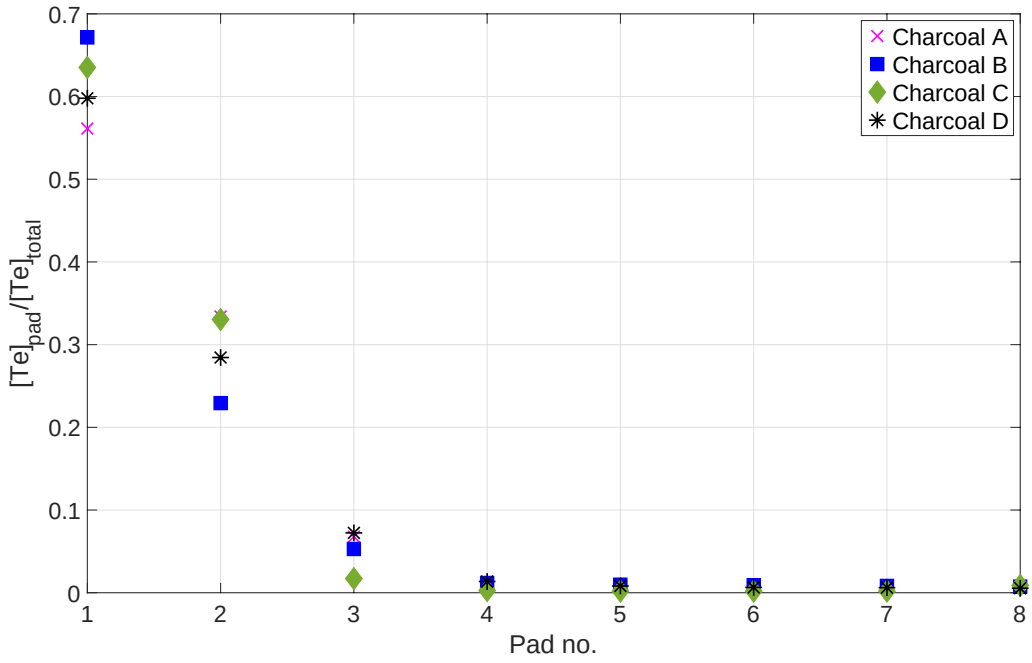

Figure 5.22. The recovered fractions of dimethyl telluride from each charcoal pad

Charcoal A obtained from disassembling a 3M 60928 respirator cartridge was chosen for further investigation. Firstly, the effect of time was explored while the flow rate was kept at 1 $Lmin^{-1}$. The results are presented in Figure 5.23. With a flow duration of 5 minutes, around 70 % adsorbed onto the first pad. This value with a 30-minute flow was 56 %. The results from the short experiments, 5 and 30 min, are quite similar with some variation in the adsorption on the 1st and 2nd pad. With short times, no tellurium was detected from the 4th pad onwards or in the traps. Significant change was observed when the flow duration was increased. With 120 minutes, the highest fraction, around 30 %, was recovered from pad no. 2. Moreover, the trend was not exponential anymore, but DMT seemed to have diffused wider in the column. In the 120-minute experiment, tellurium was recovered from the 5th pad, but nothing was detected in the last three or in the trap. By further increasing the flow duration to 330 minutes, DMT was detected in pad number 6. The graph in Figure 5.23 shows how DMT had distributed quite evenly on the first four pads after which the amounts decreased, and no detectable amount was measured on pads 7 or 8. Regardless of the flow duration used in these experiments, eight 250 mg charcoal pads were sufficient in retaining DMT. However, there seems to be some reversibility of adsorption as the DMT penetrated deeper into the column with longer experiments.

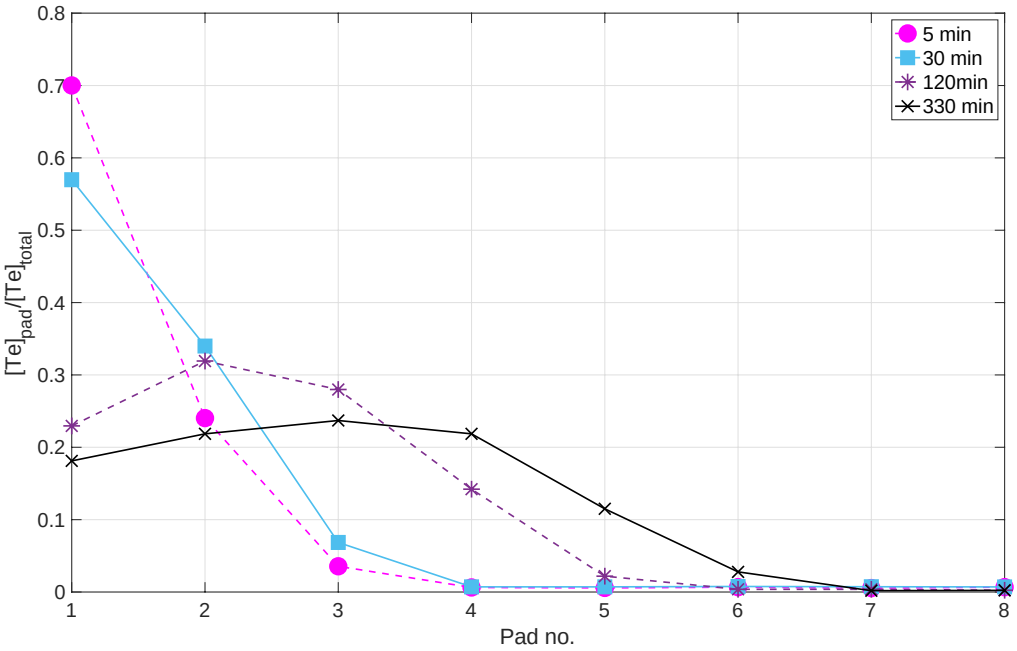

Figure 5.23. The recovered tellurium fractions from each charcoal pads using different flow durations

To gain more information on the efficiency and adsorption mechanism, Charcoal A was used for flow rate experiments. Three different flow rates, 0.5, 1 and 2 $Lmin^{-1}$, were used. The duration of the experiments was 30 minutes and otherwise the conditions were kept the same. The results of the fractions recovered as a function of pad number for the different flow rate experiments are presented in Figure 5.24. With slower flow rates, 0.5 and 1 $Lmin^{-1}$, only small variation was observed. The trend for both was exponential with the highest fractions in the first pad following the second and third. No tellurium was again recovered after the 4^{th} pad. However, when the flow rate was increased to 2 $Lmin^{-1}$, DMT was again spread wider within the column. The distribution in the first four pads was quite similar with around 20 % recovered from each pad. The fifth pad had about 10 % following the 6^{th} with only a few percent. Again, no tellurium was recovered in the last two pads or the trap. These results suggest that in addition to the time, the flow rate also has a significant effect on the adsorption of DMT onto charcoal. This likely relates to the adsorption kinetics where with a faster flow rate, the adsorption of the DMT molecules is too slow, and therefore, they diffuse deeper into the AC column.

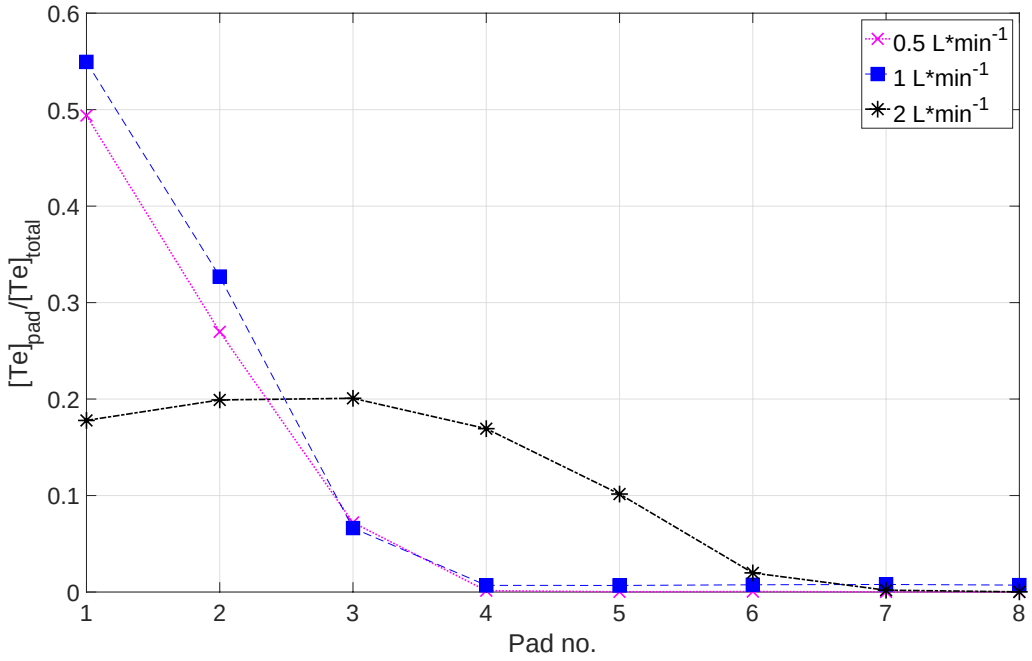

Figure 5.24. The fraction of tellurium recovered from each pad using Charcoal A with different flow rates

Efforts were made to compare the experimental results to theoretical values optimized by using a model based on Cauchy Lorentz distribution and the adsorption of radioactivity in soil[153]. The optimization was done by varying the Kd value and the x offset in the Cauchy fit. A least square method was used to fit the experimental data to the model using the solver feature in Excel. The model was given the flow rate and the duration of the flow. The results comparing the experimental results for Charcoal B and D to the calculated values are presented in Figure 5.25. As observed, the calculated results estimate around 80 % adsorption on the first pad, following around 10 % on the second pad. In the experiments, the fractions recovered in the first pads were around 68 and 60 % in Charcoal B and D, respectively. Moreover, the values for the second charcoal pads were around 25 and 30 % which are more than twice as high compared to the calculated results. From the 3rd pad onwards both the experimental and calculated results give the same low or neglectable adsorption. The differences in the calculated and experimental results suggest that the adsorption of dimethyl telluride on charcoal is not a theoretical process but more complex.

The results with higher flow rates and longer flow durations were also compared to those given by the model. However, the model grossly underestimated the diffusion deeper into the column which was observed in the experiments. This strengthens the assumption that the adsorption of dimethyl telluride is likely not a simple one compartment system.

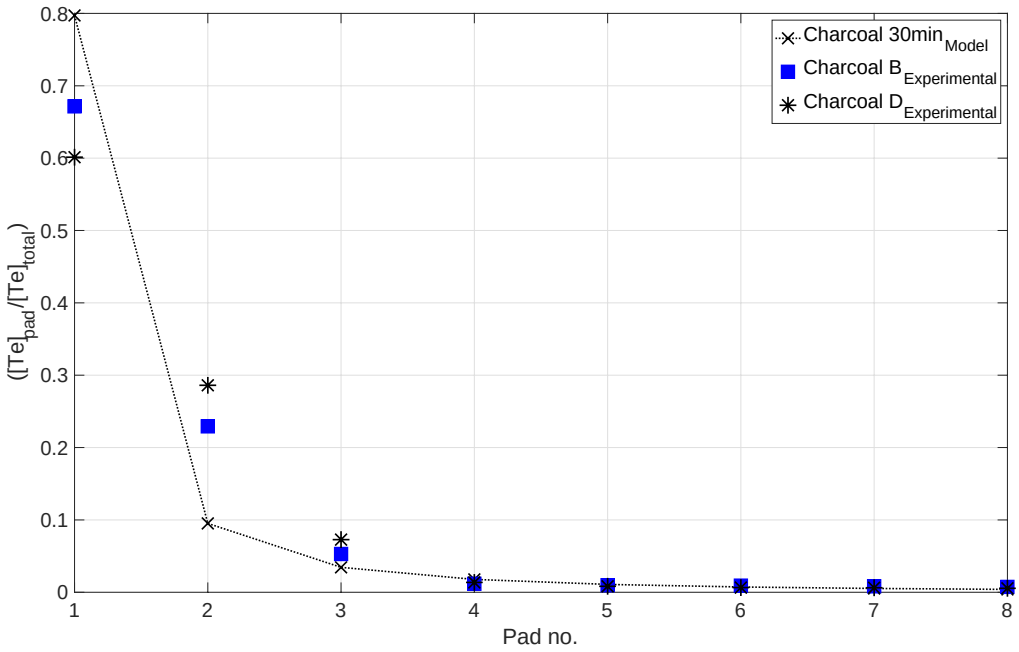

Figure 5.25. The calculated results with the experimental results for Charcoals B and D for a flow duration of 30 minutes and flow rate of 1 $Lmin^{-1}$.

By combining the results presented here, it seems like the adsorption mechanism of DMT onto charcoal is quite complex. Comparing the results obtained from similar experiments for methyl iodide, the results are do not coincide. Methyl iodide has been found to adsorb onto charcoal very efficiently[154,155] and migrate only a couple of centimeters in a 23 day experiment using the same 20 cm/s linear flow[156]. However, it is important to note that the charcoal material and column dimensions were different, and therefore, the experiments cannot be fully compared.

One possible explanation for the results is to consider the adsorption of DMT on charcoal as being a multi-compartment system. A simple schematic presentation of the multi-compartment system with two compartments is shown in Figure 5.26. This type of analysis is often used in pharmacokinetic studies where the distribution and elimination of a drug in the body is expressed with a multi-compartment curve[157]. In a single compartment system, the distribution of the drug or organic tellurium, forms a first-order curve. This applies to the short experiments and slower flow rates. However, by changing the conditions, the system involves more compartments. Then the dimethyl tellurium is transferred into at least one other compartment from which it is only slowly released. After the desorption, the dimethyl telluride molecules are captured again deeper along the charcoal column, which leads to the wider distribution seen with longer times and faster flow rates. This resembles a common drug distribution scenario[158] where the initial plasma concentration of the drug is eliminated by the kidneys (single compartment) yet is the recaptured into another compartment. This often results in a biexponential curve. However, in the case of dimethyl telluride on charcoal the curve is not biexponential but even more complex. The different compartments likely

relate to phenomena such as physisorption, chemisorption and the porous structure of charcoal.

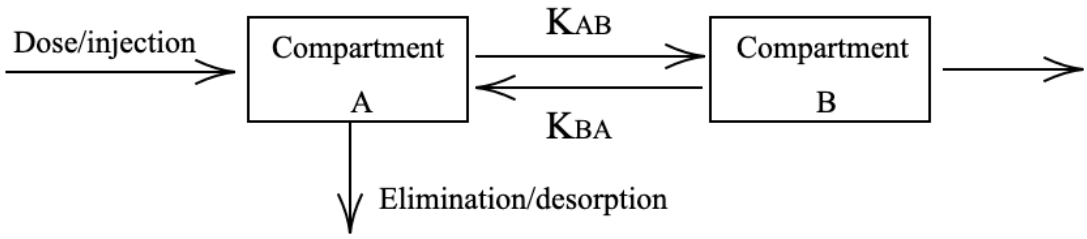

Figure 5.26. The schematic presentation of a general multi-compartment system with two compartments showing the possible paths and connections between the two compartments after the initial injection

6. Conclusion

The aim of this work was to investigate the potential reactions, phenomena and interaction tellurium can be involved in severe nuclear reactor accidents. The phenomena investigated here have not been part of any research program before although some of the reactions leading to higher mobility have been considered in literature before. However, no evidence has been presented before.

The work was divided into reaction leading to higher mobility and to the management of these species. The first part of the mobilization reactions was to study the effect of gamma irradiation on the solubility of tellurium in the containment sump (PAPER II). The results show that tellurium dioxide can oxidize to telluric acid, a species with significantly higher solubility, in the presence of oxidizing water radiolysis products. The solubility increased linearly with increasing radiation dose. No equilibrium was achieved which is likely due to incomplete oxidation and the dissolution of tellurium dioxide in the samples. In the presence of sodium thiosulfate, a strong radical scavenger, tellurium dioxide reduced to elemental tellurium. This is likely due to the thiosulfate ions scavenging the oxidizing radicals, and tellurium dioxide then reacting with the reducing products. These results indicate a higher dissolution of tellurium in the sump conditions than expected. The dissolved tellurium species could take part in further reactions investigated in the following experiments.

Of the possible interactions in the sump, the reactions between dissolved tellurium dioxide and paint solvents were the next focus in this work (PAPER III). Several organic tellurides were formed in the sump simulant under gamma irradiation. The main species formed from tellurium and texanol ester alcohol was diisopropyl telluride. Of the paint solvents, texanol and MIBK decomposed to form organic tellurides. No tellurium bearing organic species were observed in the irradiated samples with toluene. In addition to the formation of organic tellurides, tellurium dioxide was found to reduce to elemental tellurium which could indicate the reaction occurs between elemental tellurium and organic radicals rather than with the dissolved tellurium dioxide. However, no conclusive mechanism could be presented. The highest amount of organic tellurides were observed after around 1 day of irradiation (96 kGy). Since the detected amount is the sum of the organic tellurides formed and decomposed, this suggest that the tellurides are somewhat stable under gamma irradiation. The stability of a chosen organic telluride, dimethyl telluride, was further investigated in PAPER IV.

Dimethyl telluride was chosen for the stability studies because it was one of the tellurides formed in the paint experiments but also since it is the simplest telluride to synthesize. DMT was found to degrade under gamma irradiation. However, around 21 kGy dose was required to decompose all the DMT in sump conditions. In aerated water, around 6 % of the DMT was left after 21 kGy. The difference is likely due to the presence of boric acid in the sump which facilitates the oxidative decomposition by reacting with the reducing radiolysis products. Significant differences were observed with samples in deaerated water or sodium thiosulfate. The absence of oxygen decreased the rate of degradation significantly. In turn, new higher mass organic tellurides were identified in the samples. This was not observed in the aerated samples. Lastly, the degradation of DMT in the thiosulfate solution had an interesting trend where the degradation was rapid in the beginning of the experiment but stabilized and only

slightly degraded after. This was attributed to the formation of sulfate radical, a strong oxidant, and the rapid decrease of the amount of oxygen present. All the reactions presented in this work are suggestions, and none of the intermediates could be detected in the samples.

The last part of the mobilization experiments, discussed in PAPER VI, was the interaction between elemental tellurium and organic material in the gas phase. The aim was to simulate conditions present in the containment where tellurium aerosols are present with volatile organic compounds in the containment atmosphere. A clear increase in the tellurium concentrations measured in the trap solutions were observed with inert and reducing atmospheres. The increase can be a sign of the formation of organic tellurides; however, speciation analyses were inconclusive. In oxidizing atmosphere, the trap results were very similar with and without organic material. This is likely due to the oxidation of tellurium precursor, confirmed by XRD analysis, which inhibits the interactions with the organic material. This does not occur when using inert or reducing atmospheres. Adding methane gas to the feed also increased the fraction passing through the filter. These results indicate some reactions occurring in the gas phase. However, the detailed mechanism remains unclear and should be further investigated.

In order to minimize the release of radioactive material into the environment, different management actions are in place and targeted to mitigate the species formed during an accident. The first management action investigated in this work was the containment spray system (PAPER I). The CSS was tested for the removal of tellurium species formed in oxidizing and inert atmospheres, in the presence of humidity and cesium iodide. Water, alkaline borate solution with and without sodium thiosulfate were used as the spray solutions. Overall, the removal efficiencies were high, especially in oxidizing atmosphere. With the chemical sprays, the removal efficiencies were up to 99 %. In inert atmosphere, the removal was lower with water but increased when adding cesium iodide into the feed. The differences are likely a result of slight differences in the size of the aerosols fed into the system. When adding cesium iodide, there is likely more agglomeration leading to larger particles, which have a higher probability to collide with the spray droplets. Although the chemical sprays increased the removal efficiencies, the removal was expected to have occurred due to physical interactions like collisions rather than chemical reactions between the aerosols and tellurium aerosols.

The second part of the management experiments relates to the formation of organic tellurides. One of the management actions designed to trap organic species in accident scenarios is activated charcoal. Charcoal materials are found in the respirators used by the emergency workers and sampling devices. Moreover, some nuclear power plants have charcoal in their filter system. In this work, four charcoal materials were tested for the trapping of dimethyl telluride. This was the focus in PAPER V. In short flow times, and in moderate flow rates, DMT was efficiently adsorbed onto the charcoal materials. However, when increasing the flow duration from 30 minutes up to 330 minutes, DMT was found to diffuse deeper into the charcoal column. The same effect was observed when increasing the flow rate. These results indicate some irreversibility of the adsorption. In addition, the adsorption mechanism is likely a multi-compartment system where DMT is adsorbed, released and re-adsorbed later in the column. This behavior was somewhat unexpected since only minor diffusion has been

observed for methyl iodide in similar experiments. However, the exact adsorption mechanism could be something to focus on in future experiments.

Overall, the results presented here have improved the knowledge on tellurium behavior in severe nuclear reactor accident scenarios. The mobilization and formation of organic tellurides raise concerns on re-volatilization and increased source term which are worth to consider in future research. This work has increased the interest around tellurium while also showing evidence on the efficiency of different management systems. The experiments conducted and results obtained pave the way for future research on tellurium source term.

Future Work

Suggestions for further research include going forward with the organic telluride studies. The quantification of the organic tellurides formed in severe accident conditions is important to assess the actual relevance. In case, the amount is found to be sufficient to cause concern, the mitigation of the organic tellurides becomes important. For that, testing the pool scrubbing efficiency would be a suggestion.

In this work, the sump simulant was very simplified. In future research, increasing the complexity of the sump solution to ensure it is even more representative would improve the assessments.

Lastly, the collaboration between experimentalists and modelers should be enhanced, not only regarding tellurium behavior but also when studying other severe accident phenomena. Currently, work is being done with improving the chemical models in the current codes. In the future, relevant tellurium species and reactions should be applied to the codes in order to decrease the uncertainties and improve the overall safety assessments.

Acknowledgements

Thank you to my supervisor Christian Ekberg for giving me the freedom to find my own way while still keeping me on the right track all through the years.

Thank you to my co-supervisor Mark Foreman for answering to my endless questions, risking the safety of the lab for my syntheses, and for being such a great mentor.

To Henrik Glänneskog and all APRI members, thank you for your input to my work throughout the years. The perspective you've given has been very valuable and guided my research into the right direction.

Thank you, Teodora Retegan Vollmer, for all help you have given me and always finding a solution to any problem I might have faced.

To the rest of the KK/IMÅ people, thank you for making our division a great place to work, collectively laughing at my quirky jokes and helping me with whatever I have needed.

Special mention to Luis, the best office buddy a girl can ask for. Thank you for holding my hand while I submitted my first paper, for giving your valuable opinions on my defense outfit suggestions, and for handing me a tissue when I've needed one.

To Thea, Niklas, Olivia, Agnes, Fredrik, Emma, Gabriele, and the rest of the group. Thank you for the after works, game nights, lake fun, and all the shenanigans you've been part of. Also, thank you for understanding my "Finnishness" and learning to deal with it.

To my family, äiti, iskä, Saaris, Jedi, Kaarle, Eppu ja Helka. This would be just a torso of a thesis without you. Thank you for keeping me together, lifting me up, encouraging and letting me be me. Kiitos kaikesta, rakastan teitä.

Last but not least, thank you Petri for letting me chase my dreams, supporting and loving me.

References

1. INTERNATIONAL ATOMIC ENERGY AGENCY, *Nuclear Power Reactors in the World, Reference Data Series No. 2*, Vienna (2022).
2. INTERNATIONAL ATOMIC ENERGY AGENCY, "Nuclear Safety, Security and Safeguards in Ukraine Summary Report by the Director General 24 February-28 April 2022" (2022).
3. B. K. SOVACOOL, "The costs of failure: A preliminary assessment of major energy accidents, 1907-2007," Energy Policy **36** 5, 1802, Elsevier (2008); https://doi.org/10.1016/j.enpol.2008.01.040.
4. Y. LIU and T. ISHIHARA, "Fatigue failure accident of wind turbine tower in taikoyama wind farm," in European Wind Energy Association Annual Conference and Exhibition 2015, EWEA 2015 - Scientific Proceedings, pp. 121–125 (2015).
5. M. SPADA and P. BURGHERR, "An aftermath analysis of the 2014 coal mine accident in Soma, Turkey: Use of risk performance indicators based on historical experience," Accid. Anal. Prev. **87**, 134, Pergamon (2016); https://doi.org/10.1016/J.AAP.2015.11.020.
6. UNSCEAR, "SOURCES AND EFFECTS OF IONIZING RADIATION (annex D)," United Nations, New York (2008).
7. M. CHINO et al., "Preliminary estimation of release amounts of 131i and 137cs accidentally discharged from the fukushima daiichi nuclear power plant into the atmosphere," J. Nucl. Sci. Technol. **48** 7, 1129 (2011); https://doi.org/10.1080/18811248.2011.9711799.
8. B. RICHARDSON, J. SORENSEN, and E. J. SODERSTROM, "Explaining the Social and Psychological Impacts of a Nuclear Power Plant Accident," J. Appl. Soc. Psychol. **17** 1, 16 (1987); https://doi.org/10.1111/j.1559-1816.1987.tb00290.x.
9. M. MURAKAMI, Y. TAKEBAYASHI, and M. TSUBOKURA, "Lower psychological distress levels among returnees compared with evacuees after the fukushima nuclear accident," Tohoku J. Exp. Med. **247** 1, 13 (2019); https://doi.org/10.1620/tjem.247.13.
10. E. J. BROMET, J. M. HAVENAAR, and L. T. GUEY, "A 25 Year Retrospective Review of the Psychological Consequences of the Chernobyl Accident," Clin. Oncol. (2011); https://doi.org/10.1016/j.clon.2011.01.501.
11. W. RÜDIG, *Anti-nuclear movements : a world survey of opposition to nuclear energy*, Longman Current Affairs (1990).
12. J. ROBBINS and A. B. SCHNEIDER, "Thyroid Cancer Following Exposure to Radioactive Iodine," Kluwer Academic Publishers (2000).
13. K. TAGAMI et al., "Estimation of Te-132 Distribution in Fukushima Prefecture at the Early Stage of the Fukushima Daiichi Nuclear Power Plant Reactor Failures" (2013); https://doi.org/10.1021/es304730b.
14. R. S. DICKSON and G. A. GLOWA, "Tellurium behaviour in the Fukushima Dai-ichi Nuclear Power Plant accident," in Journal of Environmental Radioactivity (2019); https://doi.org/10.1016/j.jenvrad.2019.03.024.
15. INTERNATIONAL ENERGY AGENCY, "Key World Energy Statistics 2021," IEA (2021).

16. INTERNATIONAL ATOMIC ENERGY AGENCY, “The International Nuclear and Radiological Event Scale User’s Manual” (2008).
17. INTERNATIONAL ATOMIC ENERGY AGENCY, “The Information Channel on Nuclear and Radiological Events,” Nuclear Events Web-based System (NEWS); https://www-news.iaea.org/.
18. OECD NEA, *Nuclear Fuel Behaviour Under Reactivity-initiated Accident (RIA) Conditions State-of-the-art Report* (2010).
19. INTERNATIONAL ATOMIC ENERGY AGENCY, *Nuclear Power Reactors in the World*, Vienna (2022).
20. WORLD NUCLEAR ASSOCIATION, “RBMK Reactors;” 2022.
21. P. E. MACDONALD et al., “Assessment of light water reactor fuel damage during a reactivity initiated accident” (1980).
22. INTERNATIONAL ATOMIC ENERGY AGENCY, “Technical Volume 1 of 5: Description and Context of the Accident,” Fukushima Daiichi Accid. **1**, 238 (2015).
23. B. R. SEHGAL, *Nuclear safety in light water reactors: severe accident phenomenology*, Academic Press (2011).
24. L. SOFFER et al., “Accident source terms for light-water nuclear power plants,” Off. Nucl. Regul. Res., 38 (1995); https://doi.org/10.1177/2047487314530052.
25. P. A. RILEY, “Free radicals in biology: Oxidative stress and the effects of ionizing radiation,” Int. J. Radiat. Biol. **65** 1, 27, Taylor & Francis (1994); https://doi.org/10.1080/09553009414550041.
26. M. BARNETT, *The Biological Effects of Ionizing Radiation: An Overview*, US Department of Health, Education, and Welfare, Rockville, Maryland (1976).
27. Y. SHIBATA et al., “15 years after Chernobyl: new evidence of thyroid cancer,” Lancet **358** 9297, 1965, Elsevier (2001); https://doi.org/10.1016/S0140-6736(01)06971-9.
28. P. JACOB et al., “Thyroid cancer among Ukrainians and Belarusians who were children or adolescents at the time of the Chernobyl accident,” J. Radiol. Prot **26**, 51 (2006); https://doi.org/10.1088/0952-4746/26/1/003.
29. D. WILLIAMS, “Cancer after nuclear fallout: lessons from the Chernobyl accident,” Nat. Rev. Cancer 2002 27 **2** 7, 543, Nature Publishing Group (2002); https://doi.org/10.1038/nrc845.
30. N. J. MCCORMICK, “Changes in the nuclear power industry after TMI,” Prog. Nucl. Energy **10** 3, 245 (1982); https://doi.org/10.1016/0149-1970(82)90007-5.
31. J. H. JOHNSON and D. J. ZEIGLER, “Post-Chernobyl nuclear reactions in the USA,” Environ. Plan. C Gov. Policy **6** 3, 289 (1988); https://doi.org/10.1068/c060289.
32. H. OTWAY et al., “Risk Communication in Europe after Chernobyl: A Media Analysis of Seven Countries,” Ind. Cris. Q. **2** 1, 3 (1988).
33. L. SJOBERG et al., “Countermeasures to the Chernobyl accident in the Nordic countries: Public reactions (HHS-CFR-B--34)” (1998).
34. M. V RAMANA, “Nuclear policy responses to Fukushima: Exit, voice, and loyalty,” Bull. At. Sci. **69** 2, 66 (2013); https://doi.org/10.1177/0096340213477995.
35. B. B. F. WITTNEBEN, “The impact of the Fukushima nuclear accident on European energy policy,” Environ. Sci. Policy **15** 1, 1 (2012); https://doi.org/10.1016/j.envsci.2011.09.002.

36. D. JAHN and S. KOROLCZUK, “German exceptionalism: the end of nuclear energy in Germany!,” http://dx.doi.org/10.1080/09644016.2011.643374 **21** 1, 159, Routledge (2012); https://doi.org/10.1080/09644016.2011.643374.
37. T. K. BAUER, S. T. BRAUN, and M. KVASNICKA, “Nuclear power plant closures and local housing values: Evidence from Fukushima and the German housing market,” J. Urban Econ. **99**, 94 (2017); https://doi.org/10.1016/j.jue.2017.02.002.
38. WORLD NUCLEAR ASSOCIATION, “Nuclear Power in the World Today;” https://www.world-nuclear.org/information-library/current-and-future-generation/nuclear-power-in-the-world-today.aspx; (current as of Oct. 16, 2022). [Reproduced with permission]
39. X. ZEJUN et al., “Experimental research progress on passive safety systems of Chinese advanced PWR,” Nucl. Eng. Des. **225** 2–3, 305 (2003); https://doi.org/10.1016/S0029-5493(03)00178-X.
40. S. H. CHANG, S. H. KIM, and J. Y. CHOI, “Design of integrated passive safety system (IPSS) for ultimate passive safety of nuclear power plants,” Nucl. Eng. Des. **260**, 104 (2013); https://doi.org/10.1016/J.NUCENGDES.2013.03.018.
41. F. WANG et al., “Code validation and application of hydrogen mitigation by passive autocatalytic recombiner in small modular reactor,” Nucl. Eng. Des. **396**, Elsevier Ltd (2022); https://doi.org/10.1016/J.NUCENGDES.2022.111882.
42. G. SHI et al., “CAP1400 passive core cooling integral testing and application in code validation,” Ann. Nucl. Energy **154**, Elsevier Ltd (2021); https://doi.org/10.1016/J.ANUCENE.2020.107997.
43. M. DE CORT, L. BREITENBACH, and G. DE VRIES, “The on-line European Community urgent radiological information exchange (ECURIE) information system,” OECD, Nuclear Energy Agency of the OECD (NEA) (1998).
44. N. YAMAGUCHI, ICHIRO; SHIMURA, TSUTOMU; TERADA, HIROSHI; SVENDSEN, ERIC R ; KUNUGITA, “Lessons learned from radiation risk communication activities regarding the Fukushima nuclear accident,” J. Natl. Inst. Public Heal. **67** (2018).
45. S. Y. F. CHU, L. P. EKSRÖM, and R. B. FIRESTONE, “Decay Data Search;” 1999; http://nucleardata.nuclear.lu.se/toi/; (current as of Sep. 4, 2020).
46. K.-J. DREICER, M AND AARKOG, A AND ALEXAKHIN, R AND ANSPAUGH, L AND ARKHIPOV, NP AND JOHANSSON, “Consequences of the Chernobyl accident for the natural and human environments” (1996).
47. A. STOHL, P. SEIBERT, and G. WOTAWA, “The total release of xenon-133 from the Fukushima Dai-ichi nuclear power plant accident,” J. Environ. Radioact. **112**, 155, Elsevier (2012); https://doi.org/10.1016/j.jenvrad.2012.06.001.
48. M. CHINO et al., “Preliminary estimation of release amounts of 131i and 137cs accidentally discharged from the fukushima daiichi nuclear power plant into the atmosphere,” J. Nucl. Sci. Technol. **48** 7, 1129 (2011); https://doi.org/10.1080/18811248.2011.9711799.
49. G. STEINHAUSER, A. BRANDL, and T. E. JOHNSON, “Comparison of the Chernobyl and Fukushima nuclear accidents: A review of the environmental impacts,” Sci. Total Environ. **470**–**471**, 800, Elsevier (2014); https://doi.org/10.1016/J.SCITOTENV.2013.10.029.

50. J. ROBBINS and A. B. SCHNEIDER, “Thyroid Cancer Following Exposure to Radioactive Iodine,” Rev. Endocr. Metab. Disord. **1**, Kluwer Academic Publishers (2000).
51. A. P. ZHIDKIN et al., “Detailed study of post-Chernobyl Cs-137 redistribution in the soils of a small agricultural catchment (Tula region, Russia),” J. Environ. Radioact. **223**–**224**, 106386, Elsevier (2020); https://doi.org/10.1016/J.JENVRAD.2020.106386.
52. D. HOLIAKA et al., “Distributions of 137Cs and 90Sr activity concentrations in trunk of Scots pine (Pinus sylvestris L.) in the Chernobyl zone,” J. Environ. Radioact. **222**, 106319, Elsevier (2020); https://doi.org/10.1016/J.JENVRAD.2020.106319.
53. A. A. AGER et al., “The wildfire problem in areas contaminated by the Chernobyl disaster,” Sci. Total Environ. **696**, 133954, Elsevier (2019); https://doi.org/10.1016/J.SCITOTENV.2019.133954.
54. L. CUI et al., “Environmental Remediation of the difficult-to-return zone in Tomioka Town, Fukushima Prefecture,” Sci. Reports 2020 101 **10** 1, 1, Nature Publishing Group (2020); https://doi.org/10.1038/s41598-020-66726-y.
55. Y. TAIRA et al., “Assessment of localized and resuspended 137Cs due to decontamination and demolition in the difficult-to-return zone of Tomioka town, Fukushima Prefecture,” Integr. Environ. Assess. Manag. **00**, 0, John Wiley and Sons Inc (2022); https://doi.org/10.1002/IEAM.4625.
56. S. GUNTAY, D. A. POWERS, and L. DEVELL, “THE CHERNOBYL REACTOR ACCIDENT SOURCE TERM : DEVELOPMENT OF A CONSENSUS VIEW,” Organ. Econ. Co-Operation Dev. Energy Agency, Comm. Saf. Nucl. Install., 183 (1995).
57. M. P. MORRELL, “THREE MILE ISLAND UNIT 2 (TMI-2) CONTAINMENT ASSESSMENT TASK FORCE PROGRAM.,” in osti.gov **2**, pp. 1132–1153 (1980).
58. K. MÜCK et al., “A consistent radionuclide vector after the Chernobyl accident,” journals.lww.com.
59. N. KINOSHITA et al., “Assessment of individual radionuclide distributions from the Fukushima nuclear accident covering central-east Japan,” Proc. Natl. Acad. Sci. U. S. A. **108** 49, 19526 (2011); https://doi.org/10.1073/pnas.1111724108.
60. G. A. WETHERBEE et al., “Wet deposition of fission-product isotopes to North America from the Fukushima Dai-ichi incident, march 2011,” Environ. Sci. Technol. **46** 5, 2574, American Chemical Society (2012); https://doi.org/10.1021/ES203217U/SUPPL_FILE/ES203217U_SI_001.PDF.
61. J. N. SMITH et al., “Arrival of the Fukushima radioactivity plume in North American continental waters,” Proc. Natl. Acad. Sci. **112** 5, 1310, National Academy of Sciences (2015); https://doi.org/10.1073/PNAS.1412814112.
62. A.-P. LEPPÄNEN et al., “Artificial radionuclides in surface air in Finland following the Fukushima Dai-ichi nuclear power plant accident” (2013); https://doi.org/10.1016/j.jenvrad.2013.08.008.
63. P. THAKUR, S. BALLARD, and R. NELSON, “An overview of Fukushima radionuclides measured in the northern hemisphere,” Sci. Total Environ. **458**–**460**, 577, Elsevier (2013); https://doi.org/10.1016/J.SCITOTENV.2013.03.105.

64. P. P. POVINEC et al., “Dispersion of Fukushima radionuclides in the global atmosphere and the ocean,” Appl. Radiat. Isot. **81**, 383 (2013); https://doi.org/10.1016/J.APRADISO.2013.03.058.
65. N. EVANGELIOU et al., “Global Transport and Deposition of 137 Cs Following the Fukushima Nuclear Power Plant Accident in Japan: Emphasis on Europe and Asia Using High−Resolution Model Versions and Radiological Impact Assessment of the Human Population and the Environment Using Interactive Tools,” Environ. Sci. Technol **47**, 5812 (2013); https://doi.org/10.1021/es400372u.
66. S. YIN et al., “Simulation of the small modular reactor severe accident scenario response to SBO using MELCOR code,” Prog. Nucl. Energy **86**, 87, Pergamon (2016); https://doi.org/10.1016/J.PNUCENE.2015.10.007.
67. L. E. HERRANZ, M. GARCÍA, and M. P. KISSANE, “In-containment source term in accident conditions in sodium-cooled fast reactors: Data needs and model capabilities,” Prog. Nucl. Energy **54** 1, 138, Pergamon (2012); https://doi.org/10.1016/J.PNUCENE.2011.07.003.
68. T. SUZUKI et al., “A scenario of core disruptive accident for Japan sodium-cooled fast reactor to achieve in-vessel retention,” http://dx.doi.org/10.1080/00223131.2013.877405 **51** 4, 493, Taylor & Francis (2014); https://doi.org/10.1080/00223131.2013.877405.
69. P. MARCH and B. SIMONDI-TEISSEIRE, “Overview of the facility and experiments performed in Phébus FP,” Ann. Nucl. Energy **61**, 11, Pergamon (2013); https://doi.org/10.1016/J.ANUCENE.2013.03.040.
70. M. LAURIE et al., “Containment behaviour in Phébus FP,” Ann. Nucl. Energy **60**, 15, Pergamon (2013); https://doi.org/10.1016/J.ANUCENE.2013.03.032.
71. Y. PONTILLON, G. DUCROS, and P. P. MALGOUYRES, “Behaviour of fission products under severe PWR accident conditions VERCORS experimental programme - Part 1: General description of the programme,” Nucl. Eng. Des. **240** 7, 1843, Elsevier Ltd (2010); https://doi.org/10.1016/j.nucengdes.2009.06.028.
72. OECD/NEA, “Aerosol and Iodine Issues, and Hydrogen Mitigation under Accidental Conditions in Watercooled Reactors: Thermal-hydraulics, Hydrogen, Aerosols and Iodine (THAI-2) Project - Final Report” (2017).
73. G. A. GLOWA, C. J. MOORE, and J. M. BALL, “The main outcomes of the OECD Behaviour of Iodine (BIP) Project,” Ann. Nucl. Energy **61**, 179, Pergamon (2013); https://doi.org/10.1016/J.ANUCENE.2013.02.036.
74. G. WEBER et al., “Thermal-hydraulic–iodine chemistry coupling: Insights gained from the SARNET benchmark on the THAI experiments Iod-11 and Iod-12,” Nucl. Eng. Des. **265**, 95, North-Holland (2013); https://doi.org/10.1016/J.NUCENGDES.2013.07.012.
75. T. LIND et al., “Overview and outcomes of the OECD/NEA benchmark study of the accident at the Fukushima Daiichi NPS (BSAF), Phase 2 – Results of severe accident analyses for unit 3,” Nucl. Eng. Des. **376**, 111138, North-Holland (2021); https://doi.org/10.1016/J.NUCENGDES.2021.111138.
76. I. BEGHI, T. LIND, and H. M. PRASSER, “Experimental studies on retention of iodine in a wet scrubber,” Nucl. Eng. Des. **326**, 234, North-Holland (2018); https://doi.org/10.1016/J.NUCENGDES.2017.11.025.

77. N. P. GULHANE et al., “Experimental study of iodine removal efficiency in self-priming venturi scrubber,” Ann. Nucl. Energy **78**, 152, Pergamon (2015); https://doi.org/10.1016/J.ANUCENE.2014.12.008.
78. K. M. A. QASEM et al., “Radioactive iodine capture by metal organic frameworks in liquid and vapour phases: An experimental, kinetic and mechanistic study,” J. Environ. Chem. Eng. **9** 6, 106720, Elsevier (2021); https://doi.org/10.1016/J.JECE.2021.106720.
79. P. CHEN et al., “Iodine Capture Using Zr-Based Metal-Organic Frameworks (Zr-MOFs): Adsorption Performance and Mechanism,” ACS Appl. Mater. Interfaces **12** 18, 20429, American Chemical Society (2020); https://doi.org/10.1021/ACSAMI.0C02129/ASSET/IMAGES/LARGE/AM0C02129_0007.JPEG.
80. M. F. Y. L.L. HUMPHRIES, R.K. COLE, D.L. LOUIE, V.G. FIGUEROA, “MELCOR Computer Code Manuals,” Albuquerque, NM, and Livermore, CA (United States) (2015); https://doi.org/10.2172/1433918.
81. N. REINKE, K. NEU, and H. J. ALLELEIN, “ASTEC - An integral code for simulation of severe light water reactor accidents,” in International Conference on Nuclear Engineering, Proceedings, ICONE **2006** (2006); https://doi.org/10.1115/ICONE14-89280.
82. T. W. KIM et al., “Sensitivity study on severe accident core melt progression for advanced PWR using MELCOR code,” Nucl. Eng. Des. **269**, 155, North-Holland (2014); https://doi.org/10.1016/J.NUCENGDES.2013.08.022.
83. H. BONNEVILLE, L. CARENINI, and M. BARRACHIN, “Core Melt Composition at Fukushima Daiichi: Results of Transient Simulations with ASTEC,” Nucl. Technol. **196** 3, 489 (2016); https://doi.org/10.13182/NT16-27.
84. G. BANDINI and F. DE ROSA, “ASTEC validation on TMI-2 and LOFT LP-FP-2,” Nucl. Eng. Des. **272**, 163, North-Holland (2014); https://doi.org/10.1016/J.NUCENGDES.2013.10.012.
85. I. KLJENAK et al., “Thermal-hydraulic and aerosol containment phenomena modelling in ASTEC severe accident computer code,” Nucl. Eng. Des. **240** 3, 656, North-Holland (2010); https://doi.org/10.1016/J.NUCENGDES.2009.12.002.
86. L. FERNANDEZ-MOGUEL, A. RYDL, and T. LIND, “Updated analysis of Fukushima unit 3 with MELCOR 2.1. Part 1: Thermal-hydraulic analysis,” Ann. Nucl. Energy **123**, 59, Pergamon (2019); https://doi.org/10.1016/J.ANUCENE.2018.09.008.
87. L. CANTREL et al., “ASTEC V2 severe accident integral code: Fission product modelling and validation,” Nucl. Eng. Des. **272**, 195, North-Holland (2014); https://doi.org/10.1016/J.NUCENGDES.2014.01.011.
88. L. BOSLAND et al., “Modeling of Iodine Radiochemistry in the ASTEC Severe Accident Code: Description and Application to FPT-2 PHEBUS Test,” http://dx.doi.org/10.13182/NT10-A10774 **171** 1, 88, Taylor & Francis (2017); https://doi.org/10.13182/NT10-A10774.
89. T. HASTE et al., “MELCOR/MACCS simulation of the TMI-2 severe accident and initial recovery phases, off-site fission product release and consequences,” Nucl. Eng. Des. **236** 10, 1099, North-Holland (2006); https://doi.org/10.1016/J.NUCENGDES.2005.11.012.

90. S. IMOTO and T. TANABE, “CHEMICAL STATE OF TELLURIUM IN A DEGRADED LWR CORE” (1988).
91. R. DE BOER and E. H. P. CORDFUNKE, “The chemical form of fission product tellurium during reactor accident conditions,” J. Nucl. Mater. **240** 2, 124, Elsevier (1997); https://doi.org/10.1016/S0022-3115(96)00600-9.
92. R. DE BOER and E. H. P. CORDFUNKE, “Reaction of tellurium with Zircaloy-4,” J. Nucl. Mater. **223** 2, 103, North-Holland (1995); https://doi.org/10.1016/0022-3115(95)00005-4.
93. J. L. COLLINS, M. F. OSBORNE, and R. A. LORENZ, “Fission Product Tellurium Release Behavior Under Severe Light Water Reactor Accident Conditions,” Nucl. Technol. **77** 1, 18, Taylor & Francis (1987); https://doi.org/10.13182/NT87-A33948.
94. F. GARISTO, “THERMODYNAMICS OF IODINE, CESIUM AND TELLURIUM IN THE PRIMARY HEAT-TRANSPORT SYSTEM UNDER ACCIDENT CONDITIONS.,” At. Energy Canada Limited, AECL7782 (1982).
95. C. GONZÁLEZ and A. ALONSO, “Reaction kinetics of tellurium and silver aerosols at temperatures below 1,232 K),” J. Nucl. Sci. Technol. **34** 8, 799, Taylor & Francis (1997); https://doi.org/10.1080/18811248.1997.9733744.
96. F. ESPEGREN et al., “Tellurium Transport in the RCS under conditions relevant for severe nuclear accidents.”
97. B. R. BOWSHER, “Fission-product chemistry and aerosol behaviour in the primary circuit of a pressurized water reactor under severe accident conditions,” Prog. Nucl. Energy **20** 3, 199, Pergamon (1987); https://doi.org/10.1016/0149-1970(87)90006-0.
98. A. P. MALINAUSKAS et al., “The Interaction of Tellurium Dioxide and Water Vapor,” Nucl. Appl. Technol. **8** 1, 52 (1970); https://doi.org/10.13182/NT70-A28633.
99. C. GONZÁLEZ and A. ALONSO, “The kinetics of the reactions of tellurium with stainless steel surfaces and silver aerosols,” Nucl. Eng. Des. **180** 1, 1, Elsevier BV (1998); https://doi.org/10.1016/S0029-5493(97)00293-8.
100. E. C. BEAHM, “Tellurium Behavior in Containment under Light Water Reactor Accident Conditions,” Nucl. Technol. **78** 3, 295, Taylor & Francis (1987); https://doi.org/10.13182/NT87-A15995.
101. J. MCFARLANE and J. C. LEBLANC, “Fission-Product Tellurium and Cesium Telluride Chemistry Revisited Reexamen de la chimie du produit de fission tellure et du tellurure de cesium” (1996).
102. L. POSTMA, AK COLEMAN, “EFFECT OF CONTINUOUS SPRAY OPERATION ON THE REMOVAL OF AEROSOLS AND GASES IN THE CONTAINMENT SYSTEMS EXPERIMENT No. BNWL-1485.” (1970).
103. R. K. HILLIARD et al., “Removal of Iodine and Particles by Sprays in the Containment Systems Experiment,” Nucl. Technol. **10** 4, 499 (1971); https://doi.org/10.13182/nt71-a16261.
104. OECD NUCLEAR ENERGY AGENCY. COMMITTEE ON THE SAFETY OF NUCLEAR INSTALLATIONS, *Insights Into the Control of the Release of Iodine, Cesium, Strontium and Other Fission Products in the Containment by Severe Accident Management*, CSNI (2000).
105. A. SCHWENDIMAN, LC HASTY, RA POSTMA, “WASHOUT OF METHYL IODIDE BY HYDRAZINE SPRAYS. Final Report.” (1968).

106. GRIESS JC and BACARELLA AL, “The Corrosion of Materials in Reactor Containment Spray Solutions,” http://dx.doi.org/10.13182/NT71-A16264 **10** 4, 546, Taylor & Francis (2017); https://doi.org/10.13182/NT71-A16264.
107. I. BETOVA, M. BOJINOV, and T. SAARIO, “Hydrazine replacement in nuclear power plants: alternative substances and techniques(VTT Research Report; No. VTT-R-03426-16),” VTT Technical Research Centre of Finland (2016).
108. K.-H. NEEB, *The Radiochemistry of Nuclear Power Plants with Light Water Reactors*, in The Radiochemistry of Nuclear Power Plants with Light Water Reactors (2011); https://doi.org/10.1515/9783110812015.
109. S. TIETZE, M. RSTJ FOREMAN, and C. H. EKBERG, “Formation of organic iodides from containment paint ingredients caused by gamma irradiation,” J. Nucl. Sci. Technol. **50** 7, 689 (2013); https://doi.org/10.1080/00223131.2013.799400.
110. G. V. BUXTON and H. E. SIMS, “On the radiation chemistry of methyl iodide in aqueous solution,” Radiat. Phys. Chem. **67** 5, 623, Pergamon (2003); https://doi.org/10.1016/S0969-806X(02)00498-X.
111. E. C. BEAHM et al., “Organic Iodide Formation During Severe Accidents in Light Water Nuclear Reactors,” Nucl. Technol. **78** 1, 34 (1987); https://doi.org/10.13182/NT87-A34006.
112. M. KIM, T. J. KIM, and J. W. YEON, “Formation of CH3I in a NaI and methyl alkyl ketone solution under gamma irradiation conditions,” J. Radioanal. Nucl. Chem. **316** 3, 1329, Springer Netherlands (2018); https://doi.org/10.1007/s10967-018-5852-y.
113. M. KIM et al., “Change in the pH of NaI and methyl alkyl ketone solutions under gamma irradiation,” J. Radioanal. Nucl. Chem. **326** 1, 121, Springer Science and Business Media B.V. (2020); https://doi.org/10.1007/s10967-020-07346-8.
114. T. LAVONEN, “Chemical effects in the sump water pool during post-LOCA conditions: literature review,” Espoo (2014).
115. OECD/NEA, “Update Knowledge Base for Long-term Core Cooling Reliability No. NEA-CSNI-R--2013-12” (2013).
116. S. DICKINSON et al., “Experimental and modelling studies of iodine oxide formation and aerosol behaviour relevant to nuclear reactor accidents,” Ann. Nucl. Energy **74**, 200, Pergamon (2014); https://doi.org/10.1016/J.ANUCENE.2014.05.012.
117. C. B. ASHMORE, J. R. GWYTHER, and H. E. SIMS, “Some effects of pH on inorganic iodine volatility in containment,” Nucl. Eng. Des. **166** 3, 347, North-Holland (1996); https://doi.org/10.1016/S0029-5493(96)01252-6.
118. B. SIMONDI-TEISSEIRE et al., “Iodine behaviour in the containment in Phébus FP tests,” Ann. Nucl. Energy **61**, 157, Pergamon (2013); https://doi.org/10.1016/J.ANUCENE.2013.02.039.
119. D. R. LIDE, *CRC Handbook of Chemistry and Physics, 85th Edition - Google Libros*, CRC Press (2004).
120. K. ZWEIBEL, “The impact of tellurium supply on Cadmium telluride photovoltaics,” Science (80-.). **328** 5979, 699 (2010); https://doi.org/10.1126/SCIENCE.1189690.
121. N. BELZILE and Y.-W. CHEN, “Tellurium in the environment: A critical review focused on natural waters, soils, sediments and airborne particles,” Appl. Geochemistry **63**, 83, Pergamon (2015); https://doi.org/10.1016/J.APGEOCHEM.2015.07.002.

122. M. BOUROUSHIAN, *Electrochemistry of metal chalcogenides*, Springer Science & Business Media. (2010).
123. M. POURBAIX, *Atlas of electrochemical equilibria in aqueous solutions*, Oxford, New York, Pergamon Press (1966).(Copyright NACE international 2010)
124. J. C. WREN et al., "Dissolution of organic solvents from painted surfaces into water," Can. J. Chem. **78** 4, 464, National Research Council of Canada (2000); https://doi.org/10.1139/v00-042.
125. J. C. WREN et al., "The Interaction of Iodine with Organic Material in Containment," Nucl. Technol. **125** 3, 337 (1999); https://doi.org/10.13182/NT99-A2952.
126. L. ENGMAN, "Synthetic Applications of Organotellurium Chemistry," Acc. Chem. Res. **18** 9, 274, American Chemical Society (1985); https://doi.org/10.1021/AR00117A003/ASSET/AR00117A003.FP.PNG_V03.
127. A. TAYLOR, "Biochemistry of tellurium," Biol. Trace Elem. Res. **55** 3, 231 (1996); https://doi.org/10.1007/BF02785282.
128. N. KUHN, P. FAUPEL, and E. ZAUDER, "Ein einfaches verfahren zur synthese von [EMe3]I und EMe2 (E = Se, Te)," J. Organomet. Chem. **302** 1, C4, Elsevier (1986); https://doi.org/10.1016/0022-328X(86)80069-9.
129. D. M. MILLER and C. A. WINKLER, "The measurement of the absolute rates of removal of lead and tellurium mirrors by a free radical stream.," Can. J. Chem. **29** 7, 537 (1951); https://doi.org/10.1139/v51-062.
130. G. V BUXTON et al., "Critical Review of rate constants for reactions of hydrated electrons, hydrogen atoms and hydroxyl radicals (·OH/·O− in Aqueous Solution," J. Phys. Chem. Ref. Data **17** 2, 513 (1988); https://doi.org/10.1063/1.555805.
131. P. DRIVER, G. GLOWA, and J. C. WREN, "Steady-state γ-radiolysis of aqueous methyl ethyl ketone (2-butanone) under postulated nuclear reactor accident conditions," Radiat. Phys. Chem. **57** 1, 37, Elsevier Science Ltd (2000); https://doi.org/10.1016/S0969-806X(99)00309-6.
132. J. MALET, O. DEGREES DU LOU, and T. GELAIN, "Water evaporation over sump surface in nuclear containment studies: CFD and LP codes validation on TOSQAN tests," Nucl. Eng. Des. **263**, 395 (2013); https://doi.org/10.1016/j.nucengdes.2013.05.009.
133. T. SEVÓN, "A MELCOR model of Fukushima Daiichi Unit 1 accident," Ann. Nucl. Energy **85**, 1, Elsevier Ltd (2015); https://doi.org/10.1016/j.anucene.2015.04.031.
134. W. N. BISHOP and D. A. NITTI, "Stability of Thiosulfate Spray Solutions," Nucl. Technol. **10** 4, 449 (1971); https://doi.org/10.13182/NT71-A16255.
135. R. K. HILLIARD et al., "Removal of Iodine and Particles by Sprays in the Containment Systems Experiment," Nucl. Technol. **10** 4, 499 (1971); https://doi.org/10.13182/nt71-a16261.
136. L. T. VLAEV and V. G. GEORGIEVA, "Activation Energy for Electroconduction of Aqueous Solutions of Sulfuric and Selenic Acids and Potassium Tellurate," Russ. J. Electrochem. **40** 6, 674 (2004); https://doi.org/10.1023/B:RUEL.0000032021.43984.d3.
137. B. M. TOLBERT and M. H. KRINKS, "Chemical effects of ionizing radiation on pure organic compounds.," Radiat. Res. **Suppl 2**, 586 (1960); https://doi.org/10.2307/3583620.

138. M. KOIKE, E. TACHIKAWA, and T. MATSUI, “Gamma-Radiolysis of Aqueous Boric Acid Solution,” J. Nucl. Sci. Technol. **6** 4, 163 (1969); https://doi.org/10.1080/18811248.1969.9732863.
139. Z. ZHANG et al., “Combining ferrate(VI) with thiosulfate to oxidize chloramphenicol: Influencing factors and degradation mechanism,” J. Environ. Chem. Eng. **9** 1, 104625, Elsevier (2021); https://doi.org/10.1016/J.JECE.2020.104625.
140. W. ZHANG et al., “Thiosulfate enhanced degradation of organic pollutants in aqueous solution with g-C3N4 under visible light irradiation,” Chemosphere **275**, 130119, Pergamon (2021); https://doi.org/10.1016/J.CHEMOSPHERE.2021.130119.
141. J. YANG et al., “Superfast degradation of refractory organic contaminants by ozone activated with thiosulfate: Efficiency and mechanisms,” Water Res. **176**, 115751, Pergamon (2020); https://doi.org/10.1016/J.WATRES.2020.115751.
142. E. M. GLEBOV et al., “Photochemistry of sodium thiosulfate in aqueous solutions revisited,” J. Photochem. Photobiol. A Chem. **427**, Elsevier B.V. (2022); https://doi.org/10.1016/J.JPHOTOCHEM.2022.113818.
143. H. HERRMANN, A. REESE, and R. ZELLNER, “Time-resolved UV/VIS diode array absorption spectroscopy of SOx−(x=3, 4, 5) radical anions in aqueous solution,” J. Mol. Struct. **348**, 183 (1995); https://doi.org/10.1016/0022-2860(95)08619-7.
144. T. TOBIEN et al., “Time-resolved study on the reactions of organic selenides with hydroxyl and oxide radicals, hydrated electrons, and H-atoms in aqueous solution, and DFT calculations of transients in comparison with sulfur analogues,” Phys. Chem. Chem. Phys. **12** 25, 6750 (2010); https://doi.org/10.1039/b923797f.
145. G. GLOWA, P. DRIVER, and J. C. WREN, “Irradiation of MEK — II: A detailed kinetic model for the degradation of 2-butanone in aerated aqueous solutions under steady-state γ-radiolysis conditions,” Radiat. Phys. Chem. **58** 1, 49, Pergamon (2000); https://doi.org/10.1016/S0969-806X(99)00360-6.
146. G. MEISSNER et al., “Pulsradiolytische Untersuchung von Dimethylthioäther und Dimethylsulfoxyd in wäßriger Lösung,” degruyter.com **22**, 13 (1967).
147. K. NISHIKIDA and F. WILLIAMS, “The ESR spectrum and structure of the dimer radical cation of dimethyl selenide (Me2Se-SeMe+2) in a γ-irradiated single crystal,” Chem. Phys. Lett. **34** 2, 302, North-Holland (1975); https://doi.org/10.1016/0009-2614(75)85279-1.
148. L. BELCHETZ and E. K. RIDEAL, “The Primary Decomposition of Hydrocarbon Vapors on Carbon Filaments,” J. Am. Chem. Soc. **57** 7, 1168 (1935).
149. H. SHIRAISHI and K. ISHIGURE, “Possibility of formation of organic telluride under reactor accident condition - An experimental approach” (1988).
150. OECD/NEA, “State-of-the-Art Report (SOAR) on Nuclear Aerosols,” Paris (2009).
151. PARSLY LF, “SPRAY PROGRAM AT THE NUCLEAR SAFETY PILOT PLANT,” Nucl. Technol. **10** 4, 472 (1971); https://doi.org/10.13182/nt71-a16259.
152. W. E. JOYCE, “Sodium Thiosulfate Spray System for Radioiodine Removal,” Nucl. Technol. **10** 4, 444 (1971); https://doi.org/10.13182/NT71-A16254.
153. C. F. BAES and R. D. SHARP, “A Proposal for Estimation of Soil Leaching and Leaching Constants for Use in Assessment Models,” J. Environ. Qual. **12** 1, 17, John Wiley & Sons, Ltd (1983); https://doi.org/10.2134/JEQ1983.00472425001200010003X.

154. E. ANEHEIM, D. BERNIN, and M. R. S. J. FOREMAN, “Affinity of charcoals for different forms of radioactive organic iodine,” Nucl. Eng. Des. **328**, 228, Elsevier Ltd (2018); https://doi.org/10.1016/j.nucengdes.2018.01.007.
155. J. C. WREN et al., “Methyl Iodide Trapping Efficiency of Aged Charcoal Samples from Bruce-A Emergency Filtered Air Discharge Systems,” Nucl. Technol. **125** 1, 28 (1999); https://doi.org/10.13182/NT99-A2930.
156. J. C. WREN et al., “Modeling the removal and retention of radioiodine by TEDA-impregnated charcoal under reactor accident conditions,” Taylor Fr. **125** 1, 13, American Nuclear Society (2017); https://doi.org/10.13182/NT99-A2929.
157. J. FAN and I. A. M. DE LANNOY, “Pharmacokinetics,” in Biochemical Pharmacology **87** 1, pp. 93–120, Elsevier (2014); https://doi.org/10.1016/j.bcp.2013.09.007.
158. C. HULL and K. MCLEOD, “Pharmacokinetic analysis using an electrical analogue,” BJA Br. J. Anaesth. **48** 7, 677 (1976).